DESIGNING AND DEVELOPING TOOLS TO PROBE, MONITOR, AND MODULATE THE WNT SIGNALING PATHWAY

A Dissertation
Presented to
The Academic Faculty

by

Abhirup Mukherjee

In Partial Fulfillment
of the Requirements for the Degree
Doctor of Philosophy (Ph.D.) in
Chemical and Biomolecular Engineering

Georgia Institute of Technology
August 2019

DESIGNING AND DEVELOPING TOOLS TO PROBE, MONITOR, AND MODULATE THE WNT SIGNALING PATHWAY

Approved by:

Dr. Ravi S. Kane, Advisor
School of Chemical and Biomolecular Engineering
Georgia Institute of Technology

Dr. Andrés J. García
School of Mechanical Engineering
Georgia Institute of Technology

Dr. Hang Lu
School of Chemical and Biomolecular Engineering
Georgia Institute of Technology

Dr. Patrick T. McGrath
School of Biological Sciences
Georgia Institute of Technology

Dr. Julie A. Champion
School of Chemical and Biomolecular Engineering
Georgia Institute of Technology

Date Approved: [July 25, 2019]

ACKNOWLEDGEMENTS

I would like to start by thanking my thesis advisor, Prof. Ravi Kane, for his guidance and mentorship for the better part of the last six years. His input has been invaluable in shaping me as a person and a professional. Next, I would like to express my immense gratitude to my doctoral committee members Prof. Lu, Prof. Champion, Prof. García and Prof. McGrath for their critical feedback throughout my doctoral studies.

I would not have been able to even start this work if not for the hands-on guidance and mentorship from Dr. Manish Arha, Dr. Chaitanya Sudrik, Dr. Jicong Cao and Dr. Ruchir Mundra at the start of this journey at Rensselaer Polytechnic Institute. The findings presented in Chapter 4 of this thesis resulted from a collaboration between Dr. Sudrik, Dr. Arha and myself. I am grateful to my batchmates and friends from Rensselaer Polytechnic Institute for making my first two years in the United States of America fun and memorable.

I would like to thank all the past and present Kane Lab members; especially Dr. Chad Varner, Dr. Tania Rosen-Cheriyan, Dr. Neha Dhar, Dr. Jihun Park, Ammar Arsiwala, Troy Batugal, Steven Frey, Ana Castro, Nicole Hu, Geetanjali Pendyala and Mark Stathos. I would also like to express my heartfelt gratitude to my undergraduate mentees, Vivaan Patel and Nikolai Peterson for their contributions to this thesis.

I am forever indebted to my friends, Laura Weinstock, Nate Dwarshuis, Troy Batugal, Dr. Aaron Enten, Dr. Xuetian Ma, Dr. Charles Ge, Dr. Alex Bryant and Dr. Tony Du, for their help through this journey. I would especially like to acknowledge the contributions of the Georgia Tech Graduate Leadership Program in shaping my leadership and entrepreneurial leanings over the past 3 years.

I had the opportunity of a lifetime to work with some immensely gifted scientists at the Johnson & Johnson Group of Consumer Companies during the Spring and Summer of 2018. I would like to thank my manager, Wen-Hwa Li, and my team members, Dr. Prithwiraj Maitra, Dr. Ramine Parsa, Dr. Daphne Meza, Dr. Fang Liu-Walsh and Eric Liu, for a fantastic 6-month learning experience.

I would like to thank the Microscopy Core Director, Dr. Aaron Lifland and the Biopolymer Characterization Core Director, Dr. Bettina Bommarius for providing me the necessary training at the core facilities at Georgia Tech.

Finally, I would like to thank my girlfriend, Sayani Majumdar, for putting up with my tantrums and, inevitably, bringing a smile to my face in the end.

Last, but by no means the least, I would like to thank my Maa (mother), Sumita Mukherjee, and Baba (father), Dr. Abhijit Mukherjee. Without their innumerable sacrifices throughout my lifetime, I would not be here.

TABLE OF CONTENTS

LIST OF TABLES

LIST OF FIGURES

SUMMARY

An exhaustive understanding of the major cellular signaling pathways in biology is key to future innovations in oncology, regenerative medicine and gene therapy. The Wnt/β-catenin signaling pathway represents one such pathway. It influences cell proliferation, self-renewal, migration, embryonic development and cancer. In this pathway, the effect of extracellular Wnt ligands is mediated by a cytosolic effector protein, β-catenin, which activates downstream genes. However, the exact mechanism of action for this pathway remains controversial. Our analysis asserts that the *disassembly of a fraction of the intracellular destruction complexes results in the partial inhibition of both β-catenin phosphorylation and ubiquitination* and this disassembly is correlated with these destruction complexes relocating to the cellular membrane upon Wnt stimulation. In contrast to the generally accepted view, our model also suggests that β-catenin can dissociate from the complex between sequential phosphorylation and ubiquitination events. Our insights from the above model led us to strategically design synthetic multivalent molecules that can mimic the effects of the canonical Wnt ligands. The application of Wnt proteins in industrial bioprocesses and therapy are currently limited by the difficulty associated with the efficient production and characterization of the Wnt proteins and the synthetic Wnt agonists described in this work can thus serve as efficient, viable and scalable alternatives to these wild-type Wnt proteins.

In parallel to the work described above, we applied our understanding of the dynamics of the canonical Wnt receptor protein LRP6 to design a library of tunable blue light-(λ=488 nm)-sensitive photoswitches with a range of oligomerization efficiencies and dissociation

dynamics. Finally, we proposed the design of field-deployable sentinel cells to monitor the quality of cardiomyocyte production from human induced pluripotent stem cells (iPSCs) via modulation of Wnt signaling. As a proof-of-concept, we designed transcriptional switches to detect key biomarkers of different stages of cardiomyocyte differentiation specifically and assert that these reporters can form the basis of the above-mentioned sentinel cells.

Taken together, the work described in this thesis can serve as a platform for investigating the role of the canonical Wnt signaling pathway in a wide array of biological phenomena and its subsequent integration in future bioprocessing workflows.

CHAPTER 1. INTRODUCTION

1.1 Motivation

Cellular signaling pathways are biomolecular networks that have evolved to govern the activities of the cell (Kitano et al. 2002; Bhattacharyya et al. 2006). At the cellular level, these pathways are responsible for a gamut of biological functions that range from transcriptional, translational, and post-translational regulation within the cell to exerting short and long-range effects on neighboring cells (Elowitz et al. 2000; Mann et al. 2003; Culler et al. 2010). Thus, an interplay of the pathways helps cells communicate with one another to perform the most crucial biological functions in an organism. In modern medicine, our understanding of signaling pathways holds the key to unlocking new insights in regenerative medicine, as well as discovering innovative treatment regimens in oncology and congenital and hereditary diseases (Reya et al. 2001; Androutsellis-Theotokis et al. 2006; Niederreither et al. 2008). A couple of examples come immediately to mind; the recent advent of CAR-T cell therapy was made possible by decades of literature studying the pathways underlying antigen recognition and the subsequent activation of various immune cells (Kalos et al. 2011; Irving et al. 1991; Harada et al. 1993; Levine et al. 1997). The promising Cas9-mediated gene-editing approach that has captured the imagination of the scientific community was preceded by a fundamental understanding of Cas9's role in CRISPR-mediated prokaryotic immune pathways, something that was made possible by about two decades' worth of scientific studies (Landers 2016; Ishino et al. 1987; Mojica et al. 1993; Mojica et al. 2000; Jansen et al. 2002; Bolotin et al. 2005).

There is, of course, a lot that remains unexplored in these fields, and the challenges faced in these disciplines often lead back to an incomplete understanding of the underpinning pathways (Takebe et al. 2010; Gnimassou et al. 2017). Controversies regarding various aspects of these pathways, e.g. the developmental signaling pathways, are commonplace (Azzolin et al. 2014; Park et al. 2015; Lin et al. 2010; Tosi et al. 2018). It is almost never due to the lack of effort, resources or collective intellect, but rather a lack of engineering tools available to settle the dispute decisively. However, as new tools and methods emerge over time, applying such tools to revisit these controversies often lead to radically impactful insights in the above disciplines (Hell et al. 1994; Huang et al. 2010; Zhang et al. 2016; Igarashi et al. 2018). When such progress is combined with other methods, they often result in the implementation of radical new approaches in a therapeutic and/or bioprocessing context. For example, citing a previously mentioned instance, CAR-T therapy came about only when the fundamental understanding of our immune pathways was combined with an expertise in synthetic biology, clinical intervention, and scalable bioprocessing (Wu et al. 2015; Lim and June 2017).

The Wnt family of signaling pathways represents examples of the aforementioned cellular signaling pathways (Fig. 1). After the first of these pathways was discovered almost 35 years ago, research on these family of pathways has revealed that they are ubiquitous in the animal kingdom on top of being highly evolutionarily conserved like many other developmental pathways (Clevers 2006; Clevers and Nusse 2012). The capability to understand and modulate these pathways thus represents a significant milestone in modern medicine (Moon et al. 2004, Baron et al. 2013). As a result, almost predictably, there has been no shortage of conflicting opinions regarding almost all aspects

of the Wnt pathways (Desbois-Mouthon et al. 2001, Mao et al. 2001, Cselenyi et al. 2008). There is a clear need for a better understanding of the Wnt pathways, and consequently there is a need for better tools, to further probe and modulate these pathways. Hence, we decided to focus our efforts in this thesis on elucidating the nuances of the canonical Wnt signaling pathway (also known as the Wnt/β-catenin pathway). However, as we move along, we ponder how to potentially translate our approach and findings to the other (noncanonical) Wnt pathways and other developmental pathways. Additionally, our understanding of recombinant protein expression and synthetic biology represent key cornerstones of this thesis.

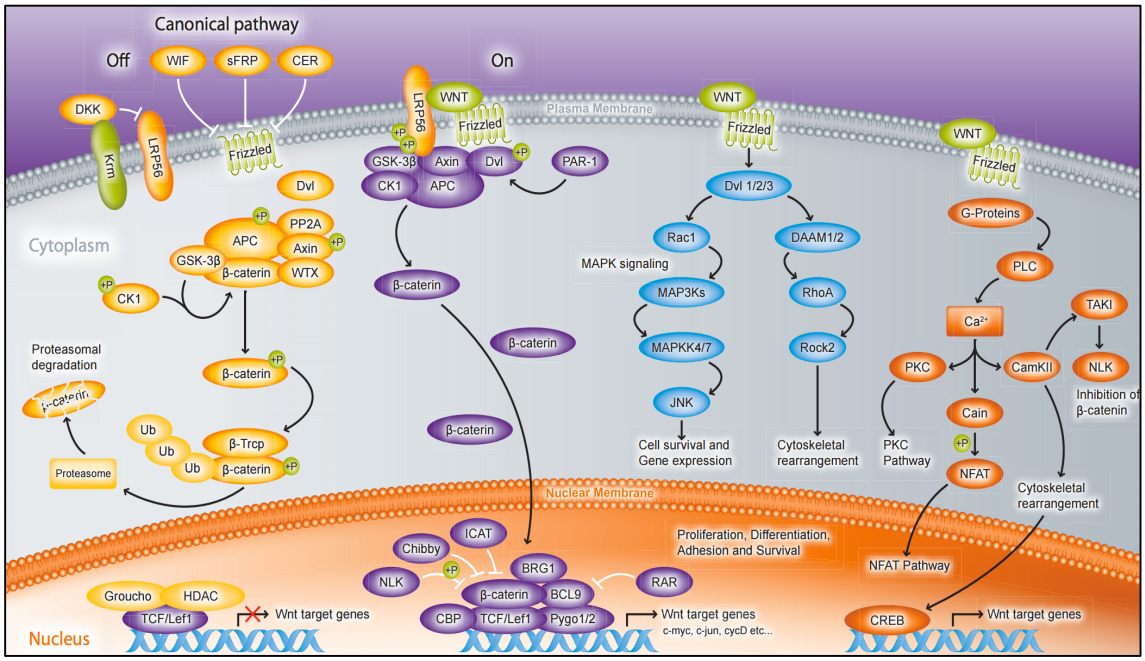

Figure 1 – Overview of the Wnt Signaling Pathways: Schematic showing the OFF and ON stages of the canonical Wnt pathway (*left, left-center*) and two noncanonical Wnt pathways, the planar cell polarity pathway (PCP) (*right-center*) and the Wnt-calcium pathway (Wnt/Ca^{2+}) (*right*). Reprinted from www.abcam.com.

1.2 Brief History of the Wnt Signaling Pathways

The first Wnt gene, the Wnt1 gene (then termed Int1), was discovered in 1982 by Harold Varmus and Roel Nusse while studying the molecular mechanism of infection by the oncogenic mouse mammary tumor virus (MMTV) (Nusse and Varmus 1982). To provide context, two of the more well-known pathways with broad-ranging implications in therapy, viz., the TGF-β and the p53 pathways were discovered in 1978 and 1979 respectively (Moses et al. 2016; DeLarco and Todaro 1978; Kress et al. 1979; Lane and Crawford 1979; Linzer and Levine 1979). In the late 1980s and early 1990s, within the first decade of the discovery of the Wnt1 gene, extensive studies in *Drosophila* and *Xenopus* indicated that the Wnt loci of genes, and the related pathways, are highly conserved among different species of the animal kingdom (Clevers and Nusse 2012).

A clearer picture of the canonical Wnt signaling pathway was predominantly developed in the 1990s. In the early 1990s, systematic epistasis studies in *Drosophila* led to the recognition of the core axis of proteins (genes) making up the Wnt transduction cascade, viz., disheveled (Dvl), armadillo (β-catenin), and GSK3 (Bhanot et al. 1996; Molenaar et al. 1996). During the same time, mutations in the adenomatous polyposis coli (APC) gene were implicated in familial adenomatous polyposis (FAP), a hereditary condition that predisposes patients to a high lifetime risk of colon cancer (Nishisho et al. 1991; Peifer and Polakis 2000). The first evidence of the Wnt pathways' involvement in diseases was reported in 1994 (Table 1), when the APC protein was shown to interact robustly with β-catenin, one of the core proteins of the Wnt axis (Su et al. 1993). In the late 1990s, the T-cell Factor/Lymphoid Enhancer-Binding Factor (TCF/LEF) family of

transcription factors was identified as key nuclear effectors of the Wnt pathway (Vandewetering et al. 1991; Behrens et al. 1996). Subsequently, the membrane receptors Frizzled and co-receptors Arrow and LRP5/6 were identified to be working together to bind the extracellular Wnt ligand and playing a key role in transducing the signal across the membrane (Wehrli et al. 2000; Cong et al. 2004).

Table 1 – Diseases Associated with Mutations in Wnt Pathway Components

Type of Mutation	Wnt Proteins	Examples of Associated Diseases
Gain-of-Function	β-catenin	Cancer
Loss-of-Function	APC	Familial Adenomatous Polyposis
Loss-of-Function	Axin1	Caudal Duplication Syndrome
Gain-of-Function	TCF4	Type II Diabetes
Loss-of-Function	LEF1	Sebaceous Skin Tumor

Since the turn of the new millennium, studies have revealed multiple additional components to the canonical Wnt pathway. Among them are the naturally secreted agonists, such as R-Spondins (RSPO) and Norrin, as well as the receptors Lgr4 and Lgr5 that specifically bind RSPO to enhance Wnt signaling *in vivo* (Xu et al. 2004; Kazanskaya et al. 2004; Glinka et al. 2011). Many naturally occurring antagonists, with different mechanisms of inhibition, have also been reported. For example, the Dickkopf (Dkk) family of proteins inhibits the Wnt signal transduction by binding the co-receptors LRP5/6 while secreted Frizzled-related proteins (sFRPs) directly bind to the canonical Wnt ligands and prevent their binding to their respective co-receptors (Glinka et al. 1998; Bovolenta et al. 2008). Identifying natural and synthetic agonists and antagonists of the canonical Wnt signaling pathway, and deciphering their role in various Wnt-modulated processes, remain an active field of research today.

In addition, multiple new members of the Wnt family of proteins and subsequently, several noncanonical Wnt pathways have been reported. To date, 19 Wnt genes (proteins) of 12 distinct subfamilies have been reported in the literature. Among the noncanonical Wnt pathways, the planar cell polarity (PCP) pathway and the Wnt-Calcium (Wnt/Ca^{2+}) signaling cascade are relatively well-known (Fig. 1) (Clevers and Nusse 2012). An alternative Wnt pathway was reported as recently as 2015 (Park et al. 2015). The mechanism of action of a large majority of these noncanonical Wnt pathways remain poorly characterized and hence their roles poorly understood from a biological standpoint.

1.3 General Overview of the Canonical Wnt Signaling Pathway

The transduction of the canonical Wnt signal is mediated by specific components in the extracellular space, the cellular membrane, the cell cytosol and the nucleus. It is a paracrine pathway and the effect of Wnt is widely considered to be a short-range, i.e., cells secreting the canonical Wnt ligands largely trigger this pathway in other cells in their immediate neighborhood (Clevers and Nusse 2012; Korkut et al. 2009; Sato et al. 2011).

In the absence of Wnt, cells (hereby referred to as Wnt OFF cells) maintain an extremely low cytosolic concentration of the Wnt effector protein, β-catenin, at steady state. This low concentration is due to the efficient functioning of a large, dynamic, multi-protein assembly known as the destruction complex (Fig. 2) (Stamos and Weis 2013). The destruction complex consists of scaffolding proteins, viz., Axin (Axin1), adenomatous polyposis coli (APC), as well as enzymes, viz., glycogen-synthase kinase 3β (GSK3β) and casein kinase 1α (CK1α). The scaffolding proteins largely ensure the proper assembly of the destruction complex, while the enzymes are responsible for the post-translational

modifications of β-catenin (Stamos and Weis 2013). In Wnt OFF cells, the cytosolic β-catenin is taken up by the destruction complex, sequentially mono-phosphorylated by CK1α, tri-phosphorylated by GSK3β and ubiquitinated by the β-TrCP E3 ubiquitin ligase complex (Hart et al. 1999; Amit et al. 2002; Liu et al. 2002; Wu et al. 2003). The ubiquitin-tagged β-catenin is then degraded extremely fast by the proteasome via the Ubiquitin-Proteasome Pathway (UPP), which in turn results in the miniscule cytosolic amounts of β-catenin (Fig. 2) (MacDonald et al. 2009).

However, the cell surface co-receptors Frizzled and LRP5/6 form a heterodimeric complex in presence of the canonical Wnt ligand (e.g. Wnt-3a) (Bhanot et al. 1996; Wehrli et al. 2000; Dann et al. 2001). Upon this complex formation, the destruction complex function in these cells (hereby referred to as Wnt ON cells) is disrupted (Cong et al. 2004). This disruption results in an accumulation of β-catenin in the cytosol over time which leads to the translocation of large amounts of β-catenin to the nucleus (Cong et al. 2004). In the nucleus, β-catenin acts as a transcriptional co-activator. It is recruited by the TCF/LEF family of transcription factors (already present in the nucleus) to the enhancer elements of the downstream Wnt target genes in the nucleus, thereby increasing the likelihood of expression of these genes (Behrens et al. 1996; vandeWetering 1997). The activation of these genes has far-reaching implications in the development of the Wnt ON cells as these genes influence key phenomena such as cell proliferation, self-renewal, differentiation etc. (Wodarz and Nusse 1998).

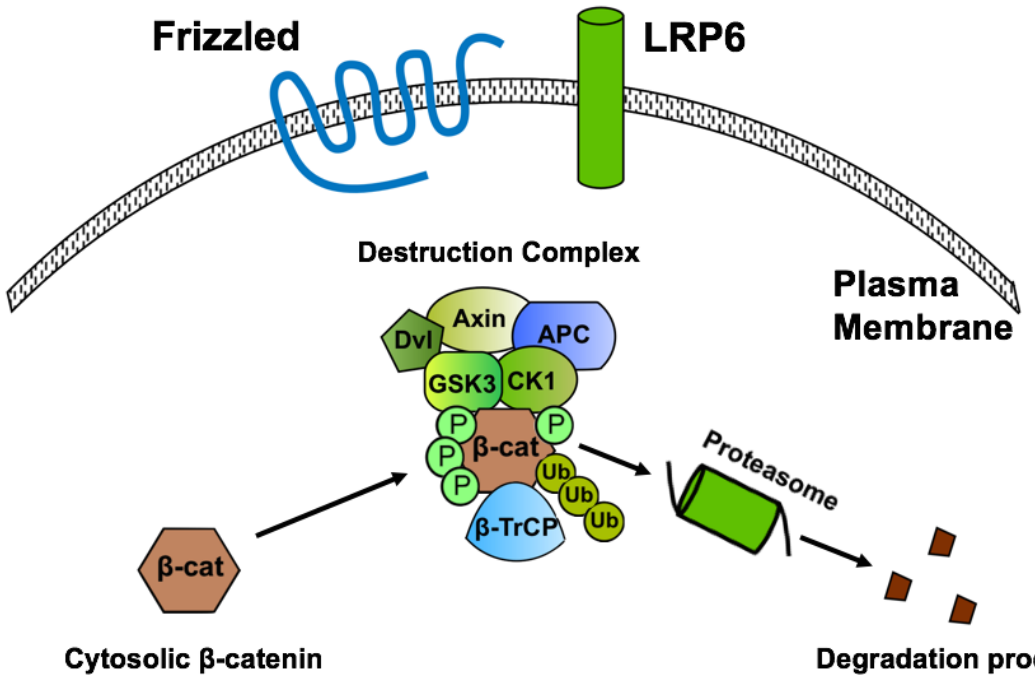

Figure 2 – Role of Destruction Complex in β-catenin Degradation: Schematic showing sequential phosphorylation by CK1α (CK1) and GSK3β (GSK3) followed by degradation by the Ubiquitin-Proteasome Pathway (UPP).

1.4 Challenges and Specific Aims

Evidently, the capability to modulate the canonical Wnt pathway represents a powerful tool for modern medicine. However, despite its discovery more than 35 years ago, this remains exquisitely challenging for a multitude of reasons.

1.4.1 Fundamental mechanism of the canonical Wnt pathway remains unclear

As mentioned above, researchers have attempted to decipher the fundamental mechanism of the canonical Wnt pathway since the early '90s. While they have discovered numerous (though, not all) essential components of the canonical Wnt pathway, the exact

biophysical mechanism underlying the signal transduction remains controversial (Hernandez et al. 2012; Li et al. 2012).

1.4.2 Challenging to produce and characterize Wnt ligands

The canonical Wnt proteins e.g. Wnt1 and Wnt-3a, are ~40 kDa proteins with multiple conserved cysteine residues (Tanaka et al. 2002). Moreover, these proteins are lipid modified and these lipids are essential for their signaling activity and may even be important for their secretion. For example, analysis of the purified mouse Wnt-3a revealed that it contains a palmitoleic acid moiety on a conserved serine residue (Janda et al. 2012; Clevers and Nusse 2012). The presence of these lipids makes the purification of the Wnt proteins extremely difficult, thus hindering the scalability of many Wnt-dependent bioprocessing workflows (Clevers and Nusse 2012; Janda et al. 2017).

1.4.3 Translating understanding of Wnt pathway to building orthogonal molecular biology tools

Understanding the details of the biophysical and biochemical phenomena associated with different components of cell biological pathways enables us to successfully develop new molecular biology tools that find potential applications in other contexts. However, our incomplete understanding of the canonical Wnt signaling pathway have limited the development of such orthogonal tools that are widely applicable.

1.4.4 Insufficient correlation between Wnt signaling and downstream pathways

As a direct consequence of the challenges associated with the pathway, it has been difficult to study the influence of the canonical Wnt signaling to its downstream signaling

networks. While it is known that Wnt plays an essential role in critical functions of the cell, especially in stem cells, such as proliferation and self-renewal, the exact chain of events that lead to these phenomena remains underexplored (Matushansky et al. 2008).

In this thesis, we attempted to address the concerns mentioned above. Our overall objective was to design an approach to derive novel insights into the fundamental mechanism of the canonical Wnt signaling pathway and subsequently, to utilize our understanding to develop a variety of cell biological tools to facilitate future investigations into the pathway. The following were our specific aims:

Specific Aim 1: Elucidate the Fundamental Mechanism of the Canonical Wnt Signaling Pathway

a. Ascertaining the rate-limiting step in inhibition of β-catenin degradation
b. Exploring the biophysical basis of Wnt signal transduction in the cytosol
c. Understanding the nature of destruction complex-β-catenin interaction

Specific Aim 2: Producing Synthetic Multivalent Agonists of Canonical Wnt Signaling

a. Standardizing the strategy and purification of divalent canonical Wnt agonists
b. Validating the activity and efficacy of Wnt agonists *in vitro*

Specific Aim 3: Designing Tunable Optogenetic Photoswitches

a. Constructing a library of optogenetic proteins with a wide range of declustering dynamics

Specific Aim 4: Designing Transcriptional Switches as Alternate Reporters in Wnt-modulated Generation of Cardiomyocytes

a. Constructing and validating transcriptional activation-based reporters of biomarkers Brachyury and Coup-TFII

CHAPTER 2. ELUCIDATE THE FUNDAMENTAL MECHANISM OF THE CANONICAL WNT SIGNALING PATHWAY

2.1 Background

Ever since the discovery of the core components of the canonical Wnt pathway in the 1990s, numerous mechanisms have been proposed in the literature to explain the increase in cytosolic β-catenin in presence of the canonical Wnt ligands. Several of these models revolved around the concept of Wnt-mediated disruption of the activity of Axin1, the protein which was widely considered the rate-limiting component of the destruction complex. Mao et al. and Zeng et al. suggested that the dephosphorylation and destabilization of Axin1 upon its membrane sequestration is largely responsible for stabilization of cytosolic β-catenin (Mao et al. 2001; Zeng et al. 2005). Along the same lines, several studies proposed the physical dissociation of Axin1 (and APC) from the destruction complex and its subsequent degradation in the cell being the key driver behind canonical Wnt signaling (Logan and Nusse 2004).

A contemporary school of thought (in the early 2000s) suggested that inhibition of phosphorylation of β-catenin is primarily responsible for its increased concentration. Cselenyi et al. and others suggested that the cytosolic domain of phosphorylated LRP6 inhibits GSK3 kinase activity whereas Taelman et al. suggested that vesicular bodies within the cytosol sequester the GSK3 enzyme to prevent it from interacting with the destruction complex and β-catenin in the first place (Cselenyi et al. 2008; Taelman et al. 2010). Some

studies also posited a role for phosphatases such as PP2A in dephosphorylating, and thus stabilizing, cytosolic β-catenin (Su et al. 2008).

As indicated by Li et al., the above studies mostly suffered from a key drawback, i.e. utilizing an overexpression strategy in probing the Wnt pathway (Li et al. 2012). A few Wnt components are present in very small amounts in the cytosol, and hence the dynamics of the Wnt pathway is severely modified when one or more of these components are expressed at a significantly higher level than that usually found in the organism. However, recent innovations have allowed us to circumvent the need for overexpression by being able to accurately detect nanomolar levels of proteins. As a result, recent controversies in the field have circled around two main competing mechanisms; a) the inhibition of phosphorylation and b) the inhibition of ubiquitination of β-catenin (Fig. 3) (Hernandez et al. 2012; Kim et al. 2013; Li et al. 2012; Azzolin et al. 2014).

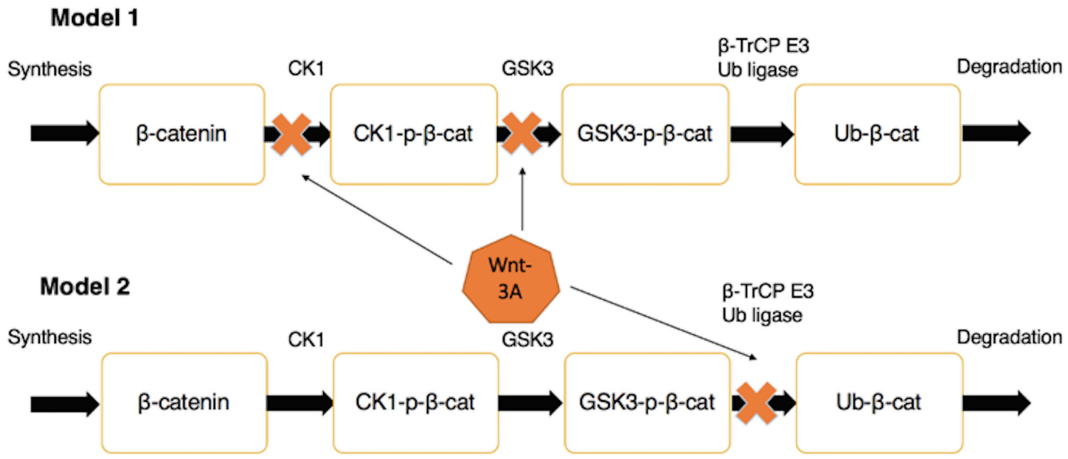

Figure 3 – Two Competing Models of Canonical Wnt Signaling: Model 1 has been proposed by Hernandez et al. and Kim et al. and asserts that CK1 and GSK3 phosphorylation are rate-limiting steps. Model 2 shows inhibition of only the ubiquitination step as suggested by Li et al. and Azzolin et al.

In 2012, Li et al. ruled out the possibility of Axin1 degradation being the key cause behind β-catenin accumulation. Upon Wnt-3a stimulation, they found that the accumulation of β-catenin was detectable after 30 minutes while any noticeable degradation of Axin1 took at least ~4 hours (Li et al. 2012). To probe the pathway, they co-immunoprecipitated Axin1 and thus pulled down the proteins associated with the destruction complex. They observed that the same proteins were pulled down along with Axin1 before and after the addition of Wnt-3a, suggesting that the destruction complex doesn't fall apart. Moreover, they reported that the concentrations of CK1-phosphorylated-β-catenin (hereby referred to as CK1-p-β-catenin) and GSK3-phosphorylated-β-catenin (hereby referred to as GSK3-p-β-catenin) associated with Axin1 increased after Wnt stimulation. They also observed that the amount of ubiquitinated GSK3-p-β-catenin associated with Axin1 decreased after Wnt stimulation. This decrease led them to conclude that "Wnt signaling suppresses β-catenin ubiquitination normally occurring within the complex, leading to complex saturation by accumulated phospho-β-catenin." (Li et al. 2012). Complex saturation would make the destruction complexes unavailable for degrading β-catenin, leading to a rise in β-catenin concentration in the cytosol. In 2014, Azzolin et al. reported that Hippo transducer proteins YAP/TAZ form a part of the destruction complex and are essential for the docking of the β-TrCP ubiquitin E3 ligase (Azzolin et al. 2014). They observed that Wnt signaling caused YAP/TAZ to be released from the destruction complex. This, in turn, prevented the docking of the E3 ligase to the destruction complex, thus inhibiting the ubiquitination of β-catenin.

In the same year, Hernandez et al. proposed a contradictory model to that of Li et al. They suggested that the CK1α (hereby referred to as CK1) and the GSK3β (hereby referred

to as GSK3)-phosphorylation of β-catenin were the rate controlling steps in the canonical Wnt signaling pathway (Hernandez et al. 2012). They arrived at this conclusion by measuring the temporal variation in concentrations of different types of cytosolic and nuclear β-catenin upon Wnt-3a stimulation in mammalian cells. They observed that the total cytosolic β-catenin concentration increased monotonically and then plateaued over time to reach a new steady-state concentration. However, the levels of CK1-phosphorylated (CK1-p-β-cat) and GSK3-phosphorylated β-catenin (GSK3-p-β-cat) decreased initially (to different extents) and subsequently recovered over time, reaching a new steady-state. They also showed that the minimum in GSK3-p-β-cat concentration coincided in time with the maximum in the rate of accumulation of total β-catenin. In 2013, Kim et al. also reported that the ratio of GSK3-p-β-catenin to total β-catenin concentration fell precipitously upon Wnt stimulation, but never recovered over time (Kim et al. 2013). They argued that this observation conclusively proved that phosphorylation was the rate controlling step. While both studies did not explicitly comment on the destruction complex, Hernandez et al. mentioned that their model was consistent with the destruction complex falling apart. Commenting on the Li et al. study, Hernandez et al. argued that an inactivation-via-saturation of the destruction complex offers no possibility of a recovery of the degradation flux. A lack of such a recovery will lead to a runaway accumulation of β-catenin in the cytosol and is thus inconsistent with the experimental observations.

2.2 Material and Methods

Antibodies

The anti-APC antibody (Cell signaling Technology, #2504) was used for co-immunoprecipitation only. The anti-Axin1 antibody (Cell Signaling Technology; #2087) was used for both co-immunoprecipitation and immunoblotting. The following antibodies were used for immunoblotting only: anti-β-catenin (BD Transduction Laboratories; #610153), anti-phospho-β-catenin antibody (Ser33/37/Thr41) (Cell Signaling Technology; #9561), anti-phospho-β-catenin antibody (Ser45) (Cell Signaling Technology; #9564), anti-LRP6 (C5C7) antibody (Cell Signaling Technology; #2560), anti-APC (Abcam, #ab15270), anti-biotin (Abcam, #ab53494), anti-α-tubulin (Abcam; #ab52866), anti-GAPDH (Abcam; #ab8245), and monoclonal rabbit IgG isotype control (Abcam, #ab172730).

Mammalian Cell Culture and Treatment with Wnt-3a and MG132

Human embryonic kidney (HEK) 293T cells were purchased from the American Type Culture Collection (ATCC) and cultured in D-10 (DMEM with 10% HI-FBS; Gibco, Thermo Scientific) media in a humidified incubator at 37°C with 5-8% CO_2. Cultured cells were treated with recombinant human Wnt-3a (Bio-Techne) at a final concentration of ~800 ng/ml. MG132 (Sigma-Aldrich) treatments were done at a final concentration of 10 μM (liquid MG132 stock diluted directly in D-10 media immediately before treatment).

Preparation of Whole-cell Lysates and Cytoplasmic and Nuclear extracts

293T cells were cultured in 6-well tissue culture plates (Corning) and grown up to 90% confluency. After treatment, the cells were washed in ice-cold DPBS (Corning) twice and 80 μL of lysis buffer, consisting of 0.5% (w/v) digitonin (pH 7.5) in DPBS (Kim et al. 2013), was added to each well. The lysis buffer was supplemented with N-ethylmaleimide (Sigma-Aldrich) at a concentration of 5 μM and phosphatase inhibitor (Sigma-Aldrich) and protease inhibitor cocktails (Thermo Scientific) at dilutions recommended by the manufacturer. The lysates were incubated on ice for 30-45 min for complete lysis and harvested using cell scrapers (Grainger). The lysates were then cleared by centrifuging at 13,000g for ~15 min. The clear, debris-free supernatant was collected for further analysis for each lysate. These represented the whole-cell lysates.

Next, we obtained the cytoplasmic and nuclear extract by incubating the above supernatant with Concanavalin A-Sepharose 4B beads (GE Healthcare) for 60 min at 4°C with continuous end-over-end mixing. The slurry was then centrifuged at 4000g for ~5 mins. The membrane-associated proteins were bound to the Concanavalin A beads and the supernatant consisted of the cytoplasmic and nuclear fractions of the lysate. The beads were then washed 5 times with DPBS and denatured directly in 2x LDS Sampling Buffer (Thermo Scientific) followed by immunoblotting (western blotting) to analyze membrane-associated proteins. The supernatants from both whole-cell and cytoplasmic and nuclear lysates were denatured in 1x LDS Sampling Buffer (Thermo Scientific) by heating at 100°C for 10-15 mins. We then proceeded to immunoblotting (western blotting) for further analysis.

Detection of Newly-Synthesized β-catenin

293T cells were cultured in 15-cm tissue culture dishes (Corning) at an initial concentration of 15 million cells per dish for 36-48 h in D-10 media. First, the cells were treated with Wnt-3a for the indicated time periods. Next, the D-10 media was removed and the cells were washed twice with DPBS followed by one wash with methionine-free, cystine-free Dulbecco's Modified Eagle Medium (DMEM) (Thermo Scientific) consisting of 4-6 mM of L-Azidohomoalanine (L-AHA) (Anaspec). The cells were then treated with the wash media containing 10 μM MG-132 (Sigma-Aldrich) and Wnt-3a for the indicated time periods. The cells were then washed twice with ice-cold DPBS (Corning) and lysed using 2% SDS in DPBS containing phosphatase and protease inhibitor cocktails at concentrations prescribed by the manufacturers. The lysates were subsequently denatured and processed as described by Dieterich et al. and Debets et al. (Dieterich et al. 2007; Debets et al. 2010).

Co-Immunoprecipitation (Co-IP)

293T cells were cultured in 15-cm tissue culture dishes (Corning) at an initial concentration of 15 million cells per dish and incubated in D-10 media until 80% confluency was achieved. Cells were treated for the indicated time periods with Wnt-3a followed by two washes in ice-cold DPBS (Corning). They were then lysed in a lysis buffer of the following recipes:

a. **For anti-Axin1 co-IP:** 150 mM NaCl, 30 mM Tris (pH 7.5), 1 mM EDTA, 1% Triton X-100, 10% Glycerol.
b. **For anti-APC co-IP:** 25 mM Tris-HCl pH 7.4, 150 mM NaCl, 1% NP-40, 1 mM EDTA, 5% glycerol.

Lysis buffers were supplemented with phosphatase inhibitor cocktails 2 & 3 (at 1:100 dilution) (Sigma-Aldrich), Halt protease inhibitor cocktail (at 1:100 dilution) (Thermo Scientific), 0.1 mM phenylmethylsulfonyl fluoride (PMSF) and 0.5 mM Dithiothreitol (DTT). The cells were then incubated on ice for 30 mins, harvested using a cell scraper and centrifuged to collect the supernatant (whole-cell lysate) as mentioned earlier in this section.

Cell lysates were pre-cleared by incubating with Rabbit IgG isotype control antibody for 4 hours followed by Pierce Protein A Magnetic beads (Thermo Scientific) for 2 hours at 4°C. The magnetic beads were then separated out using a magnetic rack (MagnaRack; Thermo Scientific) and the supernatant incubated overnight with the appropriate immunoprecipitating antibody at 4°C with constant end-over-end mixing. This represented the "pull-down" step. The lysates were then incubated in Protein A-conjugated magnetic beads for 2 hours at 4°C with constant mixing to isolate the antibody. The magnetic beads were then separated again using the MagnaRack, washed 5 times with Tris-Buffered Saline (TBS) containing 0.1% Tween-20 followed by 1 wash with TBS. The beads were then denatured in 2x LDS Sampling Buffer (containing 2% v/v 2-mercaptoethanol) by heating at 100°C for ~15 mins. The heating denatures the proteins pulled down with the Protein A beads completely. The magnetic beads were then separated using the MagnaRack and the supernatant containing the immunoprecipitated proteins further analyzed.

SDS-PAGE Gel Electrophoresis and Immunoblotting

High-molecular weight proteins (100 - 400 kDa) and medium to low-molecular weight proteins (20 kDa - 100 kDa) in the lysates were resolved using SDS-PAGE Gel

Electrophoresis in 3-8% Tris-Acetate and 4-12% Bis-Tris Polyacrylamide gels respectively using an OWL P8DS (Thermo Scientific) gel-running apparatus. The proteins were then transferred using the Trans-Blot Turbo Transfer System (Bio-Rad) to a nitrocellulose membrane.

For immunoblotting, the membrane was blocked in a blocking buffer (1x TBS with 0.1% Tween-20 and 5% non-fat dry milk or BSA; as per antibody manufacturer's recommendation) for 1 hour at room temperature. The membrane was then incubated overnight at 4°C in primary antibody diluted in 5% BSA in TBST (1x TBS containing 0.1% Tween-20). The dilution used for different primary antibodies are as follows:

a. Anti-Axin1, anti-β-catenin, anti-phospho-β-catenin antibody (Ser33/37/Thr41), anti-phospho-β-catenin antibody (Ser45), anti-LRP6 (C5C7) antibody: 1:1000

b. Anti-α-tubulin, anti-GAPDH: 1:5000

c. Anti-APC: 1:500

Next, the membrane was washed three times with TBST for 5 minutes each and then incubated in secondary antibody diluted in the blocking buffer for 1 hour at room temperature with constant mixing. An HRP-conjugated anti-mouse antibody (Jackson Immunoresearch) was used to detect total β-catenin and GAPDH at a dilution of 1:10000. All other proteins were detected using an HRP-conjugated anti-rabbit antibody (Thermo Scientific) at a dilution of 1:3000. The membrane was then imaged in a ChemiDoc MP Imaging system (Bio-Rad) after ~1 minute of incubation in the SuperSignal West Femto Maximum Sensitivity Substrate. The detected protein bands were quantified using the

analysis tools provided in the Image Lab Software (Bio-Rad) and then validated using ImageJ.

2.3 Results

2.3.1 Monitoring temporal dynamics of β-catenin upon canonical Wnt signaling

To investigate, we proceeded by monitoring temporal changes in levels of β-catenin in 293T cells upon Wnt-3a stimulation. From previous reports, we knew that a significant amount of β-catenin in these cells remain associated with the E-cadherin complexes in the plasma membrane (Hernandez et al. 2012). By current understanding, these represent a highly stable pool of β-catenin which are *not* involved in canonical Wnt signaling. Hence, to monitor changes in the level of free (cytosolic and nuclear) β-catenin over time, we incubated the whole cell lysates with Concanavalin A-Sepharose 4B beads (which selectively bind glycosylated proteins) to remove the membrane-associated (glycosylated) β-catenin fraction (Mukherjee et al. 2018). We observed that the level of total β-catenin started increasing monotonously 15 min after Wnt-3a stimulation until it reached a steady-state at an elevated concentration at ~2 hours after Wnt exposure (Fig. 4A).

We know that for any protein species, and so for total β-catenin:

$$Rate\ of\ Accumulation = Rate\ of\ Synthesis - Rate\ of\ Degradation \quad (1)$$

Hernandez et al. had previously reported that the rate of synthesis of β-catenin does not change following Wnt-3a stimulation (Hernandez et al. 2012). The observed positive rate of accumulation of β-catenin thus implied that its rate of degradation decreased

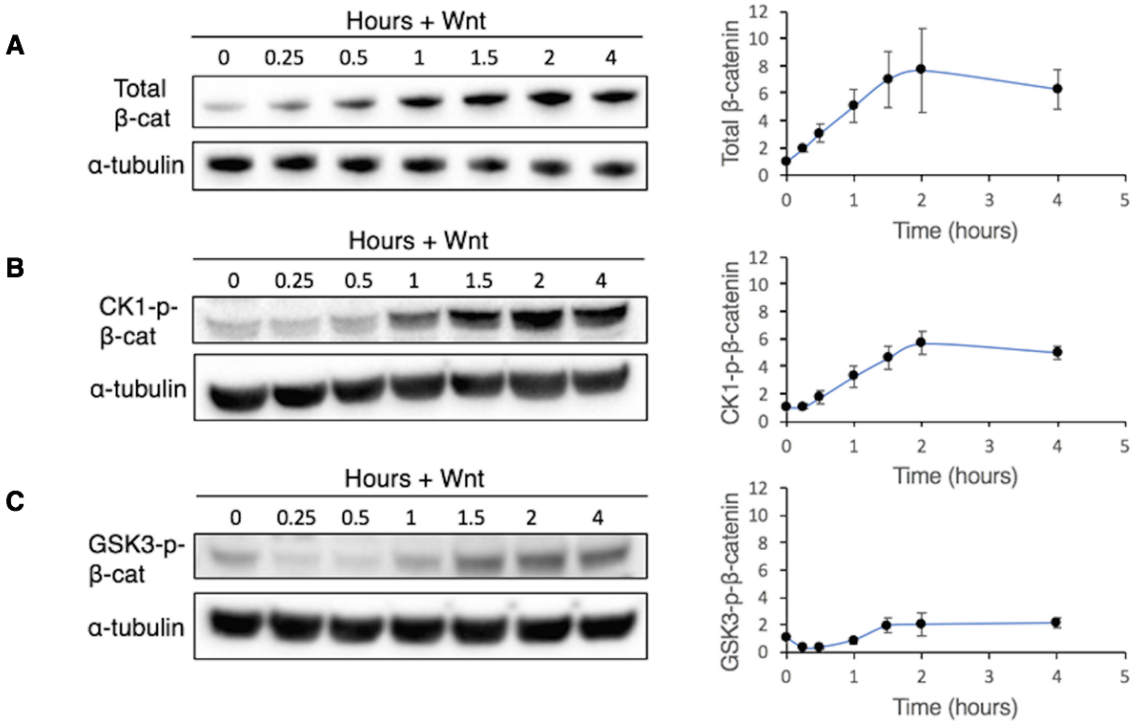

Figure 4 – Dynamics of β-catenin in Presence of Wnt-3a: Figure showing the temporal change in concentrations of (A) cytosolic total β-catenin (B) whole-cell CK1-p-β-catenin and (C) GSK3-p-β-catenin upon Wnt-3a addition at 0 hours. Each data point in the graph represent the mean (± 1 s.d) of three independent experimental repeats (n=3).

initially, which led to the observed increase in β-catenin levels. However, rate of accumulation became zero at the new steady-state observed at the 2-hour mark, suggesting that the rate of β-catenin degradation recovered to equal the rate of synthesis at that point, i.e. the rate of degradation of total β-catenin at the 2-hour mark recovered in the cell to equal its rate of degradation before Wnt-3a stimulation.

$$Rate\ of\ degradation_{t=2\ hours} = Rate\ of\ degradation_{t=0\ hour} \qquad (2)$$

Next, we wanted to observe the changes in the levels of CK1-p-β-catenin and GSK3-p-β-catenin upon Wnt stimulation. In contrast to total β-catenin, there is no

consensus about the subcellular localization of the phosphorylated species of β-catenin. So, we proceeded to measure the temporal changes of these two post-translationally modified species of β-catenin in the whole-cell lysates (as the most general case). In case of CK1-p-β-catenin, we observed temporal trends similar to that of total β-catenin i.e., levels of CK1-p-β-catenin in the cell increased with time (starting at 30 mins instead of the observed 15 mins in case of total β-catenin earlier) before attaining a steady-state at a higher concentration, ~2 hours after Wnt stimulation (Fig. 4B).

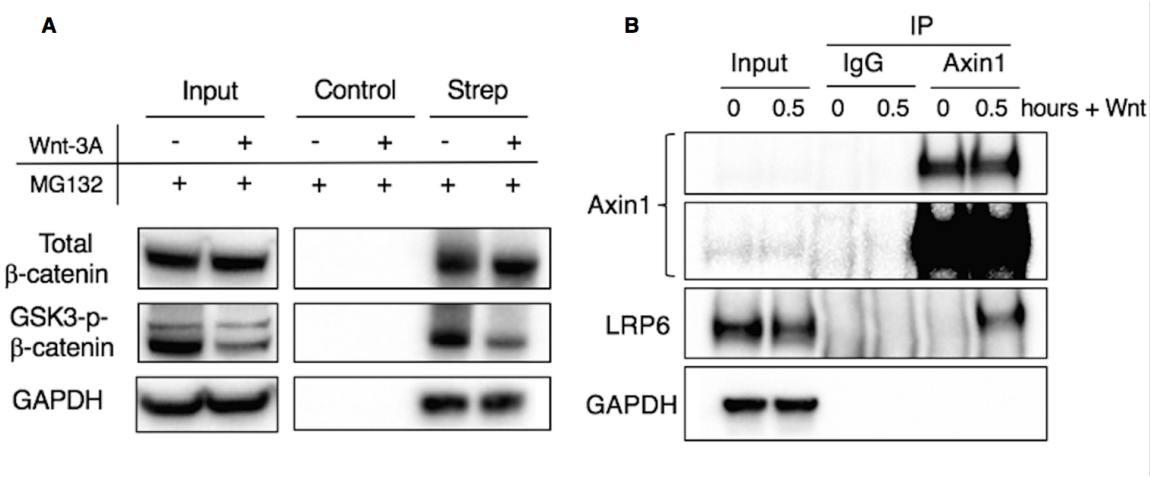

Figure 5 – Membrane Localization of Axin1 May Cause GSK3 inhibition: (A) Cumulative levels of newly-synthesized GSK3-p-β-catenin decrease while that of total β-catenin remain relatively unchanged in presence of canonical Wnt signaling. Input lanes represent whole-cell lysates of AHA-treated cells; Control lanes and Strep (streptavidin) lanes represent input lysates treated with DBCO-sulfo-biotin and subsequently pulled down with control agarose beads and streptavidin-conjugated beads respectively (B) Immunoprecipitation of Axin1 shows LRP6 co-immunoprecipitating in the presence of Wnt-3a, suggesting membrane localization of Axin1 and destruction complex. Input lanes represent whole-cell lysates of cells; IgG and Axin1 lanes represent lysates immunoprecipitated with control Rabbit IgG antibody and anti-Axin1 IgG antibody respectively.

In contrast, we found that the concentration of GSK3-p-β-catenin decreased initially (the minimum being at ~15-30-minute mark) and then recovered, reaching a new

steady-state that coincided in time with that of total and CK1-p-β-catenin i.e. at ~2 hours after Wnt stimulation (Fig. 4C). Now, this observation was inconsistent with inhibition happening solely at the downstream ubiquitination step (Mukherjee et al. 2018). As noted by Hernandez et al., inhibition of ubiquitination, but not of any other step in β-catenin degradation, would cause GSK3-p-β-catenin to continue to accumulate, much like total and CK1-p-β-catenin, until the ubiquitination flux, and hence the degradation flux, recovered their original values at a higher steady-state concentration of GSK3-p-β-catenin. Hence, the model proposed by Li et al. didn't satisfactorily explain our preliminary observations regarding the GSK3-p-β-catenin minimum (Hernandez et al. 2012).

The previous experiments showed what happens to the cell in presence of Wnt-3a relative to its initial steady-state. We proceeded to remove this background of previously present steady-state levels of proteins by measuring the concentrations of newly-synthesized total, CK1-p- and GSK3-p-β-catenin levels immediately following Wnt-3a stimulation (Fig. 5A). This was done using BioOrthogonal Noncanonical Amino Acid Tagging or BONCAT (Dieterich et al. 2007). In BONCAT, we treated the cellular media with the methionine-substitute noncanonical amino acid, L-Azidohomoalanine (L-AHA) at the same time that we started the Wnt treatment. This resulted in proteins translated after the addition of Wnt to be selectively tagged with L-AHA. To analyze the cumulative population of newly synthesized proteins, we also treated the cells with the well-known proteasomal inhibitor MG132 to significantly decrease overall protein degradation in the cell, thus boosting the signal from these low levels of proteins. L-AHA contains an azide moiety which is highly amenable for use in azide-alkyne "click" cycloaddition. Leveraging this property of L-AHA, we then labeled the newly synthesized proteins with biotin and

isolated them from the lysate using Streptavidin-Agarose beads (Debets et al. 2010). The amounts of newly synthesized total-β-catenin (Fig. 5A, top) and CK1-p-β-catenin (data not shown) were relatively unchanged (as we had hypothesized) before and after Wnt treatment. We also observed significant levels of newly-synthesized GSK3-p-β-catenin in presence as well as in absence of Wnt-3a, but the levels were significantly lowered upon Wnt treatment (Fig. 5A, middle). The above observation is consistent with the partial inhibition of β-catenin phosphorylation upon Wnt-3a stimulation. Previous studies have shown conclusively that the binding of Wnt-3a to its cellular receptors results in destruction complexes relocating to the cellular membrane (to form "signalosomes") (Bilic et al. 2007; Gerlach et al. 2018). We confirmed the above by observing that the cellular Wnt receptor LRP6 co-immunoprecipated with Axin1 upon Wnt-3a stimulation (Fig. 5B). Thus, we hypothesized that the relocalization of destruction complexes to the cellular membrane may be connected to the partial decrease in GSK3 phosphorylation, and thus in the partial loss of destruction complex activity upon Wnt-3a stimulation.

To explore this hypothesis further, we monitored the changes in levels of non-membrane-associated CK1-p-β-catenin and GSK3-p-β-catenin (i.e., the cytoplasmic and nuclear fraction) following Wnt stimulation like in the case of total β-catenin (Fig. 6A). As seen in Fig. 6B, the temporal trends for the non-membrane associated CK1-p-β-catenin and GSK3-p-β-catenin were very similar to their whole-cell counterparts. This evidence suggested that most of the phosphorylated β-catenin were *not* membrane associated. We confirmed this by further analyzing the membrane-associated proteins being pulled down with the Concanavalin A beads. In accordance with our previous observations, no

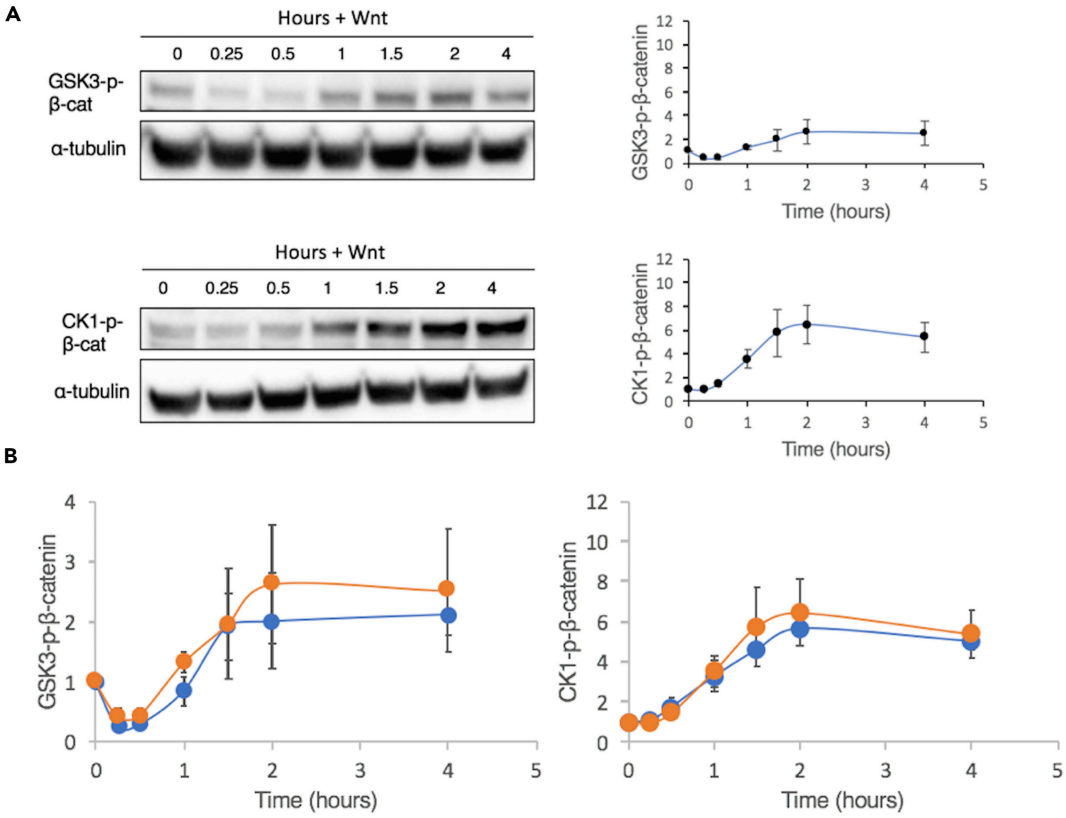

Figure 6 – Concentrations of Non-Membrane-Associated Phosphorylated β-catenin: (A) Figure shows change in concentrations of cytosolic and nuclear fractions of GSK3-p-β-catenin and CK1-p-β-catenin (B) Graphs co-plotting whole-cell (blue) and cytosolic and nuclear (orange) fractions of different forms of phosphorylated β-catenin on the same graph. Each data point in the graph represent the mean (± 1 s.d) of three independent experimental repeats (n=3).

significant levels of GSK3-p-β-catenin and CK1-p-β-catenin were pulled down in these membrane fractions (Fig. 7B). Taken together, these results indicated that an inhibition of the phosphorylation activity of the destruction complexes is correlated with the relocalization of these complexes to the membrane upon Wnt stimulation, with the residual phosphorylation activity coming primarily from the non-membrane associated (mainly cytosolic) destruction complexes.

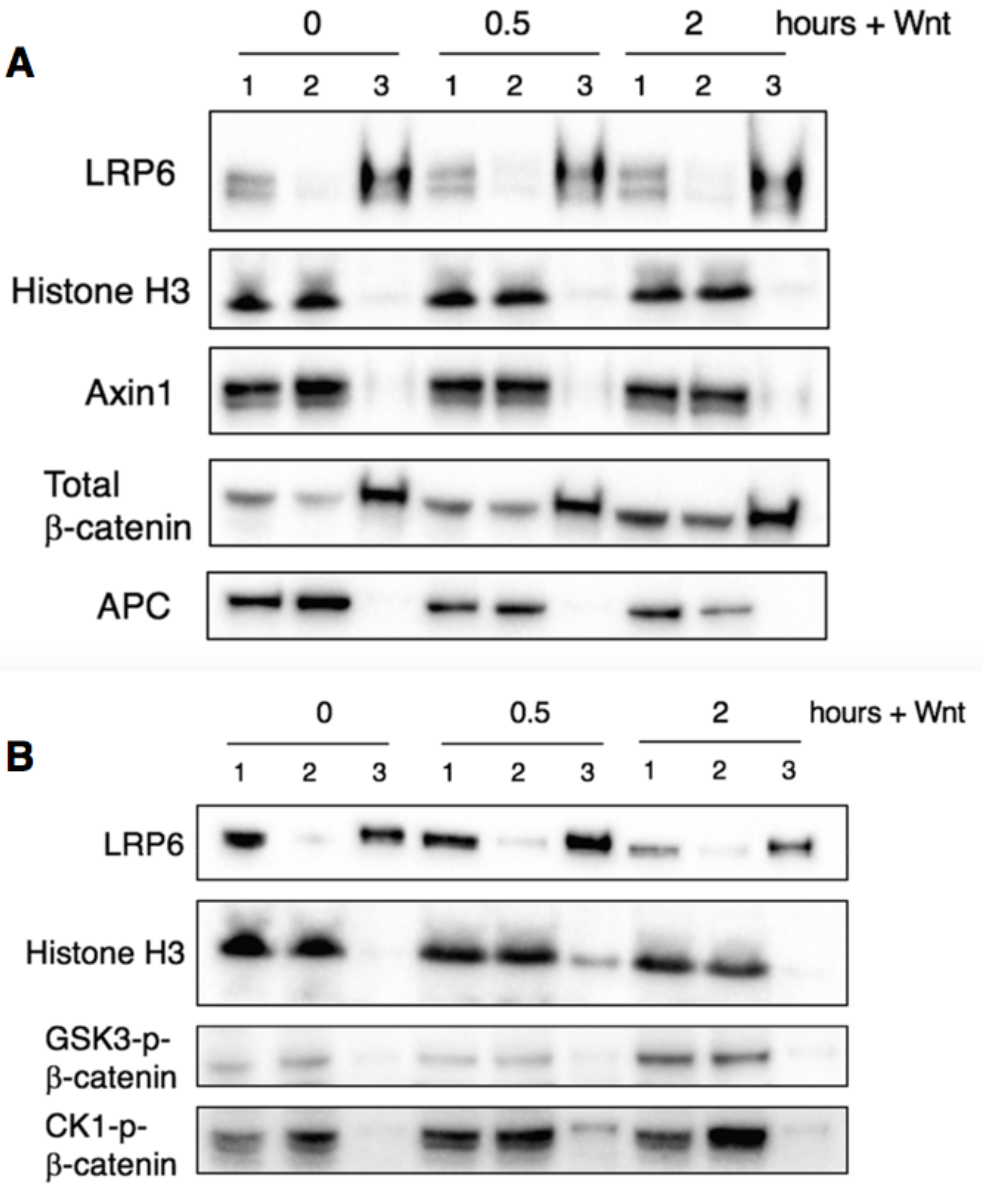

Figure 7 – Subcellular Localization of Core Canonical Wnt proteins: Figures showing temporal change in concentrations of whole-cell (Lanes 1), cytosolic and nuclear (Lanes 2) and membrane-associated fractions (Lanes 3) of core canonical Wnt proteins obtained from incubating lysates with Concanavalin A-Sepharose 4B beads.

2.3.2 Investigating the biophysics of the destruction complex upon Wnt-3a stimulation

As a natural next step, we wanted to investigate the underlying biophysical mechanism responsible for the inhibition described above. To do so, we had to design a strategy to probe the entire population of the destruction complexes. As suggested by Li et al., we proceeded to immuoprecipitate the limiting component of the destruction complex without perturbing its protein-protein interactions with the other components of the destruction complex (i.e. co-immunoprecipitation) (Li et al. 2012). However, we differed in a key way from Li et al. in that we chose to immunoprecipitate APC, and not Axin1, as in case of Li et al. This was in large parts due to multiple recent reports that APC levels are significantly lower than Axin1 levels in our cell line of choice, i.e. the HEK293T cell line, and thus is more likely to be the limiting component in the destruction complexes as opposed to the traditional view (Tan et al. 2012; Kitazawa et al. 2017). Upon co-immunoprecipitation, we measured the changes in concentrations of the major canonical Wnt proteins Axin1, GSK3-p-β-catenin and LRP6 being pulled down along with APC (Fig. 8). We immediately observed that there was a significant decrease (~56% or 0.56 times) in Axin1-APC interaction upon Wnt stimulation, similar to what Valvezan et al. observed in L cells upon Wnt stimulation (Fig. 8A and 8B) (Valvezan et al. 2012). We also observed an initial decrease in the concentration of co-immunoprecipitated GSK3-p-β-catenin, with no concomitant increase in co-immunoprecipitated LRP6 concentration (Fig. 8A).

Levels of GSK3-p-β-catenin then recovered substantially by 1.5 hours after Wnt stimulation, which was consistent with β-catenin levels approaching a new steady state

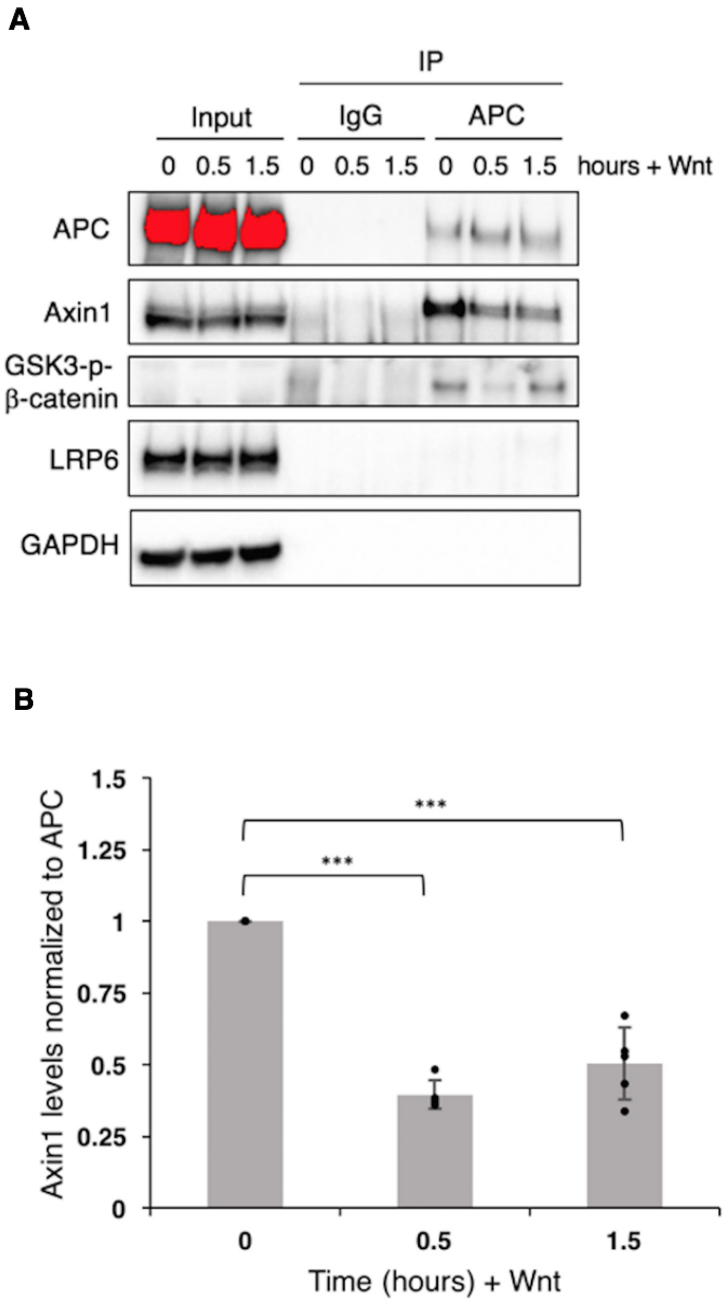

Figure 8 – Axin1 Dissociates from APC upon Wnt Signaling: Figure showing immunoprecipitation of APC. (A) Immunoblotting for key destruction complex components co-immunoprecipitating with APC. Input lanes represent whole-cell lysates of cells; IgG and APC lanes represent lysates immunoprecipitated with control Rabbit IgG antibody and anti-APC IgG antibody respectively. (B) Bar graph quantifying the decrease in Axin1-APC interaction. Bar represent the mean (± 1 s.d.) of five independent experimental repeats (n=5). ***p<0.05 from performing one-way (single-factor) ANOVA and post-hoc pairwise Tukey's HSD test.

from our previous observations (Fig. 8A; middle). Li et al.'s co-immunoprecipitation studies with Axin1 conclusively showed that Axin1's interactions with some of the other destruction complex components remained intact upon Wnt signaling. Taken together, these observations indicated that a decrease in Axin1-APC interaction, and thus a partial disassembly of destruction complexes upon Wnt stimulation results in an initial decrease in the rate of GSK3 phosphorylation and an inhibition of degradation of β-catenin.

Collectively, we see that a fraction of the destruction complexes relocates to the membrane while the remaining destruction complexes remain in the cytosol. The membrane translocation of destruction complexes is correlated with their partial disassembly and the inhibition of their activity leading to the inhibition of β-catenin degradation. The cytosolic destruction complexes remain structurally intact and active. The decrease in the levels of active destruction complexes results in an increase in the intracellular concentration of β-catenin due to an initial decrease in the rate of β-catenin degradation. The accumulating cytosolic β-catenin then causes an increase in the rate of β-catenin phosphorylation by the active destruction complexes via the principal of "mass action" which continues until the rate of degradation once again equals its rate of synthesis. This restores the β-catenin flux through the destruction complexes to its original value, thus leading to the observed new steady-state following Wnt stimulation (Mukherjee et al. 2018).

2.3.3 Kinetic modeling of β-catenin modifications in canonical Wnt signaling

We proceeded to kinetically model the dynamics of intracellular β-catenin modifications to further validate our hypothesis. In the schematic depicted in Fig. 9A, B_0,

B_1, B_2, and B_3 represent unphosphorylated β-catenin, CK1α-phosphorylated β-catenin, GSK3-phosphorylated β-catenin, and ubiquitinated β-catenin respectively (Hernandez et al. 2012).

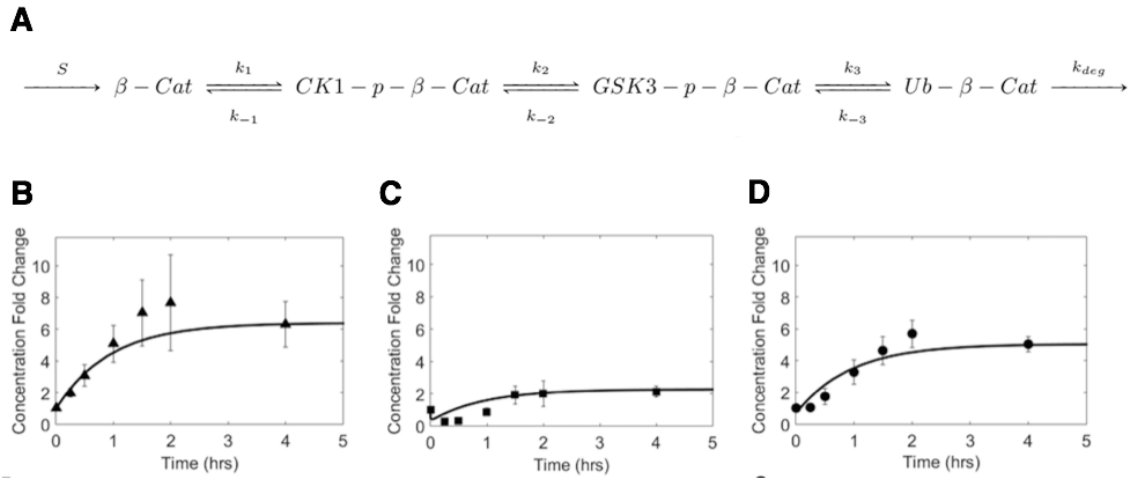

Figure 9 – Kinetic Modeling of β-catenin Dynamics: (A) Schematic showing sequence of reversible kinetic reaction equations used to model cytosolic β-catenin modifications. Graphs showing simulated curves for best fits of (B) total β-catenin (C) GSK3-p-β-catenin and (D) CK1-p-β-catenin upon decreasing k_1, k_2 and k_3 by 56%. Experimental data points are shown in respective figures for comparison.

S represents the rate of synthesis of β-catenin

$[B_i]$ denote the concentrations of the post-translationally modified β-catenin for i = 1, 2, 3

k_{deg} denotes the rate of proteasomal degradation, and

k_j denote the forward and reverse rate constants depicting phosphorylation, dephosphorylation, ubiquitination and deubiquitination, for j = ±1, ±2, ±3.

Based on the above notations, the equations governing the kinetics of phosphorylation and degradation of β-catenin can be written as (Hernandez et al. 2012):

$$\frac{d[B_0]}{dt} = S - k_1[B_0] + k_{-1}[B_1] \quad (3)$$

$$\frac{d[B_1]}{dt} = k_1[B_0] - (k_2 + k_{-1})[B_1] + k_{-2}[B_2] \quad (4)$$

$$\frac{d[B_2]}{dt} = k_2[B_1] - (k_3 + k_{-2})[B_2] + k_{-3}[B_3] \quad (5)$$

$$\frac{d[B_3]}{dt} = k_3 B_2 - (k_{deg} + k_{-3})[B_3] \quad (6)$$

In the above equations, the rate of phosphorylation by CK1, GSK3 and β-TrCP E3 ligases were assumed to be governed by the Michaelis-Menten kinetics for low substrate concentrations relative to the Michaelis constant (K_{M1});

$$k_1 = (k_{cat1}/K_{M1})[DC] \quad (7)$$

where k_{cat1} is the intrinsic catalytic rate of CK1 in the destruction complex,

[DC] is the destruction complex concentration.

First, we applied the above model to our results to predict whether the destruction complex activity was

a. "processive" i.e. β-catenin undergoes a series of phosphorylations within the destruction complex before being released from it, or
b. "distributive" i.e. β-catenin can dissociate from the complex in between sequential steps.

The generally accepted view, as suggested in Hernandez et al., is that the destruction complex activity is "processive" (Hernandez et al. 2012). However, our results were inconsistent with this assertion.

Based on Equation (1) and (2) in Page 21-22, we can say that

$$S = k_{deg}[B_3]_{t=0\ hours} \quad (8)$$

$$S = k_{deg}[B_3]_{t=2\ hours} \quad (9)$$

and S remains unchanged.

Hence, combining (8) and (9)

$$k_{deg}[B_3]_{t=0\ hours} = k_{deg}[B_3]_{t=2\ hours} \quad (10)$$

Since, proteasomal degradation remains unchanged due to canonical Wnt signaling,

k_{deg} remains unchanged over time.

So, $[B_3]_{t=0\ hours} = [B_3]_{t=2\ hours}$ (11)

In other words, the concentration of ubiquitinated β-catenin is the same at both the steady-states, regardless of whether the destruction complex is processive or distributive.

Next, we see that at the steady-states t = 0 hours and t = 2 hours, LHS of equation (6) is equal to zero, which can be written as,

$$0 = k_3[B_2]_{t=0} - (k_{deg} + k_{-3})[B_3]_{t=0} \quad (12)$$

$$0 = k_3[B_2]_{t=2} - (k_{deg} + k_{-3})[B_3]_{t=2} \quad (13)$$

Combining (11), (12) and (13), seeing that k_{deg} and k_{-3} are constant, we deduce that,

$$k_3[B_2]_{t=0} = k_3[B_2]_{t=2} \quad (14)$$

At this step, let's assume that the destruction complex is "processive". That suggests that ubiquitination can only happen inside the destruction complex. Since β-TrCP E3 ligase can be assumed to be governed by the Michelis-Menten kinetics,

$k_3 = k_{cat3}$ at both t = 0 hours and t = 2 hours steady-states (15)

Equation (14) and (15) thus asserts that, $[B_2]_{t=0} = [B_2]_{t=2}$ (16)

i.e., the concentration of GSK3-phosphorylated β-catenin must be the same at both the steady-states which is not consistent with our observations in Fig. 4C and Fig. 5A .

If we follow a similar methodology, we can deduce that in the "processive" case, the concentration of CK1-phosphorylated and GSK3-phosphorylated-β-catenin must return to their initial steady-state value at 2 hours after Wnt-3a stimulation, which is completely contradictory to what we observed in our experiments. Hence, our model infers that β-catenin's interaction with the destruction complex is "distributive" (Mukherjee et al. 2018).

In our proposed "distributive" model, the decrease in the number of active destruction complexes due to the canonical Wnt signal causes a decrease in magnitudes of the rate constants for phosphorylation and ubiquitination i.e. in k_1, k_2, and k_3 (Equation 7). We argued that the percentage of "deactivated" destruction complexes due to membrane relocation was the same as the percentage decrease in Axin1-APC interaction (Fig. 8B).

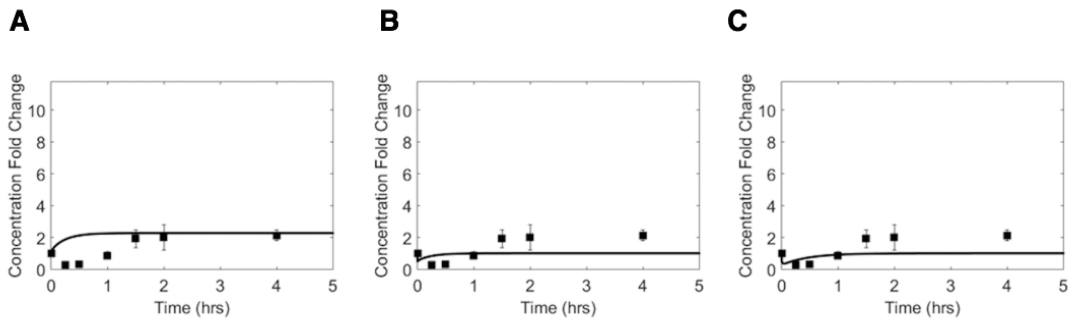

Figure 10 – Inhibiting Different Steps in Kinetic Model of β-catenin Dynamics: Graphs showing simulated GSK3-p-β-catenin curves obtained upon (A) decreasing ubiquitination (k_3) only, (B) GSK3-phosphorylation (k_2) only, or (C) CK1-phosphorylation and GSK3-phosphorylation only (k_1 and k_2) (all by 56%). Experimental data points are shown in each graph for comparison.

Logically, it followed that the fraction of active destruction complexes, with intact Axin1-APC interaction, was 0.44 times the initial destruction complex concentration (Fig. 8B). When we decreased the value of the rate constants k_1, k_2, and k_3 to 0.44 times their value before Wnt addition, the β-catenin concentrations obtained by numerical integration of the equations (3) – (6) closely matched the experimental results (Fig. 9B-D).

In contrast, if only ubiquitination was inhibited (as proposed by Li et al.), the kinetic model simulations did not show a dip in the concentration of GSK-p-β-catenin (Fig. 10A). If only phosphorylation was inhibited, but not ubiquitination (as proposed by Hernandez et al.), then the GSK3-p-β-catenin level at the new steady state recovered to its initial value, but didn't exceed it, which contradicted our experimental results (Fig. 10B and Fig. 10C). The above scenario suggested that all three β-catenin post-translational modification steps (both phosphorylation and the ubiquitination) are partially inhibited. To confirm that ubiquitination is indeed inhibited, we treated the cells with MG132 to promote a build-up of the usually short-lived ubiquitinated β-catenin. Upon Wnt-3a stimulation, we clearly

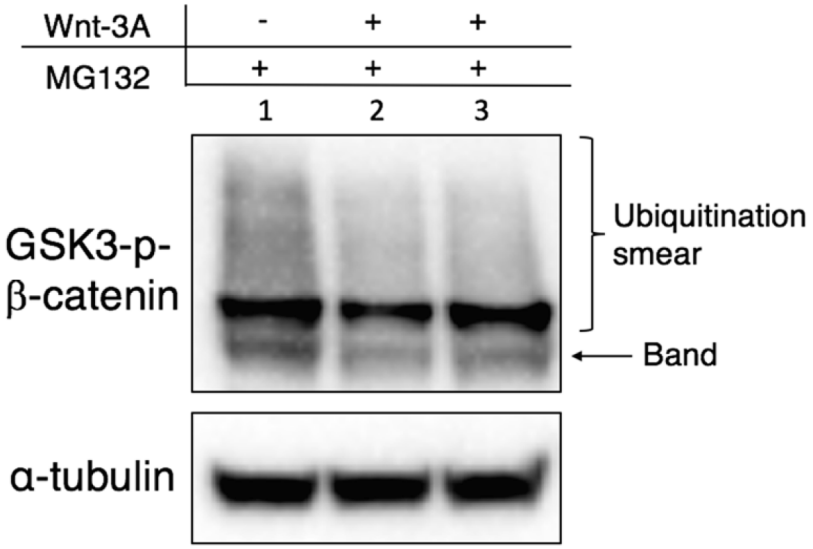

Figure 11 – Monitoring Ubiquitination of GSK3-p-β-catenin: Immunoblots showing lysates probed with anti-GSK3-p-β-catenin and anti-α-tubulin antibody (internal control) respectively. The ubiquitination of β-catenin is reflected in the intensity of the smear in Lanes 1, 2 and 3 above the indicated GSK3-p-β-catenin band. Lane 1 and Lane 3 have equal loading of GSK3-p-β-catenin.

observed a significant decrease in the concentration of ubiquitinated β-catenin that showed up as a smear in the GSK3-p-β-catenin immunoblots (Fig. 11).

In summation,

1. The canonical Wnt signal results in 56% of the destruction complexes relocating to the plasma membrane, where they associate with the Fzd-LRP6 heterodimeric complex.
2. This relocation leads to the partial disassembly of the destruction complex due to the dissociation of APC from Axin1, which inhibits the CK1 and GSK3 phosphorylation of β-catenin.
3. The remaining 44% of the destruction complexes remain structurally intact and

efficiently degrade β-catenin in the cytoplasm. However, the overall decrease in the level of active destruction complexes initially decreases the rate of degradation of β-catenin.

4. Consequently, free β-catenin accumulates in the cytosol, until "mass action" drives a recovery of the rate of degradation of β-catenin at an elevated steady-state level of β-catenin (at 2 hours after Wnt stimulation) by restoring the degradation flux through the active destruction complexes. (Fig. 12)

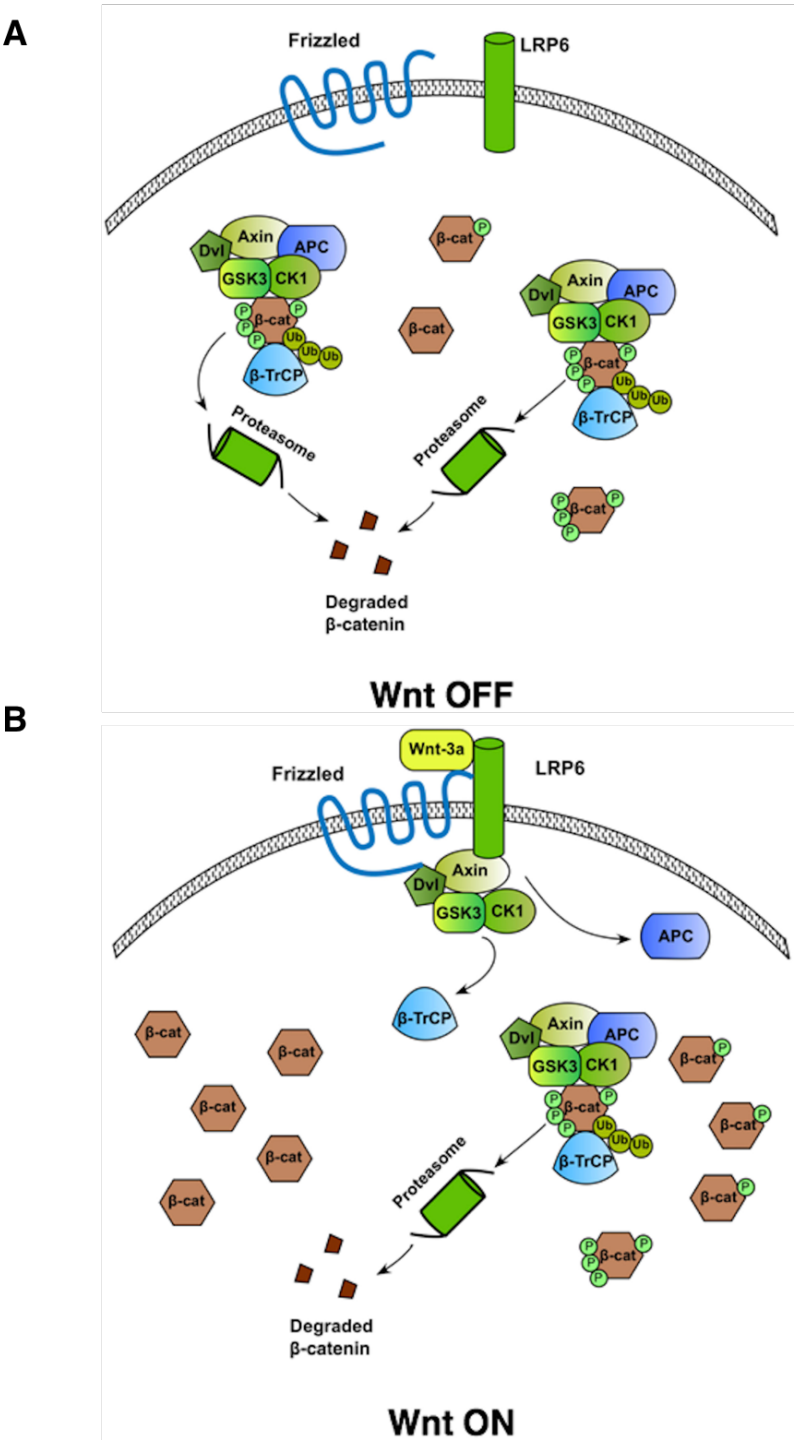

Figure 12 – Schematic Showing Proposed Model of Canonical Wnt Signaling: In (A) Wnt OFF cells, destruction complexes in the cytosol remain active and efficiently degrade cytosolic β-catenin. In (B) Wnt ON cells, a fraction of the destruction complexes relocates to the plasma membrane leading to their partial disassembly, thus inhibiting their ability to degrade β-catenin.

2.4 Discussions

2.4.1 Improving the quality of fit of theoretical model to experimental observations

We have presented a combined experimental and computational model to describe the transduction of the canonical Wnt signal through the cytosol. However, there is scope to further improve the theoretical fit of our kinetic model to our experimental observations. One aspect would involve taking into account the diffusion of the Wnt ligand through the extracellular medium. In culture, the Wnt ligand binds to different cells at different times, which leads to a heterogeneity among the cell populations regarding the initiation of assembly of the Fzd-LRP6 complexes. It is also possible that assuming Michaelis-Menten kinetics at low substrate concentrations may be too simplistic to yield a highly accurate fit. One could explore implementing other kinetic equations to simulate the enzymatic reactions described in the model and investigating the subsequent effects.

2.4.2 Generalizing our model to other cell types and culture conditions

As shown by Tan et al. (Tan et al. 2013), the expression levels of the crucial protein components of the Wnt pathway vary quite significantly among cell lines. This variation can have implications on all aspects of the Wnt pathway described above, including the nature of β-catenin and destruction complex interaction at different post-translational modification steps as well as the extent of inhibition of β-catenin degradation. To that end, our approach can be easily translated to different cell types to systematically investigate each of these phenomena and monitor the variations of Wnt transduction cascade across cell lines. To do so, one can start by confirming that the temporal trends of different post-translationally modified β-catenin species remain unchanged in different cell types. Next,

one can set up a series of end-point experiments to compare the levels of different β-catenin species at the two steady-states described above. The normalized concentration values can be evaluated using the kinetic model to derive conclusions about the nature of the rate-limiting steps and the underlying biophysical phenomena of the canonical Wnt signaling cascade.

Such a comparative study can also be extended to different culture conditions. For example, hypoxia has been hypothesized to be a key microenvironmental factor capable of influencing the proliferation and differentiation of stem cells *in vivo* (Abdollahi et al. 2011; Hawkins et al. 2013). Hypoxia has been shown to influence canonical Wnt signaling in several different cell types including stem cells and cancer cells (Xu et al. 2017). However, there have been multiple conflicting reports regarding the exact nature of such an influence (Verras et al. 2008; Varella-Nallar et al. 2014). Monitoring the intracellular concentrations of key Wnt proteins under different starting culture conditions using our approach may help characterize how various microenvironmental factors modulate the canonical Wnt signaling pathway which can be potentially impactful *in vivo*.

CHAPTER 3. SYNTHETIC MULTIVALENT AGONISTS FOR CANONICAL WNT SIGNALING ACTIVATION

3.1 Background

Our understanding of the role of canonical Wnt signaling in development and disease is ever increasing. While 19 mammalian Wnt genes have been discovered till date, the study of their respective protein products has moved at a painstakingly slow pace (Willert and Nusse 2012). Very little was known about the structure of Wnt proteins until Janda et al. published the crystal structure of the *Xenopus* Wnt8 bound to the cysteine-rich domain (CRD) of the mouse Frizzled8 (Fzd8) receptor (Willert and Nusse 2012; Janda et al. 2012). Moreover, there is significant cross-reactivity between the different Wnt proteins and the 10 different Frizzled (Fzd) surface receptors. This cross-reactivity has further hindered the discovery and attribution of specific biological functions to the different Fzd-Wnt interactions (Clevers and Nusse 2012).

The major roadblock in investigating the role of Wnt proteins in key bioprocesses and their downstream interactions with receptor proteins, is the immense difficulty associated with the purification of these Wnt proteins, which is primarily due to the myriad post-translational modifications that a Wnt protein must go through for its efficient secretion and activity (Willert and Nusse 2012). As a case study, we note that Wnt-3a contains two N-linked glycosylation sites and one palmitoylation site among its amino acid residues. Mutations in the glycosylation sites impair the secretion of the Wnt-3a protein from mammalian cells, suggesting that glycosylation is essential for the proper folding

and/or the subsequent secretion of this protein (Komekado et al. 2007; Kurayoshi et al. 2007). However, multiple Wnt proteins have been shown to be active even in the absence of glycosylation (Mason et al. 1992).

In contrast, acylation has been shown to be critical for Wnt activity. The crystal structure of Wnt8 bound to Fzd8 reported in 2012 showed that the palmitoleic acid lipid group at the conserved Ser187 residue in Wnt8 (Ser209 for Wnt-3a) projects into a deep groove in the CRD of Fzd8, thus underlining the importance of lipidation for maintaining the ability of Wnt proteins to bind to the Fzd receptors (Janda et al. 2012). Indeed, mutation of this serine residue results in impaired secretion and a complete loss of activity of the Wnt proteins (Takada et al. 2006; Komekado et al. 2007).

These necessary post-translational modifications, in turn, make the Wnt proteins highly hydrophobic and water insoluble. Thus, the purification of these proteins requires extensive use of detergents in the workflow. These properties also limit the use of Wnt as potential therapeutic agents and hinder the study of the molecular mechanisms underlying Wnt signaling (Willert and Nusse 2012; Janda et al. 2017). So, water-soluble surrogate molecules which mimic the functions of these Wnt proteins could be of immense importance in advancing our understanding of Wnt-driven processes.

In 2017, Janda et al. reported the first molecules of this kind. They designed water-soluble Fzd-LRP5/6 heterodimerizers which elicited a signature β-catenin response, much like the canonical Wnt-3a molecule (Janda et al. 2017). In this thesis, we independently developed synthetic heterodimers which bound specifically to the Wnt receptors while being orthogonal to all other cellular receptors. These heterodimers activated the canonical

Wnt signaling cascade and closely mimicked the endogenous signaling dynamics. We also demonstrated that the covalent chemistry used in the process is amenable to the "one-pot synthesis" of these heterodimers. Additionally, we also outlined a strategy to increase the potency of these synthetic agonists, which will promote its scalability and decrease the overall cost of production of these molecules, thus potentially aiding their applications in multiple Wnt-driven bioprocessing workflows.

3.2 Material and Methods

Plasmids

a. The 7x TFP Wnt luciferase reporter (Fuerer and Nusse 2010) was constructed with a pVitro2-MCS vector with a hygromycin resistance for bacterial transformation. In the first cloning site (MCS-1), the ferritin promoter was removed and replaced with a minimal promoter (minP) and the firefly luciferase nucleotide sequence was inserted downstream of minP. The CMV enhancer sequence was deleted and 7 β-catenin binding TCF enhancer sites were inserted upstream of the minP to make the reporter responsive to an increase in β-catenin concentration in the nucleus. The minP and the 7x TCF binding site sequences were custom-synthesized and inserted into the pVitro2-MCS vector by Gene Universal.
b. The Frizzled Fab (Fzd-Fab) and LRP6 Fabs (LRP6-Fab) (clones 6475 and 8168) were engineered from Frizzled antibody and LRP6 antibody sequences obtained from Gurney and Jenkins et al. respectively. The expression plasmids were constructed by inserting the respective Fab light chain and heavy chain sequences into a TGEX vector obtained from Antibody Design Labs. The TGEX vectors code

for the constant region of the human IgG heavy chain CH1 region with a C-term 6x His tag and the human kappa light chain CH1 region. The sequence for a SpyTag was inserted into the C-terminus of the heavy chain of the Fzd-Fab. The SpyCatcher sequence was inserted into the C-terminus of the LRP6 following 3x(GGGGS) linkers. All plasmids were custom-synthesized and cloned into the TGEX vector by Gene Universal.

Transfection of 293F Cells for Obtaining Secreted Proteins

45 mL 293F (Thermo Scientific) mammalian cell cultures were grown up to a density of $2.9x10^6$ cells per mL in a 125-mL Erlenmeyer flask. Cultures for Fab expression were transfected with the heavy-chain and light-chain coding plasmids in a 1:2 w/w ratio. This plasmid ratio ensured that the 6xHis-Tag containing heavy chains were present in excess and were consumed in the Fab recombination as the limiting component. Transfection was performed using the ExpiFectamine (Thermo Scientific) transfection reagent according to the manufacturer's recommendation. Recommended doses of transfection enhancers were added to the culture 20-24 hours after initial addition of transfection reagents. Post transfection, cells were incubated for 6 days and the Expi293F (Thermo Scientific) supernantant media harvested afterward to proceed in the workflow.

ELISA to Validate Binding of Ligands to Antigens

0.1 μg of commercial LRP6 ectodomain fused to a human IgG Fc region (LRP6-Fc) and Frizzled 2 (Fzd2) CRD fused to a human IgG Fc region (Fzd-Fc) were diluted in 100 μL of carbonate buffer (pH 9.6). The above antigens were used to coat a Maxisorp 96-well plate (Thermo Scientific) overnight at 4°C. After this step, each well was blocked using

5% BSA solution in TBST (TBS containing 0.05% Tween-20) for 1 hour at room temperature. The blocked wells were then incubated with the respective primary antibodies/Fabs and then by the respective secondary anti-human/anti-His antibodies (Jackson Immunoresearch; Thermo Scientific) diluted in 5% BSA solution in TBST at a concentration recommended by the manufacturer. All wells were washed thoroughly with 200 μL of TBST in between incubation steps. Finally, the wells were incubated with 100 μL TMB (Thermo Scientific) solution for 15 minutes followed by the addition of 100 μL Stop solution. Next, the plate was imaged at 450-nm using the BioTek Synergy plate reader in the Biopolymer Characterization Core in EBB.

Purifying Fzd Fab-LRP6 Fab Heterodimers

The supernatant containing unreacted Fzd Fab, LRP6 Fab and the Fzd Fab-LRP6 Fab heterodimers was first purified using the IMAC protocol using Ni-NTA (Thermo Scientific) agarose beads/resin in 30 mL columns. The Ni-NTA beads specifically bound to the 6xHis Tag on these proteins. Each Ni-NTA column was first equilibrated with 20 column volumes of equilibration (50 mM Phosphate, 500 mM NaCl, 25 mM imidazole, pH 8.0). The supernatant was then passed through the column and the flow through discarded. The column was then washed using 50 mM imidazole buffer (pH 8.0) once to get rid of non-specific protein binding in the beads/resin and the flow through was collected. The protein of interest was then eluted with ~400 mM imidazole (pH 8.0) buffer in 2 mL fractions and all the fractions were collected.

The eluted proteins were then concentrated down to ~1 mL by centrifuging at 7000g in Amicon 10kDa MWCO 15 mL spin filters (EMD Millipore). The 1 mL eluate was then

purified in a HiLoad Superdex 200 column loaded on an AKTA Pure chromatography system (GE Healthcare) using the principles of size-exclusion chromatography. All fractions were collected in PBS buffer using the fraction collector. The fractions corresponding to the peaks in A280 (absorbance at 280 nm) and A205 (absorbance at 205 nm) curves were run on an SDS-PAGE gel and analyzed for purity using Coomassie Brilliant Blue Staining or Silver Staining. All fractions with satisfactory purity (>80%) of dimers (showing up at ~110 kDa) were pooled and concentrated again in an Amicon 10kDa MWCO 15 mL spin filter. The purified proteins were then aliquoted and stored. For short-term use, purified heterodimers were stored in PBS containing >40% glycerol at -20°C. For long-term storage, purified fractions were frozen in -80°C in PBS containing >40% glycerol.

Luciferase Assay to Verify Activation of Canonical Wnt Signaling

293T cells were plated on a 6-well plate coated with poly-L-lysine and grown up to ~80% confluency. The cells were then transfected with the 7x TFP reporter plasmid, trypsinized 24 hours after transfection (0.25% Trypsin-EDTA, Thermo Scientific), re-plated in a 96-well plate (Corning) coated with poly-L-lysine (Sigma-Aldrich). Transfected cells were then treated with different concentrations of heterodimers and Wnt-3a diluted in D-10 media. The final concentrations of treatment ranged from 5 nM to 25 nM at 5 nM intervals. Each treatment was done in triplicates. After 24 hours of treatment, cells were lysed in a passive lysis buffer (Promega) and centrifuged in the 96-well plate (Corning) at 2000g for 10 minutes to remove debris from the cell lysate. The cleared cell lysates were then transferred to an opaque white-walled 96-well plate (Corning). Luminescence signal was

then measured from each well in a BioTek Synergy plate reader immediately following the addition of the Luciferase Assay Reagent (Promega).

3.3 Results

3.3.1 Expressing Frizzled-binding and LRP6-binding Fabs

To begin, we wanted to verify whether we could obtain Fabs that are capable of potently binding to Frizzled and LRP6 proteins. Full-length sequences of Frizzled- and LRP6-binding antibodies were obtained from Gurney and Jenkins et al. respectively (Jenkins et al. 2014; Gurney 2016). For the expression of each Fab, two separate plasmids were designed, one coding for the heavy chain and the other coding for the light chain. In both cases, the sequences corresponding to the variable regions obtained from the patents were inserted into TGEX-FH and TGEX-LC vectors for expressing the heavy and light chains respectively. TGEX-FH also encodes a 6xHis tag at the C-terminus of the CH1 region. The Fabs were then expressed using the 293F mammalian protein expression system by co-transfecting the plasmids encoding for both the heavy and light chains in a 1:2 w/w ratio in 30-45 mL cell cultures. The light chain plasmid was always transfected in excess to ensure that the heavy chain was effectively the "limiting" reactant in the heavy and light chain combination process to form the Fab. Upon expression and combination, the Fabs were purified using the principles of affinity chromatography in a Ni-NTA column. Since the heavy chain encoded for a 6xHis tag and was the limiting reactant, we got highly pure Fabs from this round of Ni-NTA purification. Next, we further purified the individual Fabs using size-exclusion chromatography by passing them through a HiLoad Superdex 200 column to obtain highly pure fractions. These fractions were analysed on a

4-12% Bis-Tris Gel using SDS-PAGE Gel electrophoresis via Coomassie Brilliant Blue staining. Only the highly pure fractions were pooled, concentrated, and separately run on another gel to check for purity. We proceeded with the purified Fabs only when the purity was ~90% or above (Fig. 13).

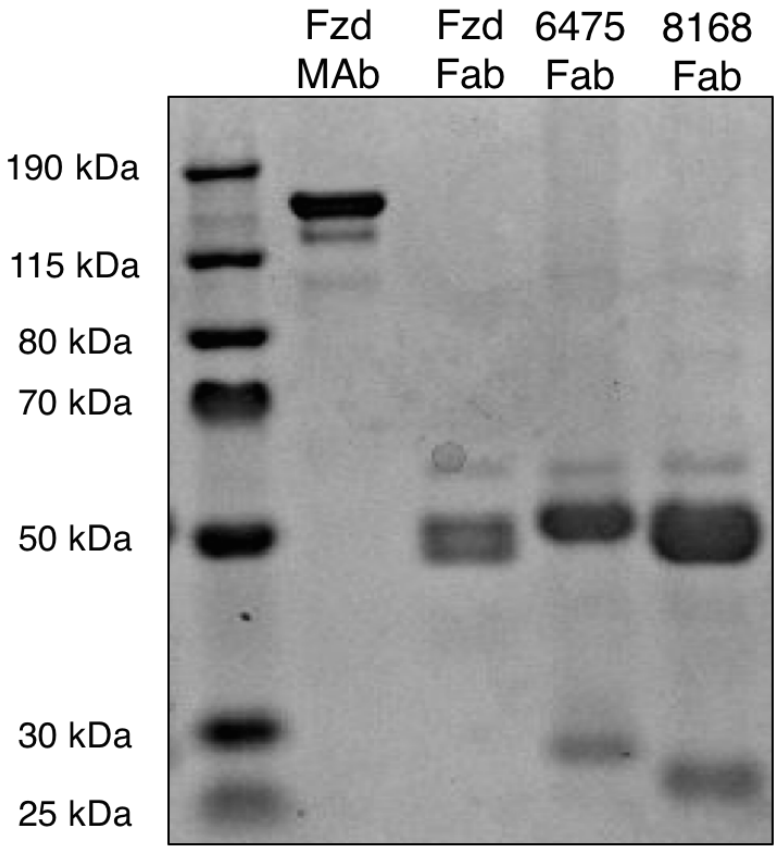

Figure 13 – Coomassie Blue Staining for Frizzled and LRP6 Ligands: Frizzled (Fzd) ligands (Fzd MAb and Fzd Fab) and LRP6 ligands (6475 Fab and 8168 Fab) imaged after SDS-Gel Electrophoresis on a 4-12% Bis-Tris Gel and subsequent Coomassie Brilliant Blue staining. The left-most lane represents the PageRuler Plus Protein Ladder.

To test whether the purified Fabs were functional, we performed an ELISA to quantify the binding of the Fabs to their respective antigens. We coated 96-well plates with pure recombinant Frizzled and LRP6 proteins with a fused human IgG Fc region diluted in

carbonate buffer (pH 9.6). The Frizzled-binding Fab (Fzd-Fab) and two separate clones (clone# 6475 and 8168) of LRP6-binding Fabs (LRP6-Fab) were found to bind robustly to their corresponding antigens (Fig. 14A). To further quantify the *in vitro* activity of the

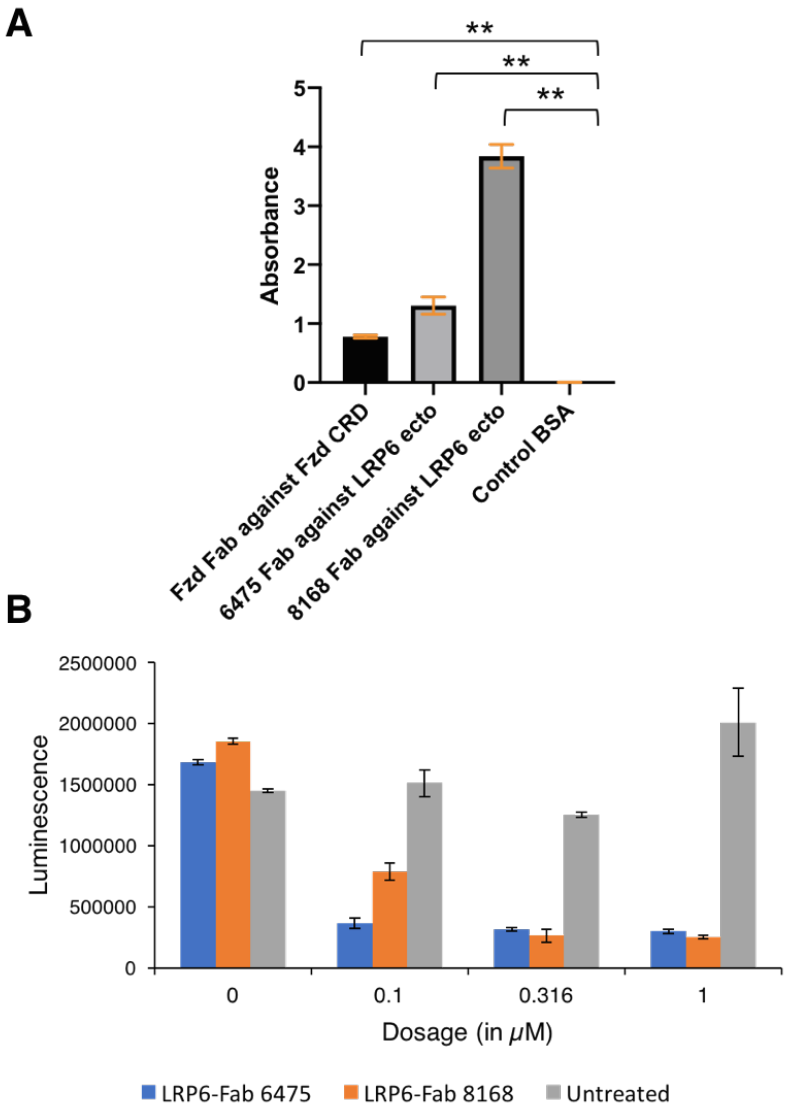

Figure 14 – Characterizing the Frizzled (Fzd-Fab) and LRP6 (LRP6-Fab-6475 and LRP6-Fab-8168) ligands: (A) ELISA showing binding of Fzd-Fab and LRP6-Fabs (6475 and 8168) to their respective antigens; Frizzled cysteine-rich domain (Fzd CRD) and LRP6 ectodomain (LRP6 ecto) respectively, both fused to a human IgG-Fc region. **p<0.05 from performing one-way (single-factor) ANOVA and post-hoc pairwise Tukey's HSD test (n=3 replicates). (B) Luciferase assay showing LRP6 Fabs blocking Wnt signal transduction in presence of Wnt-3a at different doses of Fabs.

LRP6-Fabs, we attempted to block Wnt signaling by treating 7TFP reporter-transfected 293T cells with LRP6-Fabs. We observed that both clones of LRP6-Fabs blocked Wnt signal transduction and the extents of inhibition were proportional to the dose of LRP6-Fab used in the treatment (Fig. 14B).

3.3.2 Strategy to generate anti-Fzd-LRP6 heterodimers via SpyTag-SpyCatcher chemistry

To generate the heterodimer composed of Fzd-Fab and LRP6-Fab monomers, we used the SpyTag-SpyCatcher protein coupling system. The SpyTag and SpyCatcher system was developed by Zakeri et al. by engineering a bacterial adhesin protein (Zakeri et al. 2012). SpyTag is a short peptide which spontaneously forms a covalent isopeptide bond when it encounters its protein partner, SpyCatcher.

In our case, we decided to insert the sequence for the short SpyTag on the heavy chain of the Fzd-Fab (Fzd-Fab-SpyTag) and the SpyCatcher on the light chain of the LRP6-Fabs (clones 6475 and 8168) (LRP6-Fab-SpyCatcher) (Fig. 15A). To ensure proper folding of the SpyCatcher and the LRP6-Fab, we inserted a 3x(GGGGS) flexible linker between the C-terminus of the light chain of the LRP6-Fab and the SpyCatcher sequence (Fig. 15A). To confirm that our engineered Fabs retained their activity, we expressed and purified the individual monomers and performed another ELISA along the lines of the one mentioned in 3.3.1. We found substantial binding for all the fusion proteins (Fig. 15B).

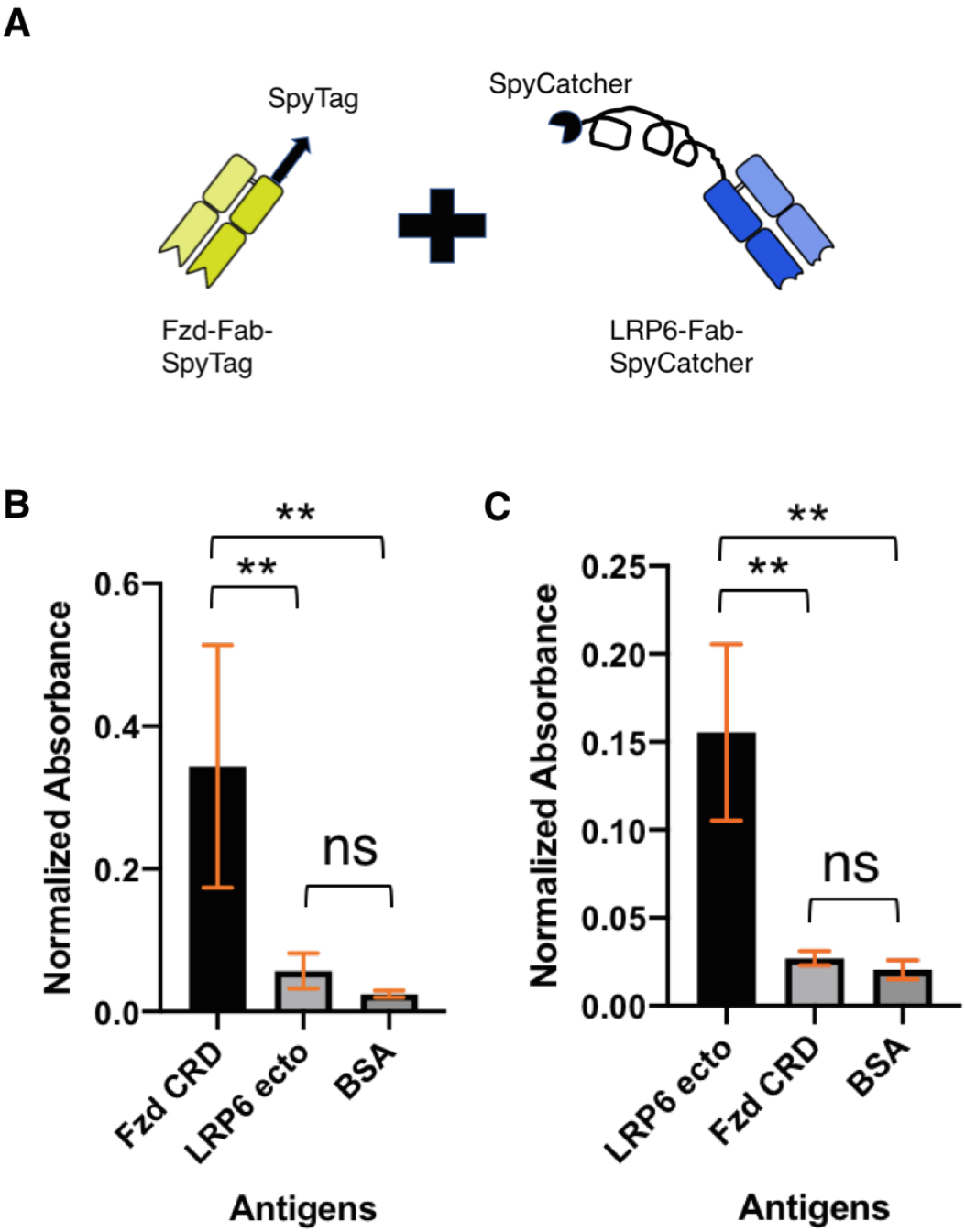

Figure 15 – Validating Activity of Fzd-Fab-SpyTag and LRP6-Fab-SpyCatcher fusion proteins: (A) Schematic showing proposed strategy of anti-Fzd-LRP6 Fab heterodimer formation. ELISA showing the binding of (B) Fzd-Fab-SpyTag and (C) LRP6-Fab-SpyCatcher fusions to their respective antigens. Each data point represents mean (± 1 s.d.) of 10 replicates (n=10). **p<0.05 by performing Kruskal-Wallis nonparametric test and post-hoc pairwise Dunn's multiple comparisons test. ns = not statistically significant.

3.3.3 Generating anti-Fzd-LRP6 heterodimers via "one-pot" reaction

The Fzd-Fab-SpyTag and the LRP6-Fab-SpyCatcher fusion proteins were expressed using the Expi293F protein expression system. Seven days after transfection of the plasmids, the 293F cell cultures were centrifuged and the supernatants analysed for the respective protein levels. The analysis was done by probing the supernatant using a primary mouse anti-6xHis-tag antibody in a dot-blot or a western blot. The bands were quantified and the Fzd-Fab-SpyTag and LRP6-Fab-SpyCatcher supernatants were mixed in ~1:1 molar stoichiometric ratios. The required volumes of supernatants were mixed in a 125-mL Erlenmeyer flask and incubated with constant shaking at 37°C for 3 hours. Reacting the fusion proteins in the already-optimized 293F medium minimized protein loss due to degradation and the extra incubation step ensured a relatively high conversion of reactants to the heterodimer product (Fig. 16A).

The resulting product-reactant mixture was then dialyzed overnight in PBS at 4°C. The dialyzed mixture was then affinity-purified on a Ni-NTA column and analysed using SDS-Gel Electrophoresis and Coomassie Brilliant Blue staining. As expected, the reaction mixture showed three prominent protein bands on the Bis-Tris gel, corresponding to the heterodimer product (~110 kDa band of the PageRuler Plus Protein ladder), the unreacted LRP6-Fab-SpyCatcher (~60 kDa) and the unreacted Fzd-Fab-SpyTag (~50 kDa). Next, we further purified the Ni-NTA elution using size-exclusion chromatography (SEC) to separate the ~110 kDa desired heterodimer from the smaller unreacted fusion proteins. The dilute fractions obtained from SEC were analysed again via SDS-PAGE Gel Electrophoresis and Coomassie Blue staining.

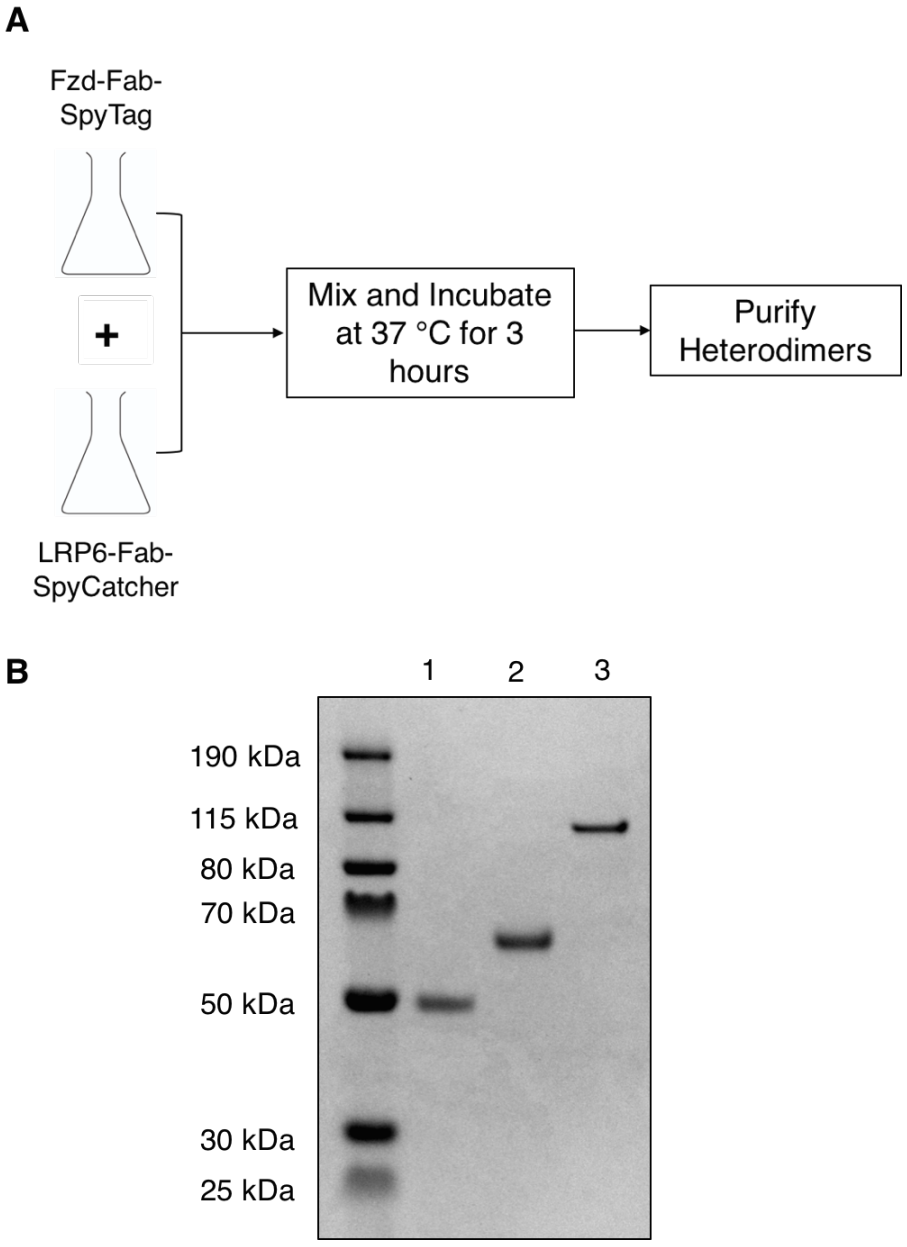

Figure 16 – Generating anti-Fzd-LRP6-Fab Heterodimers from Individual Monomers: (A) Schematic showing proposed "one-pot" strategy of generating anti-Fzd-LRP6-Fab heterodimers without intermediate purification. (B) Gel Image showing the formation of pure heterodimer 8168 (Lane 3) from the Fzd-Fab-SpyTag (Lane 1) and LRP6-Fab-Spycatcher (Lane 2) fusions.

The highly pure fractions, mostly devoid of any unreacted LRP6-Fab-SpyCatcher, Fzd-Fab-SpyTag and partially degraded heterodimers, were pooled, concentrated using a centrifuge filter, and quantified using either a BCA or a microBCA assay. Hereon, we refer

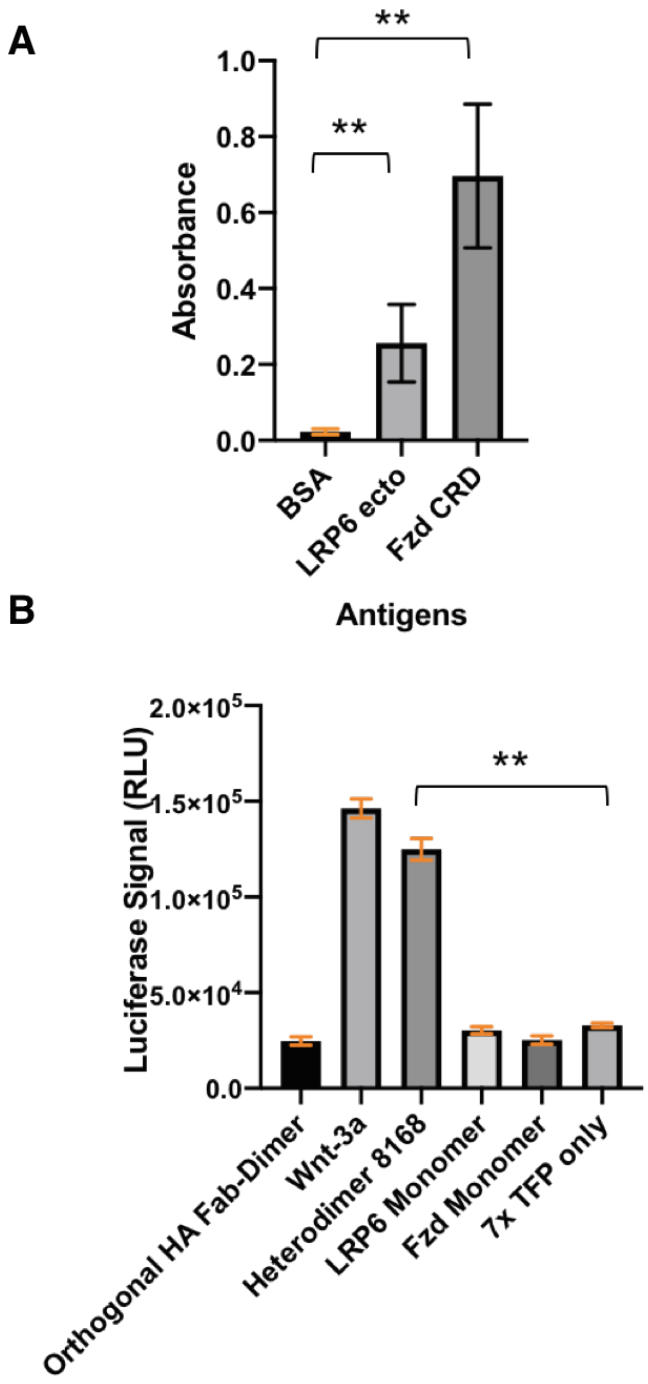

Figure 17 – Characterizing Activity of Heterodimer 8168: A) ELISA showing the avidity of Heterodimer 8168 towards both Frizzled and LRP6. Each data point represents the mean (± 1 s.d.) of 10 replicates (n=10). **p<0.05 by Kruskal-Wallis nonparametric test and post-hoc pairwise Dunn's multiple comparisons test. B) Luciferase assay showing activation of Wnt signaling by Heterodimer 8168. **p<0.05 by one-way (single-factor) ANOVA followed by post-hoc pairwise Tukey's HSD test.

to the individual heterodimers as “heterodimer 6475” or “heterodimer 8168” based on the clone of LRP6-Fab used to synthesize each one (Fig. 16B).

3.3.4 Activation of canonical Wnt signaling by Fzd-LRP6 Fab heterodimers

As a preliminary check, we wanted to test the ability of heterodimer 8168 to bind to both Frizzled and LRP6. As is evident from Figure 17, we observed heterodimer 8168 binding robustly to both Frizzled and LRP6 with comparable avidity (Fig. 17A).

To check activation of canonical Wnt signaling, 7x TFP-luciferase reporter-transfected 293T cells were treated with 15 nM of purified heterodimer 8168. The luciferase signal, which corresponded to the level of canonical Wnt signal transduction from the heterodimer 8168-treated samples, was comparable to that of samples treated with Wnt-3a at a similar concentration, indicating robust activation of canonical Wnt signaling by heterodimer 8168. In contrast, the individual monomers and an orthogonal Fab-dimer did not show any elevation of luciferase signal (Fig. 17B).

To characterize heterodimer 8168 further, we treated the 7x TFP reporter-transfected 293T cells with various doses of Wnt-3a and heterodimer 8168. Based on our preliminary experiments, we observed that heterodimer 8168 was more potent than Wnt-3a at lower doses (i.e. 5 nM and 10 nM) in activating the Wnt signaling pathway (Fig. 18). However, the level of signaling induced by heterodimer 8168 stagnated relative to Wnt-3a at higher concentrations of the ligands (i.e. 15 nM – 25 nM) (Fig. 18). Multiple independent biological repeats of the above experiment are underway to test the statistical significance of the phenomena. Qualitatively, we observed that the potency of heterodimer 8168 was comparable to wild-type Wnt-3a at various doses (Fig. 18).

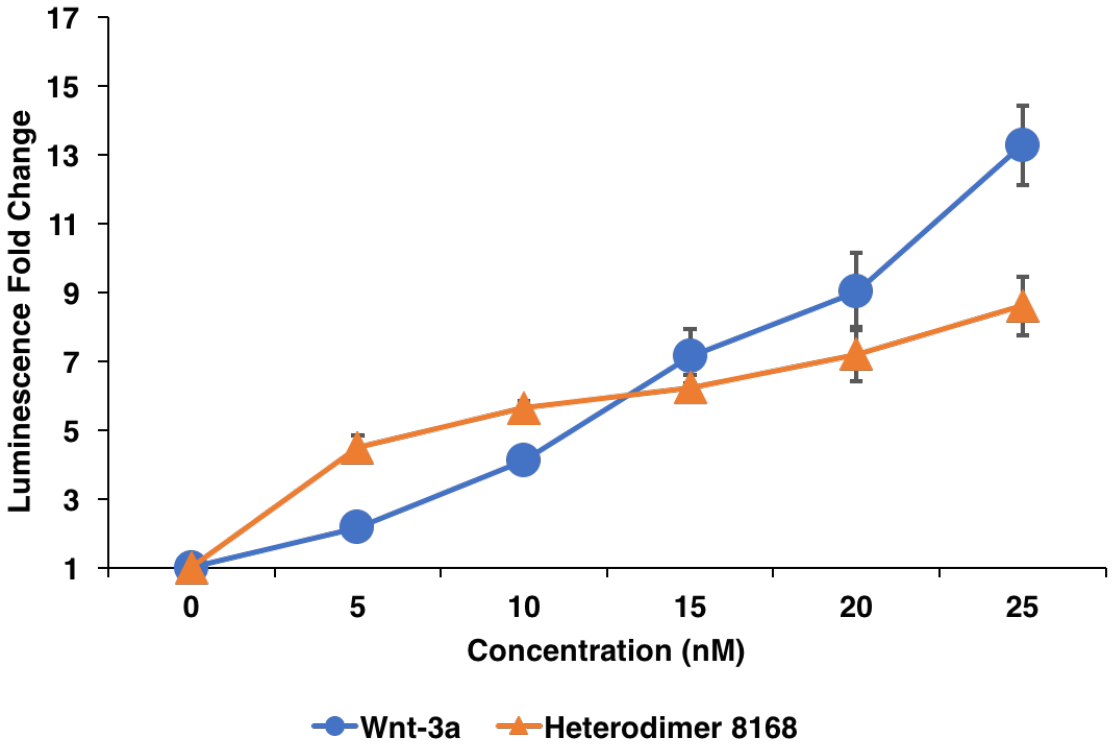

Figure 18 – Preliminary Dose-Dependent Activation of Wnt-responsive 7x TFP Reporter: Both Wnt-3a and heterodimer 8168 robustly activate canonical Wnt signaling at the indicated doses. Each data point represents the mean of three technical replicates (mean ± 1 s.d.).

To conclude,

1. We established a robust protocol to synthesize potent heterodimers capable of binding to Frizzled and LRP6.
2. The protocol is effectively one-pot and can be completed within 48 hours of harvesting cell cultures expressing unreacted monomeric Fab-fusions.
3. Heterodimers generated from this protocol were active and capable of triggering the endogenous canonical Wnt signaling pathway.

3.4 Discussions

3.4.1 Potential advantages of Fab-based heterodimers

The strategy described above to generate Fab-based heterodimers e.g. heterodimer 8168, can potentially have several advantages over the natural and/or single-chain ligand-based surrogate Wnt agonists described in Janda et al. (Janda et al. 2017). Firstly, the workflow to generate highly specific Fabs with relatively low non-specific interactions has been well-established in this industry. Hence, our approach can be translated relatively easily to generate heterodimers that can dimerize or oligomerize other receptor pairs specifically. Finding specific natural ligands to these receptors, with low levels of non-specific side effects, can be a far more daunting prospect. Secondly, tuning the potency of these agonists via multivalency can also be achieved relatively easily in the case of the heterodimers described earlier in this chapter. It is relatively simple to introduce recombinant tags, such as AviTag, to our heterodimers which can subsequently be used to conjugate them to rigid or flexible multivalent scaffolds to increase their potency. Lastly, a natural ligand-based agonist design may not be feasible to activate other signaling pathways that involve receptor heterodimerization. Some such receptors may be "orphan" receptors with no known natural ligand, thus making it difficult to implement the strategy described in Janda et al. In contrast, we can proceed by generating antibodies, and subsequently Fabs, against such orphan receptors to design and develop potent synthetic agonists to activate diverse signaling networks.

3.4.2 Increased potency of heterodimer at low concentrations

There are a number of possible explanations for the observed higher potency of the heterodimer 8168 compared to Wnt-3a at doses between 0 nM – 15 nM. One reason may be that the individual monomers, and hence the heterodimer, bind with a higher affinity (avidity, in case of the dimer) towards Frizzled and LRP6 than wild-type Wnt-3a. Alternatively, this increased potency may be because the LRP6-Fab monomer (clone 8168) binds to the β-propeller domains 1 and 2 (E1E2) of LRP6 in contrast to Wnt-3a, which binds to the β-propeller domains 3 and 4 (E3E4). The different binding sites may result in a change in the extent of receptor oligomerization which may result in the observed difference in the level of Wnt activation. Further investigation is needed to resolve which of the above two scenarios are relevant in this case.

3.4.3 Implications for differential binding kinetics of the heterodimer

As described in Chapter 2, the interaction between the Fzd-LRP6 receptor complex and Axin1 plays a key role in transducing the canonical Wnt pathway. The formation of the Fzd-LRP6 heterodimeric complex is directly related to the binding dynamics of the extracellular Wnt/surrogate Wnt ligand to these membrane receptors. To accurately investigate the influence of such binding dynamics, monitoring the changes in levels of intracellular core Wnt proteins upon heterodimer 8168 treatment will be key. Comparing these levels to the ones observed in case of Wnt-3a may provide more insights regarding the potential advantages and disadvantages of such synthetic Wnt substitutes.

CHAPTER 4. DESIGNING OPTOGENETIC PROTEINS WITH TUNABLE CLUSTERING PROPERTIES

4.1 Background

Visible light is a key mediator of signal transduction pathways in some prokaryotic and eukaryotic cells. In recent times, it has also emerged as a versatile tool to probe and investigate multiple biological phenomena which are generally light-orthogonal (Deisseroth 2011; Fenno et al. 2012; Repina et al. 2017). The field of "Optogenetics" uses genetically encoded light-responsive systems to modulate a variety of processes in living cells, that include, but are not limited to, controlling transcription and translation, triggering signaling pathways, and effecting neuronal responses (Yizhar et al. 2011; Konermann et al. 2013; Cao et al. 2013; Tischer and Weiner 2014; Zhang and Cu 2015). Compared to traditional methods for probing signal transduction processes, such as gene overexpression strategies and using soluble ligands, light offers several key advantages. Firstly, light is largely orthogonal to most endogenous signaling cascades, thus significantly reducing the probability of off-target effects which is one of the key concerns associated with overexpressed proteins and ligands. Secondly, irradiating visible radiation through lasers enables us to obtain high degrees of spatiotemporal control over the stimulation of specific cells. Thirdly, the rapid ON/OFF kinetics and the ease of modulation, which are hallmarks of optogenetic systems, offer us unprecedented capabilities in probing hitherto "un-probable" features of traditional signal transduction cascades (Repina et al. 2017). Keeping this in mind, in collaboration with Sudrik et al. (Sudrik 2014), we attempted to design novel optogenetic tools by engineering a previously reported optogenetic Wnt activation

photoswitch based on our understanding of the canonical Wnt signaling pathway. Several optogenetic systems have been reported in literature in the last decade (Repina et al. 2017), but for our purpose, we chose to focus our efforts on the *A. Thaliana* Cryptochrome2-based dimerizing and clustering photoswitches as they formed the basis of the optogenetic Wnt activator mentioned earlier.

Cryptochrome2-based Dimerizers

Wild-type Cryptochrome2 (Cry2) is a blue-light sensitive homodimer in *Arabidopsis thaliana* which remains localized in the nucleus and acts as a transcriptional effector. The Cry2 protein is bound to the endogenous cofactors flavin adenine dinucleotide (FAD) and 5,10-methanyltetrahydrofolate (MTHF) (Liu et al. 2008). These cofactors act as chromophores which help Cry2 absorb blue light, resulting in its conformational change. This conformational change enables the Cry2 protein to interact with several other regulatory proteins in the nucleus, one of which is the cryptochrome-interacting basic helix-loop-helix protein (CIB1) (Liu et al. 2008; Zuo et al. 2011).

In 2010, Kennedy et al. identified the minimal interacting domains of Cry2 and CIB1 and identified a pair of truncated proteins consisting of the photolyase homology region (PHR) of Cry2 (Cry2PHR) and the N-terminal residues 1-170 for CIB1 (termed CIBN), which retained their dimerizing activity (Kennedy et al. 2010). The authors mutated the nuclear localization signal (NLS) residues from both proteins, resulting in robust cytosolic expression and activity of both Cry2PHR and CIBN. Both Cry2-CIB1 and the Cry2PHR-CIBN dimerizing systems have since been used in several articles for various cell biological applications (Hughes et al. 2012; Wang et al. 2012; Lee et al. 2014). One such application was the light-induced sequestration of target intracellular effectors via a

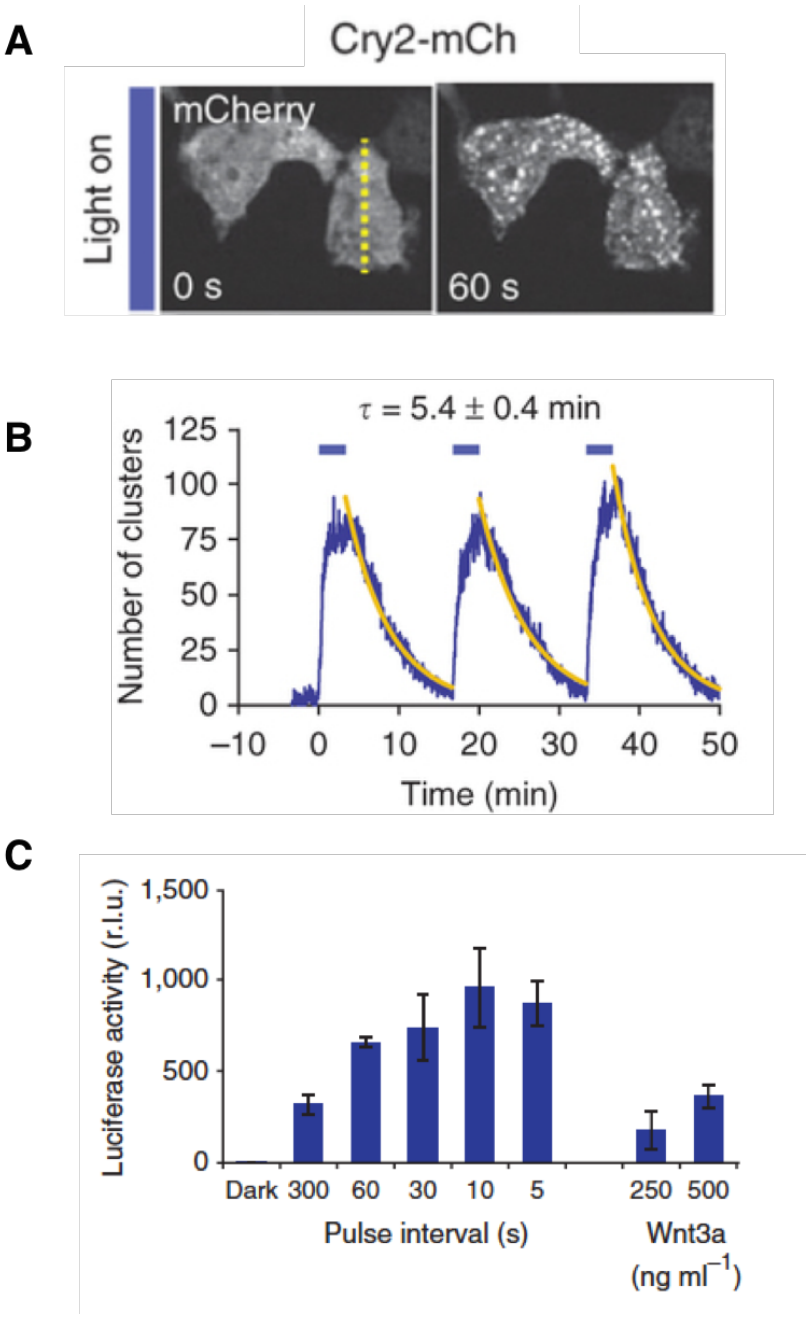

Figure 19 – Clustering of Cry2PHR-mCherry as reported by Bugaj et al. (A) Cry2-mCherry fusions form clusters upon blue light exposure. (B) These clusters have an average characteristic dissociation time ($t_{1/2}$) of ~5.4 minutes. (C) Cry2PHR-mCherry-LRP6c fusions robustly activate Wnt signaling in presence of blue light. Reprinted with permission from Nature Publishing Group (Bugaj et al. 2013).

multimeric protein (MP). In 2014, Lee et al. demonstrated that the fusion of a subunit of a multimeric protein (MP) and CIB1 formed a complex architecture with Cry2-mCherry in

the cytosol (Lee et al. 2014). Upon conjugating antigen-specific single-domain antibodies to Cry2, Lee et al. optically trapped specific proteins and disrupted their activity in the cell.

Cryptochrome2-based Clustering Tools

In 2013, Bugaj et al. reported that Cry2PHR is capable of clustering robustly by itself when exposed to blue light (Fig. 19A-B) (Bugaj et al. 2013). In the same article, they fused the cytosolic domain of the Wnt co-receptor LRP6 (termed LRP6c) to the C-terminus of Cry2PHR and showed that Wnt signaling was robustly activated when the fusion protein Cry2PHR-mCherry-LRP6c underwent clustering upon blue light exposure, as predicted by Cong et al. in 2004 (Fig. 19C) (Cong et al. 2004). They further went on to use the clustering properties of Cry2PHR to activate Rho-GTPases, RhoA and Rac1, thus establishing its utility in triggering diverse signal transduction cascades.

In 2014, Taslimi et al. reported another optogenetic clustering tool termed Cry2olig containing a single E490G mutation in Cry2PHR that dramatically increased the clustering efficiency of the construct previously reported by Bugaj et al. (Taslimi et al. 2014). In contrast to Lee et al., whose method required the additional expression of a separate CIB1-fused multimeric protein, Taslimi et al. perturbed protein activity by just fusing an effector protein to Cry2olig, requiring no other protein partners.

Previously, Sudrik had reported the novel clustering tool CL6m5 which underwent robust clustering when exposed to blue light (Sudrik 2014). In this study, we validated his findings and extended the idea to develop a library of novel clustering tools (called CL6mN) with a range of clustering dissociation half-lives, high clustering efficiencies and large sizes by engineering the Cry2PHR-mCherry-LRP6c fusion protein reported by Bugaj et al. These clustering tools have half-lives intermediate to that reported by Bugaj et al. and

Taslimi et al. and can thus be used to probe protein-protein interactions at several time scales.

4.2 Material and Methods

Plasmids

The CL6mN constructs (N=3,5) were prepared in a pmCherry-N1 vector backbone (Addgene#26866) expressing the Cry2(1-498)-mCherry fusion protein. The LRP6c fragments with the appropriate number of mutated PPPSP motifs were custom-synthesized from GenScript and cloned in between the Bsr GI and Xba I sites in the C-terminus of the pCry2PHR-mCherry insert (Addgene#26866). The Wnt-responsive 7x TFP-luciferase reporter plasmid was constructed as mentioned in section 3.2.

Cell Culture and Transfections

293T cells were cultured in a 4-chamber 35 mm glass-bottomed (1.5) dish (Cellvis) coated with poly-L-lysine using the conditions mentioned in previous chapters. Cells were grown up to ~90% confluency in each chamber (~24 hours after plating) and transfected with the respective CL6mN constructs using the Lipofectamine 2000 transfection reagent following the manufacturer's protocol for 24-well plates.

Confocal Microscopy

CL6mN and Cry2PHR-mCherry transfected cells in the imaging dishes were handled exclusively in the dark or in the presence of a monochromatic red LED strip (Superbright LEDs) to avoid accidental clustering in presence of white/blue light. Cells were washed with imaging media consisting of 90% Fluorobrite DMEM (Thermo Fisher) supplemented

with 10% Fetal Bovine Serum (FBS), 1x Glutamax and 20 mM HEPES buffer. After washing, the cells in each chamber were incubated in 500 μL of above-mentioned imaging media. The imaging dish was then wrapped completely in an aluminum wrap (to prevent accidental clustering) before proceeding to image in the Optical Microscopy Core. The 488-nm (GFP) laser in the Perkin Elmer Spinning Disk Microscope (located in the Optical Microscopy Core at EBB) was used to trigger the clustering of CL6mN and Cry2PHR cells at 10% and 100% intensity with a 1-second exposure per pixel. The clustering and declustering dynamics were observed using the 561-nm (RFP) channel.

Quantifying Number of Clusters in Confocal Microscopy Image

ImageJ version 1.48v was used to analyze all confocal microscopy images. Manual thresholding was applied individually to each image so that only the clusters were visible. The "Analyze Particles" feature of ImageJ was then used to count the number of clusters in each image. The calculated number of clusters were plotted against the respective time-points in GraphPad Prism or MS Excel to obtain the clustering and declustering curves.

4.3 Results

4.3.1 Generating optogenetic clustering proteins by mutating PPPS/TP motifs in Cry2PHR-mCherry-LRP6c

In their seminal paper in 2013, Bugaj et al. reported the fusion protein Cry2PHR-mCherry-LRP6c that triggered canonical Wnt signaling in a blue-light dependent fashion (Bugaj et al. 2013). When we monitored the cluster formation of the above fusion protein, we observed significantly different ON/OFF kinetics to that of wild-type Cry2PHR-

mCherry (data not shown). Based on this observation, we hypothesized that variants of Cry2PHR-mCherry-LRP6c – mutated so that the protein could no longer activate Wnt signaling – would act as novel scaffolds for optogenetic proteins with vastly different and tunable dynamics compared to Cry2PHR-mCherry.

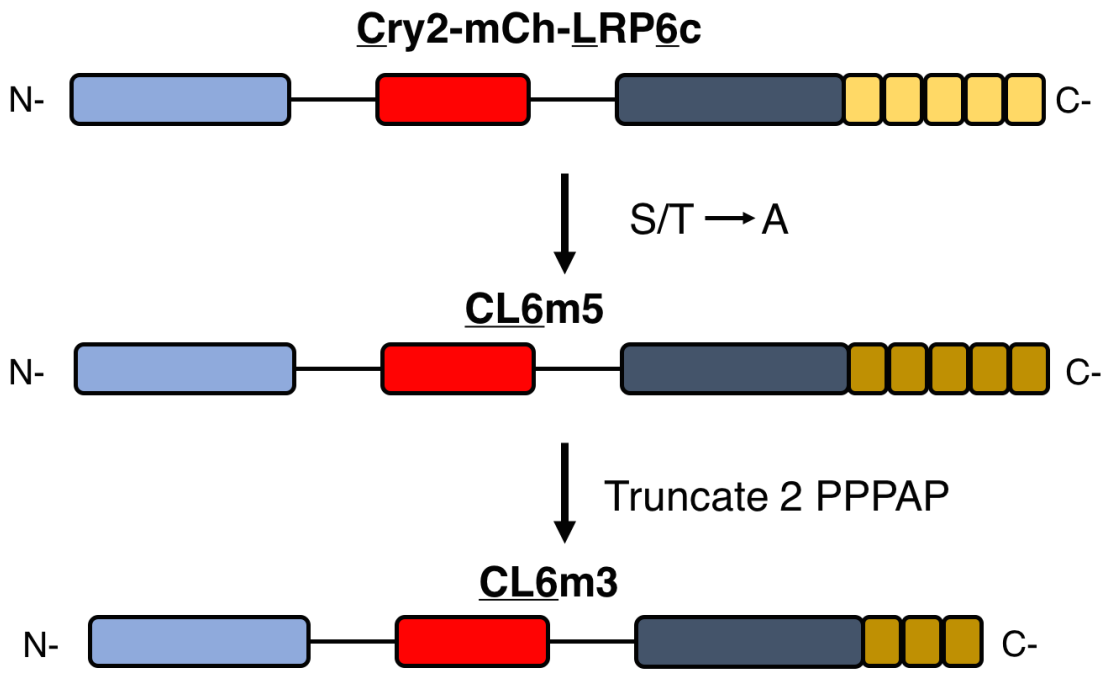

Figure 20 – Schematic Showing Strategy to Generate CL6mN Mutants: CL6m5 mutant is constructed by mutating five Ser/Thr residues in Cry2-mCh-LRP6c to Ala. CL6m3 mutant is constructed by truncating 2 PPPAP motifs from the C-terminus of CL6m5.

Since the Cry2PHR-mCherry-LRP6c fusion protein activates canonical Wnt signaling in presence of blue light, eliminating the above signaling activity upon clustering represented a key first step in generating a broadly applicable and tunable optogenetic scaffold. Macdonald et al. in 2008 reported that five PPPS/TP motifs in the cytosolic domain of LRP6 play a key role in its capability to trigger Wnt signaling upon oligomerization (Macdonald et al. 2008). They showed that mutating these PPPS/TP motifs

and/or eliminating two or more such motifs completely abrogated the signaling activity of LRP6. Taking a page out of their book, we replaced the LRP6c in the Cry2PHR-mCherry-LRP6c fusion protein with the mutated LRP6m5 protein, which contains five S/T→A mutations in the five PPPS/TP motifs (Fig. 20). Macdonald et al. also alluded to inter-motif interactions among the PPPSP motifs contributing to LRP6 oligomerization during Wnt signaling activation. We hypothesized that changing the number of "sticky" PPPAP motifs could result in tunable clustering/declustering dynamics in the mutated Cry2PHR-mCherry-LRP6c proteins.

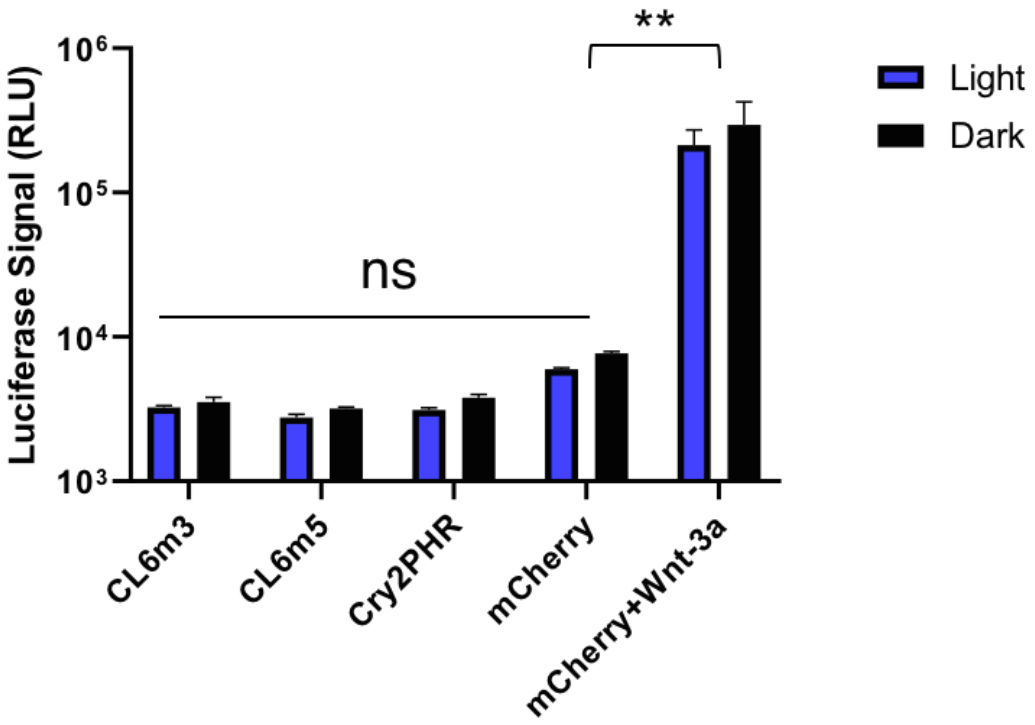

Figure 21 – Luciferase Assay to Monitor Wnt Signaling Activity of CL6mN (N=3,5) Mutants in Light and Dark: Cry2PHR and mCherry were negative controls, transiently transfected instead of CL6mN on the same vector backbone. Wnt-3a + mCherry transfected sample was the positive control. Two-way (mixed model) ANOVA was performed to analyze the effect of i) light and ii) transfected constructs on the cells. $p<0.05$ for the effect of transfected constructs (H_2); $p>>0.05$ for the effect of light (H_1) and interaction between light and transfected constructs (H_3). **$p<0.05$ by performing post-hoc pairwise Tukey's HSD test. ns = not statistically significant.

The resulting fusion protein library was termed CL6mN (Cry2PHR-mCherry-LRP6 with N mutated PPPSP motifs), where N represented the number of PPPAP motifs in the C-terminus of the fusion protein (N=3,5).

4.3.2 CL6mN does not trigger canonical Wnt signaling pathway

To test whether CL6mN triggered the canonical Wnt signaling pathway, we co-transfected 293T cells with the 7xTFP-luciferase reporter and the CL6mN constructs. Upon exposure to blue light, no significant increase in luciferase signal was observed for cells transfected with any of the CL6mN constructs (Fig. 21). In contrast, the Wnt-3a transfected cells showed high luciferase signals both in the presence and absence of blue light (Fig. 21). This experiment confirmed that CL6mN constructs do not activate canonical Wnt signaling in the presence or absence of blue light in the cell.

4.3.3 CL6mN exhibited robust clustering in the presence of blue light

To analyse whether the CL6mN constructs retain their clustering activity, we transfected multiple wells of 293T cells with plasmids expressing CL6mN proteins. We subsequently imaged these samples using confocal microscopy approximately 24 hours after transfection. When imaged using the λ=561 nm (RFP) laser, all the CL6mN constructs appeared homogenously distributed within the cell in the absence of blue light (λ=488 nm). However, upon irradiation with the 488-nm laser, bright red puncta formed within the cell, suggesting that CL6mN proteins clustered robustly in the presence of blue light (Fig. 22). Combining our observations from Fig. 21 and Fig. 22, we concluded that the CL6mN proteins are capable of clustering in the presence of blue light while exhibiting no canonical Wnt signaling activity.

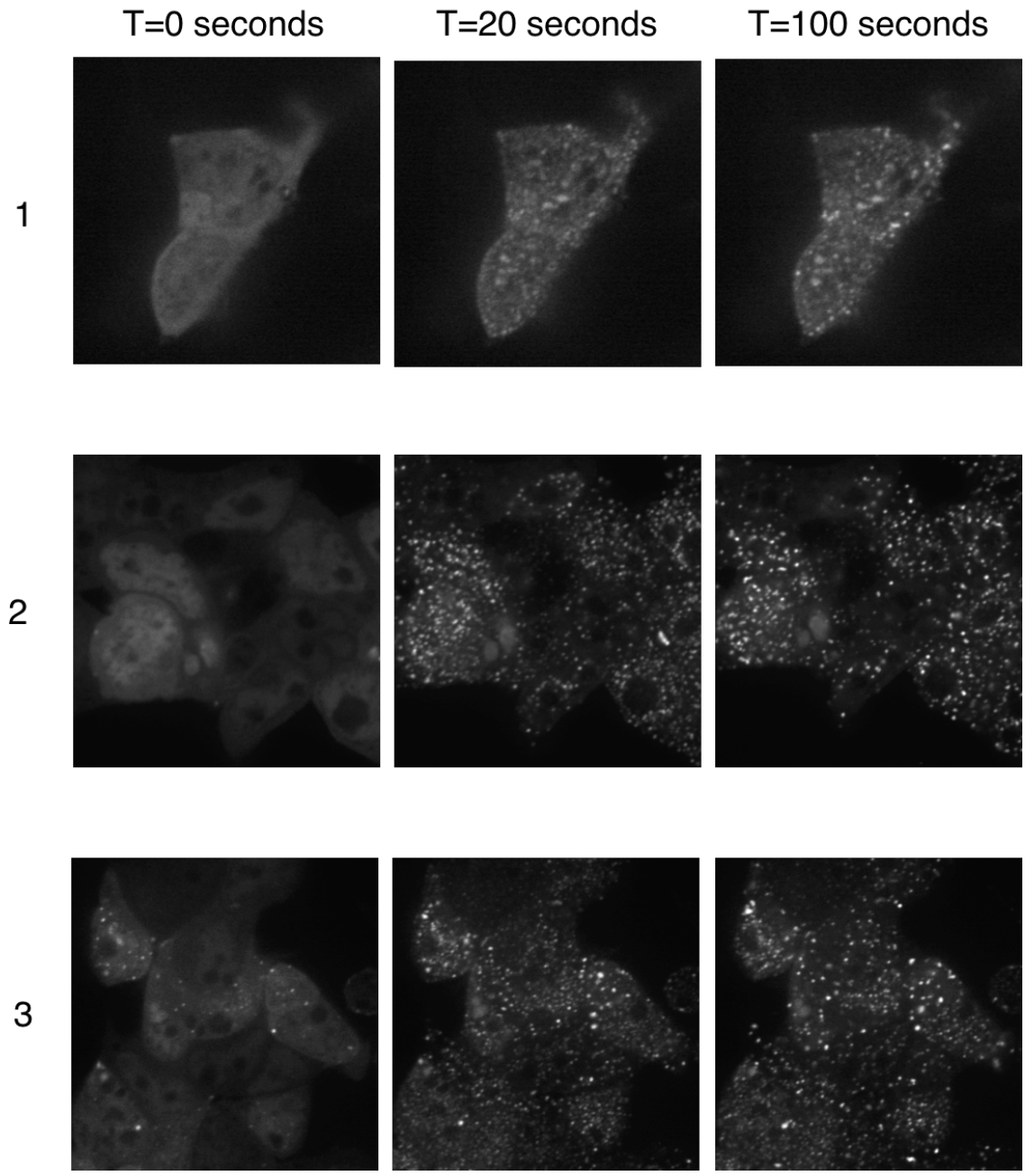

Figure 22 – Confocal Microscopy Images Showing Clustering of Cry2PHR-mCherry (Row 1), CL6m3 (Row 2) and CL6m5 (Row 3) at Various Time Points (T) after Blue Light (λ=488-nm) Exposure Visualized under the RFP (λ=561-nm) channel. The clustering is characterized by the formation of distinct puncta by the fused mCherry fluorescent protein. Cry2PHR-mCherry transfected cells (Row 1) serve as positive controls.

4.3.4 Differences in Cry2PHR-mCherry, CL6m3 and CL6m5 clustering (ON rate) dynamics are not statistically significant

To monitor the clustering dynamics (the ON rate) of the CL6mN constructs, we transfected 293T cells in a 4-chambered imaging dish with respective CL6mN constructs. Using the 561-nm laser in the confocal microscope, we first imaged a transfected cell with a homogenous mCherry, and thus CL6mN, signal. We then triggered the clustering of CL6mN by exposing the cell to the blue (λ=488 nm) laser at 100% intensity for ~1 sec and used the RFP channel to obtain images at a 10 second interval for 100 seconds. Next, we used ImageJ to analyse the number of clusters in each image to obtain the temporal dynamics of CL6mN clustering. When these clustering curves were compared, we observed that the differences in half-maximal clustering times of Cry2PHR, CL6m3 and CL6m5 constructs were not statistically significant (Fig. 23A-C).

4.3.5 Preliminary evidence suggests half-lives of CL6mN clusters can be increased by increasing the number (N) of PPPAP motifs

To characterize the declustering dynamics of different CL6mN constructs, we exposed the CL6mN expressing cells to the 488-nm laser at 10% intensity four times to ensure maximal clustering of CL6mN. Upon doing so, we imaged the samples every 30 seconds using the RFP channel for a total of 20 minutes. Next, we used ImageJ to measure the number of clusters in each image (corresponding to a distinct time-point) to construct a temporal declustering plot for each of the CL6mN constructs (Fig. 24).

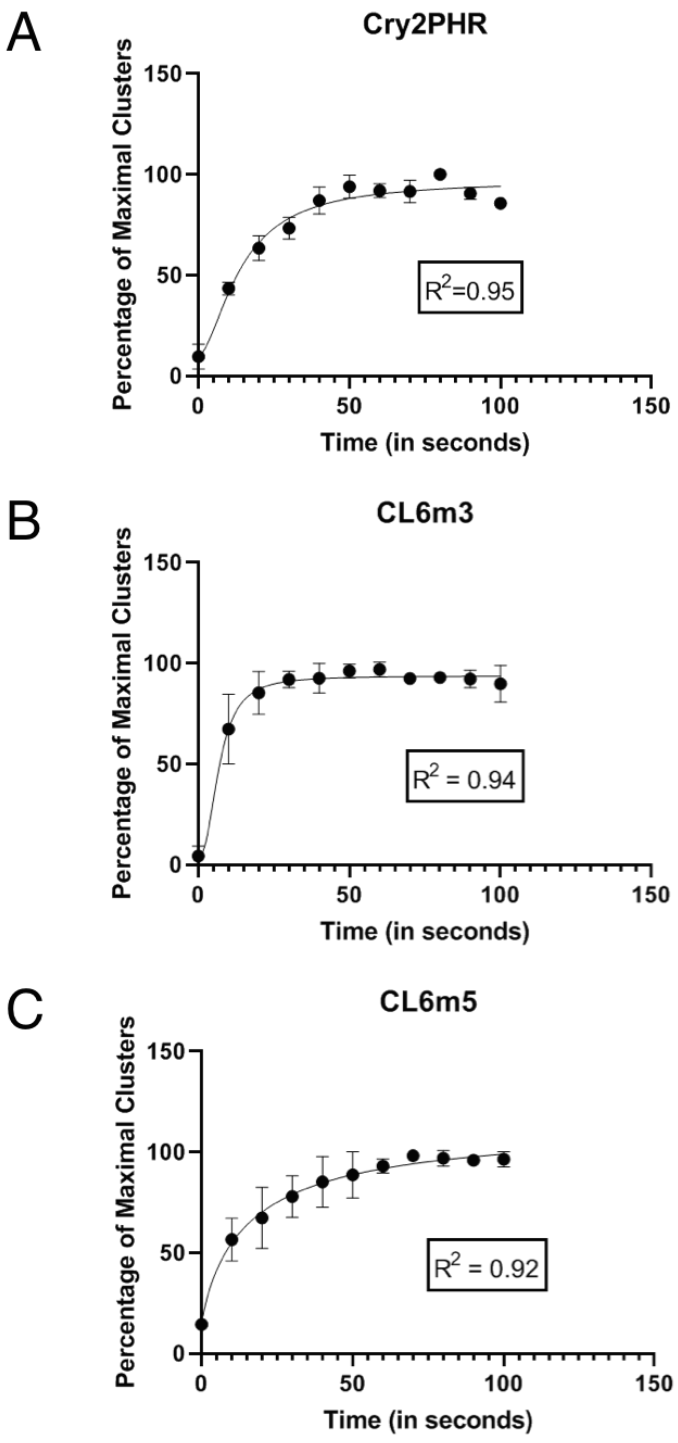

Figure 23 – Comparison of the Clustering Dynamics of (A) Cry2PHR, (B) CL6m3 and (C) CL6m5 upon blue light exposure. Each data point represents the mean (± 1 s.d.) of three independent experimental repeats (n=3 replicates). A variable slope Hill curve is fitted to the experimental observations to estimate $T_{1/2}$, the time at which the half-maximal number of clusters are observed.

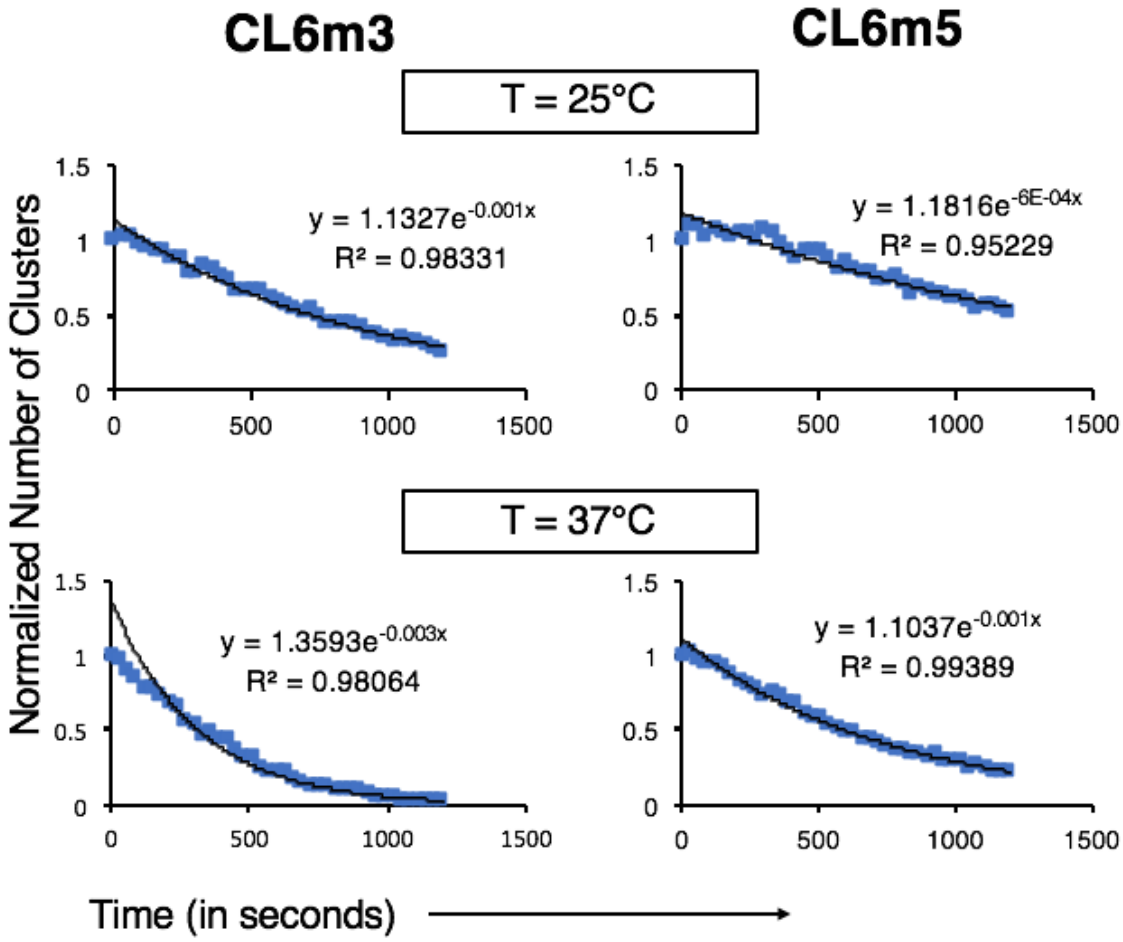

Figure 24 – Representative Plots Showing the Declustering Dynamics of CL6m3 and CL6m5 at Different Temperatures (T=25°C and T=37°C respectively). Each data point represents the normalized number of clusters from one experimental repeat. An exponential curve was used to fit the temporal dissociation dynamics of CL6m3 and CL6m5. Final declustering half-life estimates for CL6m3 and CL6m5 were obtained from three independent experimental repeats, which are reported in Table 2.

We observed that the half-lives of the CL6mN clusters increased with the number of PPPAP motifs, i.e., the half-life of CL6m5 > CL6m3 > Cry2PHR with the average half-life of CL6m5 being ~24.8 minutes (Fig. 24, Table 2) compared to ~11.55 minutes for CL6m3 (Fig. 24, Table 2) and ~3.85 minutes for Cry2PHR (Fig. 19B). Additionally, the declustering half-lives of the CL6mN mutants vary considerably with temperature,

decreasing to ~3.85 minutes and ~11.55 minutes at 37°C for CL6m3 and CL6m5 respectively (Fig. 24, Table 2). From a qualitative perspective, the CL6mN constructs showed higher clustering efficiency and formed much more stable clusters than wild-type Cry2PHR, thus suggesting that CL6mN can be continuously clustered using much lower doses of light than is needed in case of Cry2PHR.

Table 2 – Declustering Half-Lives of CL6mN at Different Temperatures

Optogenetic Proteins	**Dissociation Half-Lives (in minutes)**	
	At 25°C (mean ± s.d.) n = 3 replicates	At 37°C (mean ± s.d.) n = 3 replicates
CL6m3	11.55 ± 0.0	3.85 ± 0.0
CL6m5	24.83 ± 7.0	11.55 ± 0.0

To summarize,

1. We have constructed a library of optogenetic tools which undergo robust, reversible and efficient clustering in presence of blue light.
2. The optogenetic tools do not exhibit significantly different clustering dynamics but they have very different declustering half-lives, thus expanding the applicability of these tools in investigating biological phenomena of different time scales.
3. The dissociation kinetics of these optogenetic photoswitches are temperature-dependent, with the half-lives of dissociation decreasing with increasing temperature.

4.4 Discussions

4.4.1 Potential reasons for temperature-dependence of declustering dynamics

The exact mechanisms behind blue-light dependent cryptochrome2 (Cry2) clustering and declustering are not known. However, it has been hypothesized that in the presence of blue light, the Cry2 proteins undergo conformational changes that favour Cry2-Cry2 interaction, resulting in the formation of visible clusters. Presumably, the absence of blue light results in the relaxation of the chromophores FAD and MTHF, resulting in Cry2 reverting to its "inactive" conformation. Based on our observations, we hypothesize that the time scale associated with the conformational change of Cry2 stemming from the relaxation of its chromophores may be temperature-dependent, i.e. increased temperature results in a faster conformational change of the Cry2 monomer. To test this hypothesis, we can compare the declustering half-lives of wild-type Cry2 or Cry2PHR at different temperatures and monitor if the difference is significant.

Alternatively, the temperature-dependent variation in declustering dynamics may be an exclusive property of the CL6mN mutants, and not of wild-type Cry2PHR. The interaction between the PPPAP motifs may vary with temperature, with a higher temperature favouring faster dissociation of these PPPAP motifs. Further studies are required to confirm which of the above scenarios is more realistic.

4.4.2 Implications for PPPAP cooperativity in CL6mN

In 2008, Macdonald et al. reported a role for cooperativity and synergy among the PPP(S/T)P motifs of LRP6 in activating the canonical Wnt signaling cascade. Firstly, the

observed difference of declustering dynamics among the Cry2PHR and CL6mN constructs suggests that the cooperativity and synergies among the motifs are retained even after the mutation of the Ser/Thr residues to Ala. Secondly, the ability of the PPPAP motifs to effectively increase the lifetime of these Cry2-based homo-oligomers (clusters) suggests that such cooperativity may in fact involve both intra- and/or inter-protein interactions. In the future, one can design constructs with different numbers and types of unmutated PPP(S/T)P motifs on the C-terminus of the Cry2-mCh-LRP6c. Monitoring the dissociation dynamics of the resulting proteins may give us important clues in delineating the roles of each distinct PPP(S/T)P motif in transducing the canonical Wnt signal via phosphorylation and oligomerization of LRP6.

4.4.3 Considerations for generating stably transfected cell lines

To further characterize and use the CL6mN constructs for other applications, one will presumably have to develop novel cell lines stably expressing the CL6mN constructs. We recommend that special attention is given to the steady-state level of the CL6mN proteins in such cell lines. We have observed that, at high intracellular concentrations, the CL6mN proteins show a tendency to cluster in the absence of blue light, as evidenced by significant puncta formation in the mCherry channel even in the dark. In transient transfection-based assays, researchers have bypassed this problem by either imaging the cells within specific time windows following transfection, or by treating the cells with cycloheximide to inhibit protein synthesis to maintain a desired intracellular protein concentration. In case of stable cell lines, however, controlling the genomic site of integration and the strength of the upstream promoter for the respective CL6mN constructs can ensure an optimal intracellular

concentration. The above-mentioned considerations are by no means exhaustive, but rather represent a “starting point” for the development of any such transgenic cell line.

CHAPTER 5. DESIGNING TRANSCRIPTION ACTIVATION BASED REPORTERS FOR MONITORING CARDIOMYOCYTE DIFFERENTIATION

5.1 Background

Spatiotemporally controlling the self-renewal, proliferation and differentiation of various kinds of stem cells, e.g., embryonic stem cells, neural stem cells, mesenchymal stem cells, represents the central aim of regenerative medicine (Nusse 2008; Vallier et al. 2009; Tabar and Studer 2014). Over the last 20 years, it has become evident that the above phenomena are intricate stepwise processes involving a defined sequence of changes in cell fate (Tabar and Studer 2014). Such changes are rarely accomplished by any one developmental signal, but rather by a combination of several signals. Moreover, in contrast to having a binary response to these signals, concentrations of these signaling molecules, finely controlled by the microenvironmental niche of the residing stem cells, have been shown to play a key role in moderating the lineage commitment of the stem cells (Blank et al. 2008). A number of pivotal signaling pathways have been identified to influence these processes, involving molecules belonging to the Wnt, Hedgehog, BMP, FGF families (Pires DaSilva and Sommer 2003; Nusse 2008).

As is the signature of a nascent field, the role of Wnt signaling in controlling stem cell fate remains largely controversial (Sato et al. 2004; Reya and Clevers 2005; Davidson et al. 2012). In the early 2000-s, canonical Wnt signaling was largely thought to promote the maintenance of undifferentiated embryonic stem cells and even self-renewal in embryonic and neural stem cells (Sato et al. 2004; Reya and Clevers 2005). However,

several studies in the late 2000-s and early 2010-s reported the dual nature of Wnt signaling by highlighting its role in promoting multi-lineage differentiation of embryonic stem cells (Davidson et al. 2012; Szemes et al. 2018). What is evident is that canonical Wnt signaling remains mired in controversy and further studies are required to satisfactorily correlate the role of Wnt signaling to stem cell fate in a context-dependent manner. To do so, designing a variety of robust reporters capable of correlating Wnt activity to various cell lineages and phenotypes holds great promise.

In 2012, Lian et al. robustly generated human cardiomyocytes from human pluripotent stem cells by exclusively controlling canonical Wnt signaling temporally (Lian et al. 2012; Lian et al. 2013; Lian et al. 2015). Subsequently in 2017, Bao et al. used a similar strategy of temporally controlling Wnt signaling to generate long-term self-renewing epicardial cells from human pluripotent stem cells (hPSCs) (Bao et al. 2017). The close alignment of these processes provides the ideal test bed for us to try and explore how canonical Wnt signaling influences the process of different lineages arising from similar initial cell populations.

In the state-of-the-art reporters, unique biomarkers for the different intermediate stages of hPSC differentiation are detected usually via flow cytometry or immunoblotting (Lian et al. 2013; Bao et al. 2017; Schwach et al. 2017). Despite having moderate success, such reporters are largely low-throughput and have severe limitations under certain conditions. The following work is a primer describing our strategy to design transcriptional-activation based switches as reporters for the different intermediate stages of differentiation as the hPSC population commits to one fate or the other. Successfully deploying these reporters in stably transfected “sentinel” cells could help us satisfactorily

correlate canonical Wnt activity to cardiomyocyte differentiation in human pluripotent stem cells.

5.2 Material and Methods

Plasmids

The Brachyury and Coup-TFII transcription factor sequences were inserted into the first cloning site (cloning site-1) of the pVitro2-MCS vector (with hygromycin resistance; Invivogen). A DsRed fluorescent protein sequence was inserted into the second cloning site as a marker for positive transfection of the plasmid.

The 4x- and 8x-Brachyury reporters were constructed on the custom WT1-GFP plasmid backbone which was a gift from the Palecek lab (Bao et al. 2017). The 4x and 8x repeats of the consensus binding sequence of Brachyury were inserted upstream of a custom-synthesized minimal promoter (minP) sequence which controlled the expression of a recombinant firefly luciferase protein downstream. The baseline expression of firefly luciferase acted as a marker for positive transfection of the reporter.

The Coup-TFII reporter was constructed on a pVitro2-MCS backbone at the first cloning site. A custom-synthesized minimal promoter (minP) was cloned in place of the ferritin promoter in cloning site-1 and the CMV enhancer sequence was deleted. The minimal promoter sequence was preceeded by the consensus sequence of a promoter containing Coup-TFII binding sites. The firefly luciferase sequence was inserted downstream of the minimal promoter.

All custom gene synthesis steps were performed by Gene Universal.

Luciferase Assay to Detect Transcription Activation

293T cells were seeded in 96-well plates coated with poly-L-lysine at an initial density of 60,000 cells per well and grown up to ~90% confluency in ~24 hours. Cells were co-transfected with two separate plasmids, one encoding the transcription factor or a control protein, and the other encoding the reporter or an appropriate control. Transfection was performed by using the Lipofectamine 2000 reagent according to the manufacturer's protocol. After transfection, cells were incubated for 36 hours, washed twice with DPBS and lysed in a passive lysis buffer (Promega). Luciferase Assay Substrate (Promega) was subsequently added to the lysate upon transferring to a white-walled opaque 96-well plate (Corning) and the luminescence read in the BioTek Synergy plate reader in the EBB Biopolymer Characterization Core.

5.3 Results and Discussion

5.3.1 Brachyury and Coup-TFII as biomarkers for mesodermal precursor cells and cardiomyocytes

In 2012, Lian et al. first reported obtaining functional (beating) cardiomyocytes from human pluripotent stem cells (hPSCs) by modulating the canonical Wnt signal only over time (Lian et al. 2012). The seminal study was followed by multiple reports between 2014 – 2017 by Lian et al. and Bao et al. that described the generation of endothelial cell and long-term self-renewing epicardial cell populations respectively by hPSC differentiation (Fig. 25).

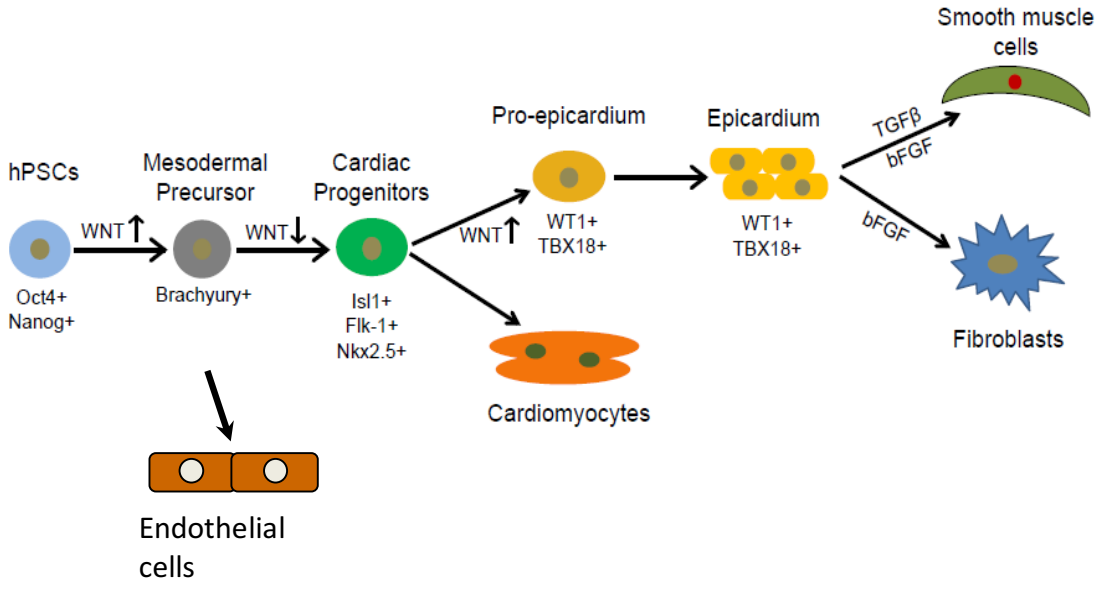

Figure 25 – Flow Chart showing the Intermediate Cell Types in the Differentiation of human Pluripotent Stem Cells (hPSCs) to form Epicardial cells, Endothelial cells and Cardiomyocytes. Reprinted with permission from Nature Publishing Group (Bao et al. 2017).

The process through which hPSCs differentiate to form three distinct cell populations is largely thought to follow the sequence described in Fig. 25. Upon Wnt activation, hPSCs differentiate to form mesodermal precursor cell populations which can, in turn, form endothelial cell layers if Wnt remains turned on. Subsequently, when Wnt is downregulated, mesodermal precursors differentiate to form cardiac progenitor cells which can give rise to multiple different types of cardiac cells, depending on the temporal variation of Wnt signaling. If canonical Wnt signaling remains downregulated, cardiac progenitors are thought to predominantly give rise to atrial and ventricular cardiomyocytes, whereas a second Wnt upregulation step leads to the formation of epicardial cells.

To leverage the above process for robust and scalable synthesis of cardiomyocytes, it is thus imperative to have suitable quality indicators for this multi-day protocol. In this

case, biological reporters that are specific to the signature biomarkers of these intermediate cell specifications, i.e. mesodermal precursors, cardiac progenitor cells, atrial and ventricular cardiomyocytes, can serve as these necessary quality indicators.

Based on a vast literature review, we found that

a. The T-box transcription factor Brachyury is a specific marker for mesodermal precursor cells (Wilson et al. 1995; Kubo et al. 2004; Tada et al. 2005; Bao et al. 2017).
b. The transcription factors Isl1 and Nkx2.5 can serve as biomarkers for the cardiac progenitor cell population (Cai et al. 2003; Elliott et al. 2011)
c. The transcription factors Coup-TFII and GATA4 are specifically expressed in the atrial and ventricular cardiomyocyte cell populations respectively (Holtzinger et al. 2010; Wu et al. 2013).

In this chapter, we analyzed the sequences and structures of the transcription factors Brachyury and Coup-TFII. Based on our findings, we designed and tested reporters that upregulated the expression of luciferase upon the expression of the above-mentioned transcription factors.

5.3.2 Biophysics of Brachyury and Coup-TFII Transcription Factors

Brachyury belongs to the family of T-box transcription factors and is capable of binding to the specific T-box consensus DNA sequence 5'-TCACACCT-3' (Kusch et al. 2002; Lolas et al. 2014). Brachyury has a relatively large DNA binding domain that spans amino acid residues 51-219, which is roughly 1/3rd the length of the entire 436 amino acid-long protein. Brachyury functions as a dimer *in vivo* and each subunit of the Brachyury dimer binds to the consensus T-box sequence (Fig. 26A) (Muller and Herrmann 1997).

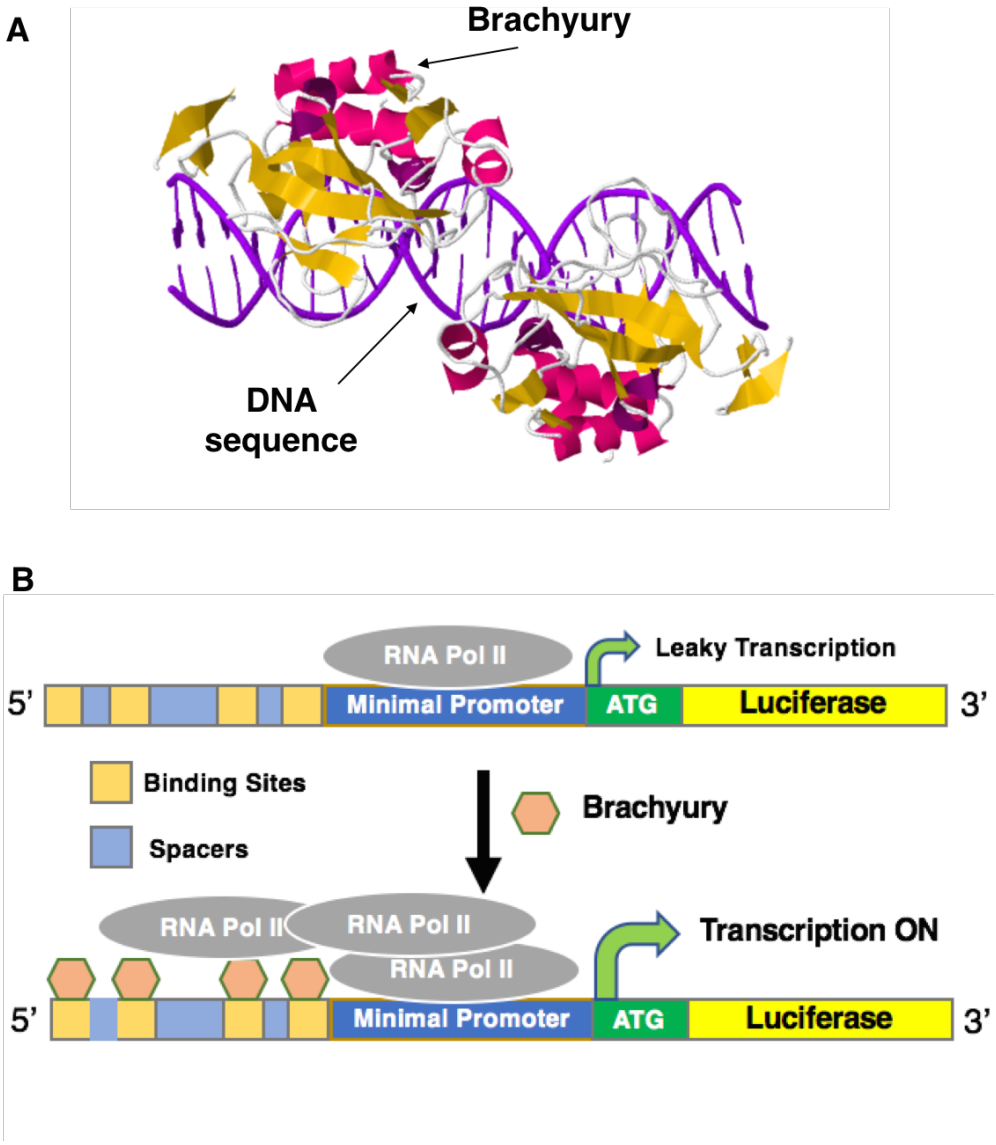

Figure 26 – Activation of Transcription by Brachyury: (A) Crystal structure showing that Brachyury is capable of binding to the consensus T-box DNA sequence (Uniprot# 6F58). (B) Schematic showing the strategy to design transcription-activation based reporters of Brachyury activity.

Once bound to the consensus sequence in the enhancer regions, the Brachyury dimer is capable of recruiting RNA Polymerase II and upregulating the transcription of downstream genes (Fig. 26B).

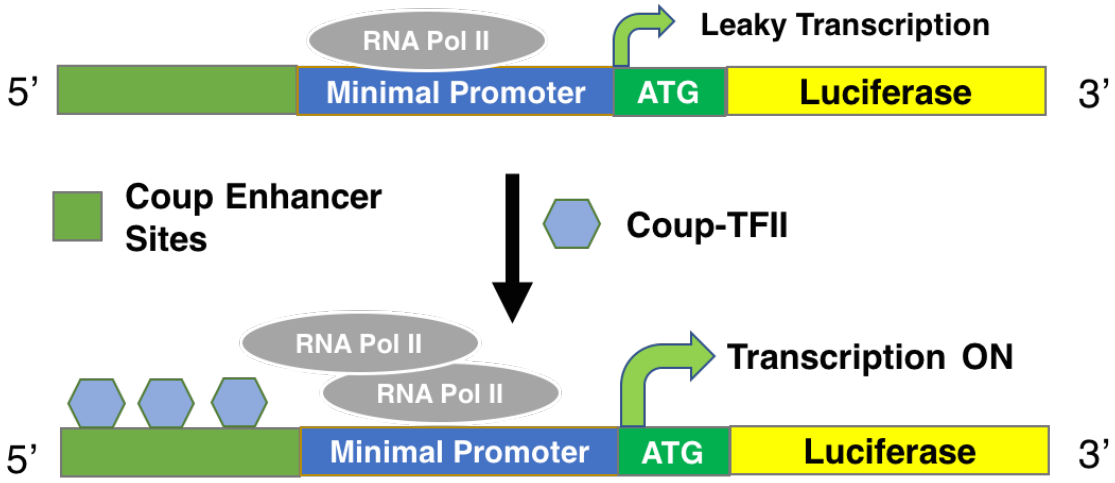

Figure 27 – Schematic Showing Proposed Strategy to Design Coup-TFII-responsive Transcription-Activation Based Reporter.

The chicken ovalbumin upstream promoter-transcription factor II (Coup-TFII) is an orphan nuclear receptor which is hypothesized to be a ligand-activated transcription factor, but the activating ligands have not been identified conclusively *in vivo* (Kruse et al. 2008). Like Brachyury, it contains a DNA binding domain that spans amino acids 76-151. However, unlike Brachyury, Coup-TFII contains two zinc finger domains which are thought to enable its interactions with other protein partners in the nucleus to upregulate transcription. Coup-TFII has been reported to bind to imperfect direct repeats of the DNA hexamer 5'-AGGTCA-3' in the promoter regions of downstream genes to upregulate transcription in a promoter-dependent fashion (Fig. 27) (Lee et al. 2012). Unlike Brachyury, no direct evidence has been reported to date as to whether binding to the consensus DNA hexamer is sufficient for Coup-TFII to recruit RNA Polymerase II and thus upregulate transcription.

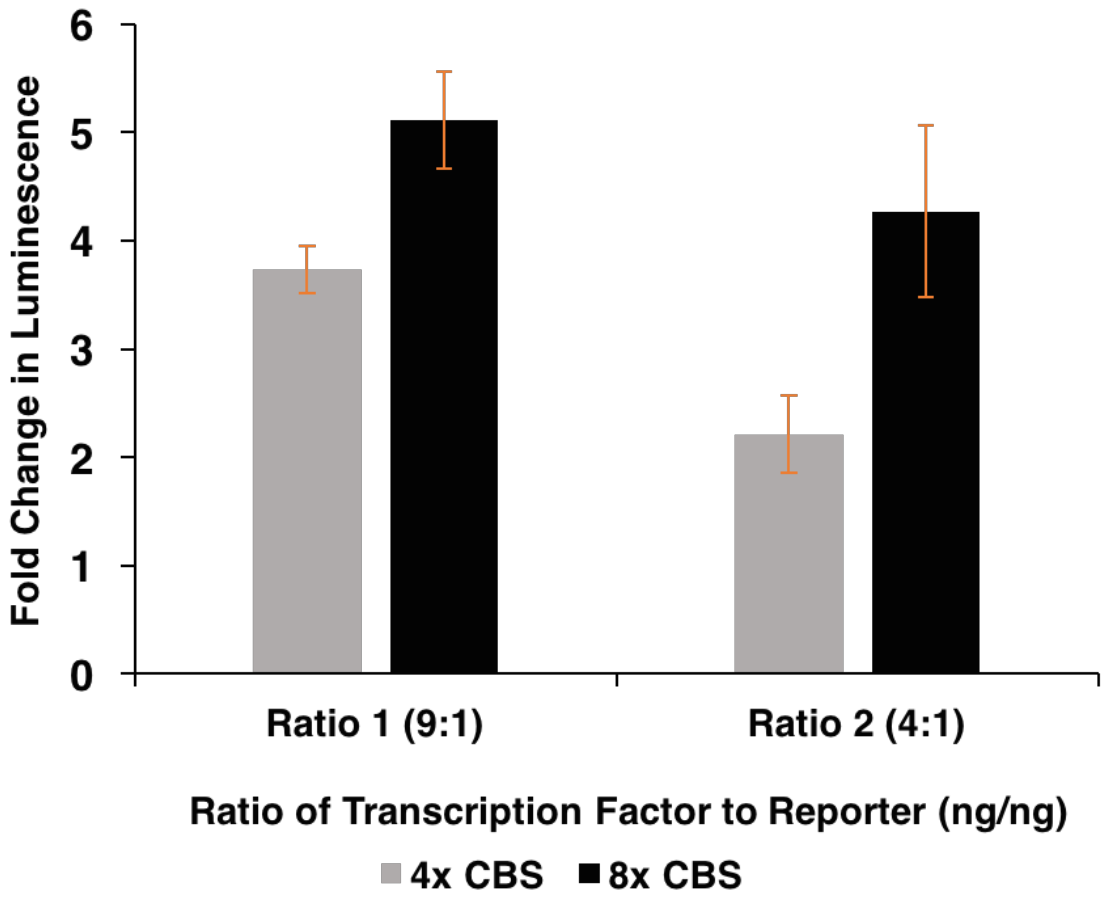

Figure 28 – Preliminary Evidence of Transcription-Activation Based Reporters (4x and 8x) Showing Significant Fold Increase in Luminescence in presence of Brachyury. The fold change increases with increase in Brachyury-to-reporter ratio for both 4x and 8x reporters. Each bar represents the mean (± 1 s.d.) of 3 replicates (n=3).

5.3.3 Transcription Activation-based Reporters for Brachyury and Coup-TFII

The Brachyury and Coup-TFII transcription activation-based reporters were constructed on custom plasmids containing the homology-directed repair (HDR) arms for editing the locus expressing the WT1 gene in the human genome. We designed two distinct Brachyury-responsive reporters, one with 4 repeats and the other with 8 repeats of the consensus T-box DNA octamer sequence 5'- TCACACCT-3' in the enhancer region (Lolas et al. 2014). The octamer sequences were upstream of a minimal promoter which controlled

the expression of a downstream luciferase gene. The spacing between successive repeats alternated between 5 bp and 22 bp to account for the *in vivo* dimerized form of active Brachyury. Upon transient transfection of the reporters along with a plasmid expressing recombinant human Brachyury or an orthogonal vector control plasmid, both 4x- and 8x-CBS (consensus binding site) reporters showed robust increase in luciferase expression in presence of Brachyury compared to the orthogonal control (Fig. 28). Predictably, the fold activation was higher in case of the reporter containing 8 CBS repeats (~5 folds compared to ~4 folds). Interestingly, the magnitude of the luminescence signals was lower in case of the 8x-reporter (data not shown), thus posing a potential signal-to-noise optimization problem for the future.

For Coup-TFII, we used the same vector backbone, but in this case, we inserted a truncated, functional region of the Coup-responsive enhancer upstream of the minimal promoter and luciferase gene (Kruse et al. 2008). Following a similar transient transfection strategy described above, we confirmed that the Coup-TFII reporter showed a ~3-fold increase in downstream luciferase expression in presence of the Coup-TFII transcription factor expressing plasmid compared to an orthogonal control (Fig. 29).

To conclude,

1. We conceptualized a transcription-activation based strategy to distinguish specific cell populations in the cardiomyocyte differentiation process.
2. As a proof-of-concept, we designed robust transcriptional-activation based reporters which were responsive to the human transcription factors, Brachyury and Coup-TFII.

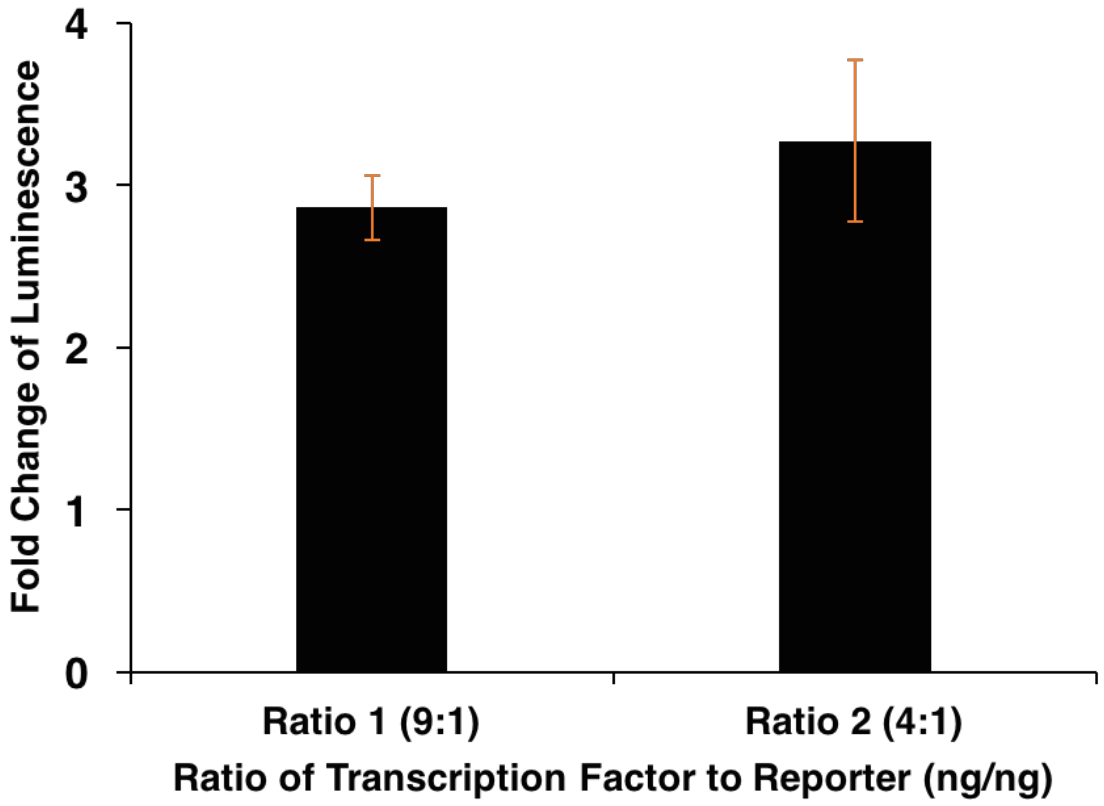

Figure 29 – Preliminary Evidence of Coup-TFII Transcription-Activation Based Reporter Showing Fold Increase in Luminescence in Presence of Coup-TFII at Various Levels of Transfected Reporter and Transcription Factor. Each bar represents the mean (± 1 s.d.) of 3 replicates (n=3).

CHAPTER 6. POTENTIAL FUTURE WORK

In this thesis, we established a model elucidating the fundamental mechanism of canonical Wnt signal transduction through the cytosol. The model can serve as a reliable framework to evaluate the nuances of canonical Wnt signaling across different cell types and culture conditions. Next, we proceeded to leverage our understanding of Wnt signaling to design synthetic agonists capable of robustly triggering the canonical Wnt pathway. Our approach is highly synergistic with bioprocesses that are well-established in the industry and can thus serve as a platform to synthesize alternatives to the canonical Wnt ligand(s). We further applied our understanding of the structure of LRP6, a membrane-bound receptor pivotal in Wnt signal transduction, to design a library of optogenetic photoswitches possessing tunable declustering dynamics. The above optogenetic proteins, termed CL6mN, can be deployed to significantly reduce cytotoxicity and to probe cellular phenomena of wide-ranging time scales. In this chapter, we discuss some potentially promising applications of these tools for the future.

6.1 Correlating Destruction Complex Localization to Cell Fate

We established in Chapter 5 that the role of the canonical Wnt signal in stem cell fate determination is highly context-dependent. In 2013, Habib et al. wanted to probe the consequences of local Wnt signals on cultured embryonic stem cells (ESCs) and found that during cell division, the Wnt-proximal daughter cells inherited high levels of nuclear β-catenin and pluripotency genes whereas Wnt-distal daughter cells showed signs of differentiation (Habib et al. 2013). *In vivo*, this result magnifies the significance of the spatial distribution and the gradient of Wnt molecules in the microenvironment of stem

cells. A binary model of Wnt signaling (where signaling is either ON or OFF) does not satisfactorily explain the nuances involved in this process of cell fate determination. In our model, we find that a certain fraction (56%) of the destruction complexes relocates to the membrane and this fraction is key in determining the fold increase in cytosolic β-catenin, and thus the extent of downstream signaling. Since this relocation is primarily thought to be driven by the interaction of Axin1 and Wnt-activated LRP6, we can speculate that the percentage of destruction complex relocating is a function of the concentration and affinity/avidity of heterodimeric Fzd-LRP6 complexes formed upon Wnt-3a stimulation towards the intracellular destruction complexes. Our model thus provides a fundamental basis for correlating destruction complex localization to the extent of Wnt-downstream gene activation. In the future, an extensive model-driven study may be warranted to investigate whether certain regimes of Wnt signaling correlate to specific cell fates. The questions to ask will be:

1. Is the percentage of destruction complex relocating to the membrane tunable? If so, what are the contributing factors?
2. Do we observe any experimental limits (both higher and lower) of destruction complex localization in the presence of Wnt-3a?
3. Do these limits correspond to certain cell fates in human pluripotent stem cells?

Any correlation observed would be immensely impactful for scientific and therapeutic purposes.

6.2 Potent Multivalent Wnt Agonists for Unexplored Regimes of Wnt Signaling

In Chapter 3, we provided a proof-of-concept that synthetic heterodimers can successfully activate canonical Wnt signaling. To further enhance the potency of the agonists, we propose designing variants with higher valencies of the receptor-binding ligands. We propose three distinct strategies to do so.

1. Using SpyTag-SpyCatcher chemistry, we intend to conjugate an anti-Fzd monoclonal antibody (mAb) to two LRP6 Fabs to obtain a "dimer of dimers" capable of triggering canonical Wnt signaling.
2. In the second approach, we propose to tether multiple copies of the synthetic heterodimer onto the surfaces of bacteriophage MS2 virus-like particles (VLPs) and investigate their potency in triggering canonical Wnt signaling. Introducing an AviTag into the sequence of a Fab heavy chain will allow us to conjugate a biotin to the Wnt heterodimer. Coating the VLP surface with streptavidin will allow us to robustly generate multivalent Wnt agonists of tunable potency.
3. Finally, we can use flexible scaffolds in place of the MS2 VLPs to generate another class of multivalent Wnt agonists.

On a different note, we can extend this strategy of coupling specific antibodies or single chain/multi-unit antibody fragments to target other aspects of the canonical, and even non-canonical, Wnt pathways. Recently, Luca et al. reported surrogate R-Spondin agonists which further amplify the effect of canonical Wnt ligands, a pathway that can also be successfully targeted using our strategy (Luca et al. 2019). Further, multiple noncanonical Wnt pathways mediated by Wnt-5a are hypothesized to propagate through the assembly of

co-receptors Frizzled and ROR2 or RYK proteins, which are tyrosine-kinase like receptors in the plasma membrane (Ho et al. 2012; Green et al. 2014). One key reason why these pathways have remained unexplored is the significant lack of natural ligands that specifically target ROR2 and RYK, so much so that these receptors were thought to be "orphan receptors" until very recently. However, antibody and/or antibody fragments specific to these proteins are abundant, which gives our strategy a unique advantage in generating synthetic noncanonical Wnt agonists.

6.3 Potent Optogenetic Activators of Rho GTPases

Optogenetic signaling activators hold immense promise in providing several novel insights into a variety of cellular phenomena. Along the way, blue-light mediated cytotoxicity may become a roadblock. Using the CL6mN photoswitches instead of the wild-type Cry2 or Cry2PHR may ameliorate this problem to a certain extent. In their seminal 2013 article, Bugaj et al. reported the activation of the Rho GTPase-s Rac1 and RhoA upon blue-light mediated oligomerization of the fusion proteins Cry2-Rac1 and Cry2-RhoA respectively. One can fuse the Rac1 and RhoA constructs to the C-terminus of CL6mN constructs and characterize their level of activation upon blue-light exposure, in a very similar vein to that of Bugaj et al. Upon doing so, one can compare the levels of activated Rho GTPases in the Cry2-Rho GTPase fusion and the CL6mN-Rho GTPase fusion respectively. We hypothesize that for similar levels of Rho GTPase activation, significantly less blue-light exposure will be required, thus supporting CL6mN-s' ability to reduce blue-light mediated cytotoxicity in cell biological applications.

6.4 Optogenetic Inhibitors of Nuclear Translocation of β-catenin

The effects of introducing developmental signals on several key cellular phenomena have been well-characterized in the past several decades. How the cell responds to the withdrawal of such signals, however, remains largely unexplored. The optogenetic tools developed in this thesis can offer us an avenue to investigate aspects of such signal withdrawal in a variety of developmental pathways. As a proof-of-concept, we may proceed by generating a blue-light dependent Wnt OFF switch. To do so, we can use fusion proteins consisting of the CL6mN proteins on the N-terminus and a single-chain β-catenin binding protein on the C-terminus. Such a fusion protein may be able to recruit β-catenin in a CL6mN cluster in a blue-light dependent fashion. The large size of these clusters may subsequently render the recruited β-catenin incapable of translocating to the nucleus.

In theory, such an OFF switch can be generated for several such developmental pathways, e.g. the TGF-β pathways, which involve the translocation of transcriptional co-activator SMAD proteins to the nucleus, and the Hippo signaling pathway, which involves the YAP/TAZ proteins migrating to the nucleus from the cytosol. If successfully implemented, such switches can provide fundamental insights into a hitherto unexplored regime of developmental signaling pathways.

6.5 Stably-transfected "Sentinel Cells" to Correlate Wnt Signaling with Stem Cell Fate and Monitor Therapeutic Cell Quality

We intend to strategically deploy the transcription-activation based reporters we designed in Chapter 5 to monitor the quality of cardiomyocytes produced from human

induced pluripotent stem cells (iPSCs). To do so, we first need to design robust reporters for cardiac progenitor cells as well as for ventricular cardiomyocytes. Transcription factors such as Isl-1 or Nkx2.5 may form the basis of such reporters in cardiac progenitor cells while GATA4 may be used to detect ventricular cardiomyocytes. Upon establishing the library of reporters, we intend to use Cas9-mediated genome editing to stably integrate these reporters into induced pluripotent stem cells (iPSCs). Putting multiple types of luciferase or fluorescent indicators downstream of these reporters will enable us to accurately report the cell specifications in the cardiomyocyte differentiation process. The successful deployment of these reporters will not only make it possible to generate high quality cardiomyocytes from human pluripotent stem cells, but will also provide us insights into the interplay between canonical Wnt signaling and subsequent cell fate determination.

REFERENCES

1. Abdollahi H, Harris LJ, Zhang P, McIlhenny S, Srinivas V, et al. 2011. The Role of Hypoxia in Stem Cell Differentiation and Therapeutics. Journal of Surgical Research 165:112-7
2. Amit S, Hatzubai A, Birman Y, Andersen JS, Ben-Shushan E, et al. 2002. Axin-mediated CKI phosphorylation of beta-catenin at Ser 45: a molecular switch for the Wnt pathway. Genes & Development 16:1066-76
3. Androutsellis-Theotokis A, Leker RR, Soldner F, Hoeppner DJ, Ravin R, et al. 2006. Notch signalling regulates stem cell numbers in vitro and in vivo. Nature 442:823-6
4. Azzolin L, Panciera T, Soligo S, Enzo E, Bicciato S, et al. 2014. YAP/TAZ Incorporation in the beta-Catenin Destruction Complex Orchestrates the Wnt Response. Cell 158:157-70
5. Bao X, Lian X, Hacker TA, Schmuck EG, Qian T, et al. 2017. Long-term self-renewing human epicardial cells generated from pluripotent stem cells under defined xeno-free conditions. Nature Biomedical Engineering 1
6. Baron R, Kneissel M. 2013. WNT signaling in bone homeostasis and disease: from human mutations to treatments. Nature Medicine 19:179-92
7. Behrens J, vonKries JP, Kuhl M, Bruhn L, Wedlich D, et al. 1996. Functional interaction of beta-catenin with the transcription factor LEF-1. Nature 382:638-42
8. Bhanot P, Brink M, Samos CH, Hsieh JC, Wang YS, et al. 1996. A new member of the frizzled family from Drosophila functions as a Wingless receptor. Nature 382:225-30
9. Bhattacharyya RP, Remenyi A, Yeh BJ, Lim WA. 2006. Domains, motifs, and scaffolds: The role of modular interactions in the evolution and wiring of cell signaling circuits. Annu. Rev. Biochem. 75:655-80
10. Bilic J, Huang YL, Davidson G, Zimmermann T, Cruciat CM, et al. 2007. Wnt induces LRP6 signalosomes and promotes dishevelled-dependent LRP6 phosphorylation. Science 316:1619-22

11. Blank U, Karlsson G, Karlsson S. 2008. Signaling pathways governing stem-cell fate. Blood 111:492-503
12. Bolotin A, Ouinquis B, Sorokin A, Ehrlich SD. 2005. Clustered regularly interspaced short palindrome repeats (CRISPRs) have spacers of extrachromosomal origin. Microbiology-Sgm 151:2551-61
13. Bovolenta P, Esteve P, Ruiz JM, Cisneros E, Lopez-Rios J. 2008. Beyond Wnt inhibition: new functions of secreted Frizzled-related proteins in development and disease. Journal of Cell Science 121:737-46
14. Bugaj LJ, Choksi AT, Mesuda CK, Kane RS, Schaffer DV. 2013. Optogenetic protein clustering and signaling activation in mammalian cells. Nature Methods 10:249-52
15. Cai CL, Liang XQ, Shi YQ, Chu PH, Pfaff SL, et al. 2003. Isl1 identifies a cardiac progenitor population that proliferates prior to differentiation and contributes a majority of cells to the heart. Developmental Cell 5:877-89
16. Cao J, Arha M, Sudrik C, Bugaj LJ, Schaffer DV, Kane RS. 2013. Light-inducible activation of target mRNA translation in mammalian cells. Chemical Communications 49:8338-40
17. Clevers H. 2006. Wnt/beta-catenin signaling in development and disease. Cell 127:469-80
18. Clevers H, Nusse R. 2012. Wnt/beta-Catenin Signaling and Disease. Cell 149:1192-205
19. Cong F, Schweizer L, Varmus H. 2004. Wnt signals across the plasma membrane to activate the beta-catenin pathway by forming oligomers containing its receptors, frizzled and LRP. Development 131:5103-15
20. Cselenyi CS, Jernigan KK, Tahinci E, Thorne CA, Lee LA, Lee E. 2008. LRP6 transduces a canonical Wnt signal independently of Axin degradation by inhibiting GSK3's phosphorylation of beta-catenin. Proceedings of the National Academy of Sciences of the United States of America 105:8032-7
21. Culler SJ, Hoff KG, Smolke CD. 2010. Reprogramming Cellular Behavior with RNA Controllers Responsive to Endogenous Proteins. Science 330:1251-5

22. Dann CE, Hsieh JC, Rattner A, Sharma D, Nathans J, Leahy DJ. 2001. Insights into Wnt binding and signalling from the structures of two Frizzled cysteine-rich domains. Nature 412:86-90
23. Davidson KC, Adams AM, Goodson JM, McDonald CE, Potter JC, et al. 2012. Wnt/beta-catenin signaling promotes differentiation, not self-renewal, of human embryonic stem cells and is repressed by Oct4. Proceedings of the National Academy of Sciences of the United States of America 109:4485-90
24. Debets MF, van Berkel SS, Schoffelen S, Rutjes F, van Hest JCM, van Delft FL. 2010. Aza-dibenzocyclooctynes for fast and efficient enzyme PEGylation via copper-free (3+2) cycloaddition. Chemical Communications 46:97-9
25. Deisseroth K. 2011. Optogenetics. Nature Methods 8:26-9
26. Delarco JE, Todaro GJ. 1978. Growth-Factors From Murine Sarcoma Virus-Transformed Cells. Proceedings of the National Academy of Sciences of the United States of America 75:4001-5
27. Desbois-Mouthon C, Cadoret A, Blivet-Van Eggelpoel MJ, Bertrand F, Cherqui G, et al. 2001. Insulin and IGF-1 stimulate the beta-catenin pathway through two signalling cascades involving GSK-3 beta inhibition and Ras activation. Oncogene 20:252-9
28. Dieterich DC, Lee JJ, Link AJ, Graumann J, Tirrell DA, Schuman EM. 2007. Labeling, detection and identification of newly synthesized proteomes with bioorthogonal non-canonical amino-acid tagging. Nature Protocols 2:532-40
29. Elliott DA, Braam SR, Koutsis K, Ng ES, Jenny R, et al. 2011. NKX2-5eGFPw hESCs for isolation of human cardiac progenitors and cardiomyocytes. Nature Methods 8:1037-+
30. Elowitz MB, Leibler S. 2000. A synthetic oscillatory network of transcriptional regulators. Nature 403:335-8
31. Fenno L, Yizhar O, Deisseroth K. 2011. The Development and Application of Optogenetics. In Annual Review of Neuroscience, Vol 34, ed. SE Hyman, TM Jessell, CJ Shatz, CF Stevens, HY Zoghbi, 34:389-412. Number of 389-412 pp.
32. Fuerer C, Nusse R. 2010. Lentiviral Vectors to Probe and Manipulate the Wnt Signaling Pathway. Plos One 5

33. Gerlach JP, Jordens I, Tauriello DVF, van' t Land-Kuper I, Bugtera JM, et al. 2018. TMEM59 potentiates Wnt signaling by promoting signalosome formation. Proceedings of the National Academy of Sciences of the United States of America 115:E3996-E4005
34. Glinka A, Dolde C, Kirsch N, Huang YL, Kazanskaya O, et al. 2011. LGR4 and LGR5 are R-spondin receptors mediating Wnt/beta-catenin and Wnt/PCP signalling. Embo Reports 12:1055-61
35. Glinka A, Wu W, Delius H, Monaghan AP, Blumenstock C, Niehrs C. 1998. Dickkopf-1 is a member of a new family of secreted proteins and functions in head induction. Nature 391:357-62
36. Gnimassou O, Francaux M, Deldicque L. 2017. Hippo Pathway and Skeletal Muscle Mass Regulation in Mammals: A Controversial Relationship. Frontiers in Physiology 8
37. Green J, Nusse R, van Amerongen R. 2014. The Role of Ryk and Ror Receptor Tyrosine Kinases in Wnt Signal Transduction. Cold Spring Harbor Perspectives in Biology 6
38. Gurney AL. 2016. Patent No. US 09499630
39. Habib SJ, Chen B-C, Tsai F-C, Anastassiadis K, Meyer T, et al. 2013. A Localized Wnt Signal Orients Asymmetric Stem Cell Division in Vitro. Science 339:1445-8
40. Harada H, Kawano MM, Huang N, Harada Y, Iwato K, et al. 1993. Phenotypic Difference Of Normal Plasma-Cells From Mature Myeloma Cells. Blood 81:2658-63
41. Hart M, Concordet JP, Lassot I, Albert I, del los Santos R, et al. 1999. The F-box protein beta-TrCP associates with phosphorylated beta-catenin and regulates its activity in the cell. Current Biology 9:207-10
42. Hawkins KE, Sharp TV, McKay TR. 2013. The role of hypoxia in stem cell potency and differentiation. Regenerative Medicine 8:771-82
43. Hell SW, Wichmann J. 1994. Breaking The Diffraction Resolution Limit By Stimulated-Emission-Depletion Fluorescence Microscopy. Optics Letters 19:780-2
44. Hernandez AR, Klein AM, Kirschner MW. 2012. Kinetic Responses of beta-Catenin Specify the Sites of Wnt Control. Science 338:1337-40

45. Ho H-YH, Susman MW, Bikoff JB, Ryu YK, Jonas AM, et al. 2012. Wnt5a-Ror-Dishevelled signaling constitutes a core developmental pathway that controls tissue morphogenesis. Proceedings of the National Academy of Sciences of the United States of America 109:4044-51
46. Holtzinger A, Rosenfeld GE, Evans T. 2010. Gata4 directs development of cardiac-inducing endoderm from ES cells. Developmental Biology 337:63-73
47. Huang B, Babcock H, Zhuang XW. 2010. Breaking the Diffraction Barrier: Super-Resolution Imaging of Cells. Cell 143:1047-58
48. Hughes RM, Bolger S, Tapadia H, Tucker CL. 2012. Light-mediated control of DNA transcription in yeast. Methods 58:385-91
49. Igarashi M, Nozumi M, Wu LG, Zanacchi FC, Katona I, et al. 2018. New observations in neuroscience using superresolution microscopy. Journal of Neuroscience 38:9459-67
50. Irving BA, Weiss A. 1991. The Cytoplasmic Domain Of The T-Cell Receptor Zeta-Chain Is Sufficient To Couple To Receptor-Associated Signal Transduction Pathways. Cell 64:891-901
51. Ishino Y, Shinagawa H, Makino K, Amemura M, Nakata A. 1987. Nucleotide-Sequence Of The Iap Gene, Responsible For Alkaline-Phosphatase Isozyme Conversion In Escherichia-Coli, And Identification Of The Gene-Product. Journal of Bacteriology 169:5429-33
52. Janda CY, Dang LT, You CJ, Chang JL, de Lau W, et al. 2017. Surrogate Wnt agonists that phenocopy canonical Wnt and beta-catenin signalling. Nature 545:234-+
53. Janda CY, Waghray D, Levin AM, Thomas C, Garcia KC. 2012. Structural Basis of Wnt Recognition by Frizzled. Science 337:59-64
54. Jansen R, van Embden JDA, Gaastra W, Schouls LM. 2002. Identification of genes that are associated with DNA repeats in prokaryotes. Molecular Microbiology 43:1565-75
55. Jenkins D, Lei M, Loew A, Zhou L. 2014. Patent No. US 08883735

56. Kalos M, Levine BL, Porter DL, Katz S, Grupp SA, et al. 2011. T Cells with Chimeric Antigen Receptors Have Potent Antitumor Effects and Can Establish Memory in Patients with Advanced Leukemia. Science Translational Medicine 3
57. Kazanskaya O, Glinka A, Barrantes ID, Stannek P, Niehrs C, Wu W. 2004. R-spondin2 is a secreted activator of Wnt/beta-catenin signaling and is required for Xenopus myogenesis. Developmental Cell 7:525-34
58. Kennedy MJ, Hughes RM, Peteya LA, Schwartz JW, Ehlers MD, Tucker CL. 2010. Rapid blue-light-mediated induction of protein interactions in living cells. Nature Methods 7:973-U48
59. Kim SE, Huang H, Zhao M, Zhang XJ, Zhang AL, et al. 2013. Wnt Stabilization of beta-Catenin Reveals Principles for Morphogen Receptor-Scaffold Assemblies. Science 340:867-70
60. Kitano H. 2002. Systems biology: A brief overview. Science 295:1662-4
61. Kitazawa M, Hatta T, Ogawa K, Fukuda E, Goshima N, Natsume T. 2017. Determination of Rate-Limiting Factor for Formation of Beta-Catenin Destruction Complexes Using Absolute Protein Quantification. Journal of Proteome Research 16:3576-84
62. Komekado H, Yamamoto H, Chiba T, Kikuchi A. 2007. Glycosylation and palmitoylation of Wnt-3a are coupled to produce an active form of Wnt-3a. Genes to Cells 12:521-34
63. Konermann S, Brigham MD, Trevino AE, Hsu PD, Heidenreich M, et al. 2013. Optical control of mammalian endogenous transcription and epigenetic states. Nature 500:472-+
64. Korkut C, Ataman B, Ramachandran P, Ashley J, Barria R, et al. 2009. Trans-Synaptic Transmission of Vesicular Wnt Signals through Evi/Wntless. Cell 139:393-404
65. Kress M, May E, Cassingena R, May P. 1979. Simian-Virus 40-Transformed Cells Express New Species Of Proteins Precipitable By Anti-Simian Virus-40 Tumor Serum. Journal of Virology 31:472-83

66. Kruse SW, Suino-Powell K, Zhou XE, Kretschman JE, Reynolds R, et al. 2008. Identification of COUP-TFII orphan nuclear receptor as a retinoic acid-activated receptor. Plos Biology 6:2002-15
67. Kubo A, Shinozaki K, Shannon JM, Kouskoff V, Kennedy M, et al. 2004. Development of definitive endoderm from embryonic stem cells in culture. Development 131:1651-62
68. Kurayoshi M, Yamamoto H, Izumi S, Kikuchi A. 2007. Post-translational palmitoylation and glycosylation of Wnt-5a are necessary for its signalling. Biochemical Journal 402:515-23
69. Kusch T, Storck T, Walldorf U, Reuter R. 2002. Brachyury proteins regulate target genes through modular binding sites in a cooperative fashion. Genes & Development 16:518-29
70. Lander ES. 2016. The Heroes of CRISPR. Cell 164:18-28
71. Lane DP, Crawford LV. 1979. T-Antigen Is Bound To A Host Protein In Sv40-Transformed Cells. Nature 278:261-3
72. Lee K-N, Jang W-G, Kim E-J, Oh S-H, Son H-J, et al. 2012. Orphan Nuclear Receptor Chicken Ovalbumin Upstream Promoter-Transcription Factor II (COUP-TFII) Protein Negatively Regulates Bone Morphogenetic Protein 2-induced Osteoblast Differentiation through Suppressing Runt-related Gene 2 (Runx2) Activity. Journal of Biological Chemistry 287:18888-99
73. Lee S, Park H, Kyung T, Kim NY, Kim S, et al. 2014. Reversible protein inactivation by optogenetic trapping in cells. Nature Methods 11:633-+
74. Levine BL, Bernstein WB, Connors M, Craighead N, Lindsten T, et al. 1997. Effects of CD28 costimulation on long-term proliferation of CD4(+) T cells in the absence of exogenous feeder cells. Journal of Immunology 159:5921-30
75. Li VSW, Ng SS, Boersema PJ, Low TY, Karthaus WR, et al. 2012. Wnt Signaling through Inhibition of beta-Catenin Degradation in an Intact Axin1 Complex. Cell 149:1245-56
76. Lian X, Bao X, Zilberter M, Westman M, Fisahn A, et al. 2015. Chemically defined, albumin-free human cardiomyocyte generation. Nature Methods 12:595-6

77. Lian X, Hsiao C, Wilson G, Zhu K, Hazeltine LB, et al. 2012. Robust cardiomyocyte differentiation from human pluripotent stem cells via temporal modulation of canonical Wnt signaling. Proceedings of the National Academy of Sciences of the United States of America 109:E1848-E57
78. Lian X, Zhang J, Azarin SM, Zhu K, Hazeltine LB, et al. 2013. Directed cardiomyocyte differentiation from human pluripotent stem cells by modulating Wnt/beta-catenin signaling under fully defined conditions. Nature Protocols 8:162-75
79. Lim WA, June CH. 2017. The Principles of Engineering Immune Cells to Treat Cancer. Cell 168:724-40
80. Lin FY, Yang XA. 2010. TGF-beta signaling in aortic aneurysm: another round of controversy. Journal of Genetics and Genomics 37:583-91
81. Linzer DIH, Levine AJ. 1979. Characterization Of A 54k Dalton Cellular Sv40 Tumor-Antigen Present In Sv40-Transformed Cells And Uninfected Embryonal Carcinoma-Cells. Cell 17:43-52
82. Liu CM, Li YM, Semenov M, Han C, Baeg GH, et al. 2002. Control of beta-catenin phosphorylation/degradation by a dual-kinase mechanism. Cell 108:837-47
83. Liu H, Yu X, Li K, Klejnot J, Yang H, et al. 2008. Photoexcited CRY2 Interacts with CIB1 to Regulate Transcription and Floral Initiation in Arabidopsis. Science 322:1535-9
84. Logan CY, Nusse R. 2004. The Wnt signaling pathway in development and disease. Annual Review of Cell and Developmental Biology 20:781-810
85. Lolas M, Valenzuela PDT, Tjian R, Liu Z. 2014. Charting Brachyury-mediated developmental pathways during early mouse embryogenesis. Proceedings of the National Academy of Sciences of the United States of America 111:4478-83
86. Luca VCM, Y.; Li, X; Hollander, M.J.; Kuo, C.J.; Garcia, K.C. 2019. Surrogate R-spondins for tissue-specific potentiation of Wnt signaling. BioRxiv.
87. MacDonald BT, Tamai K, He X. 2009. Wnt/beta-Catenin Signaling: Components, Mechanisms, and Diseases. Developmental Cell 17:9-26

88. MacDonald BT, Yokota C, Tamai K, Zeng X, He X. 2008. Wnt signal amplification via activity, cooperativity, and regulation of multiple intracellular PPPSP motifs in the wnt co-receptor LRP6. Journal of Biological Chemistry 283:16115-23
89. Mao JH, Wang JY, Liu B, Pan WJ, Farr GH, et al. 2001. Low-density lipoprotein receptor-related protein-5 binds to Axin and regulates the canonical Wnt signaling pathway. Molecular Cell 7:801-9
90. Mason JO, Kitajewski J, Varmus HE. 1992. Mutational Analysis Of Mouse Wnt-1 Identifies 2 Temperature-Sensitive Alleles And Attributes Of Wnt-1 Protein Essential For Transformation Of A Mammary Cell-Line. Molecular Biology of the Cell 3:521-33
91. Matushansky I, Maki RG, Cardo CC. 2008. A context dependent role for Wnt signaling in tumorigenesis and stem cells. Cell Cycle 7:720-4
92. Mojica FJM, Diez-Villasenor C, Soria E, Juez G. 2000. Biological significance of a family of regularly spaced repeats in the genomes of Archaea, bacteria and mitochondria. Molecular Microbiology 36:244-6
93. Mojica FJM, Juez G, Rodriguezvalera F. 1993. Transcription At Different Salinities Of Haloferax-Mediterranei Sequences Adjacent To Partially Modified PstI Sites. Molecular Microbiology 9:613-21
94. Molenaar M, vandeWetering M, Oosterwegel M, PetersonMaduro J, Godsave S, et al. 1996. XTcf-3 transcription factor mediates beta-catenin-induced axis formation in Xenopus embryos. Cell 86:391-9
95. Moon RT, Kohn AD, De Ferrari GV, Kaykas A. 2004. WNT and beta-catenin signalling: Diseases and therapies. Nature Reviews Genetics 5:689-99
96. Moses HL, Roberts AB, Derynck R. 2016. The Discovery and Early Days of TGF-beta: A Historical Perspective. Cold Spring Harbor Perspectives in Biology 8
97. Mukherjee A, Dhar N, Stathos M, Schaffer DV, Kane RS. 2018. Understanding How Wnt Influences Destruction Complex Activity and beta-Catenin Dynamics. Iscience 6:13-+
98. Muller CW, Herrmann BG. 1997. Crystallographic structure of the T domain DNA complex of the Brachyury transcription factor. Nature 389:884-8

99. Niederreither K, Dolle P. 2008. Retinoic acid in development: towards an integrated view. Nature Reviews Genetics 9:541-53
100. Nishisho I, Nakamura Y, Miyoshi Y, Miki Y, Ando H, et al. 1991. Mutations Of Chromosome-5q21 Genes In Fap And Colorectal-Cancer Patients. Science 253:665-9
101. Nusse R. 2008. Wnt signaling and stem cell control. Cell Research 18:523-7
102. Nusse R, Varmus HE. 1982. Many Tumors Induced By The Mouse Mammary-Tumor Virus Contain A Provirus Integrated In The Same Region Of The Host Genome. Cell 31:99-109
103. Park HW, Kim YC, Yu B, Moroishi T, Mo JS, et al. 2015. Alternative Wnt Signaling Activates YAP/TAZ. Cell 162:780-94
104. Peifer M, Polakis P. 2000. Cancer - Wnt signaling in oncogenesis and embryogenesis - a look outside the nucleus. Science 287:1606-9
105. Pires-daSilva A, Sommer RJ. 2003. The evolution of signalling pathways in animal development. Nature Reviews Genetics 4:39-49
106. Repina NA, Rosenbloom A, Mukherjee A, Schaffer DV, Kane RS. 2017. At Light Speed: Advances in Optogenetic Systems for Regulating Cell Signaling and Behavior. In Annual Review of Chemical and Biomolecular Engineering, Vol 8, ed. JM Prausnitz, 8:13-39. Number of 13-39 pp.
107. Reya T, Clevers H. 2005. Wnt signalling in stem cells and cancer. Nature 434:843-50
108. Reya T, Morrison SJ, Clarke MF, Weissman IL. 2001. Stem cells, cancer, and cancer stem cells. Nature 414:105-11
109. Sato N, Meijer L, Skaltsounis L, Greengard P, Brivanlou AH. 2004. Maintenance of pluripotency in human and mouse embryonic stem cells through activation of Wnt signaling by a pharmacological GSK-3-specific inhibitor. Nature Medicine 10:55-63
110. Sato T, van Es JH, Snippert HJ, Stange DE, Vries RG, et al. 2011. Paneth cells constitute the niche for Lgr5 stem cells in intestinal crypts. Nature 469:415-+

111. Schwach V, Verkerk AO, Mol M, Monshouwer-Kloots JJ, Devalla HD, et al. 2017. A COUP-TFII Human Embryonic Stem Cell Reporter Line to Identify and Select Atrial Cardiomyocytes. Stem Cell Reports 9:1765-79
112. Stamos JL, Weis WI. 2013. The beta-Catenin Destruction Complex. Cold Spring Harbor Perspectives in Biology 5
113. Su LK, Vogelstein B, Kinzler KW. 1993. Association Of The APC Tumor-Suppressor Protein With Catenins. Science 262:1734-7
114. Su YY, Fu CJ, Ishikawa S, Stella A, Kojima M, et al. 2008. APC Is Essential for Targeting Phosphorylated beta-Catenin to the SCF beta-TrCP Ubiquitin Ligase. Molecular Cell 32:652-61
115. Sudrik C. 2014. Design strategies for molecular switches in mammalian cells. Doctoral Dissertation. Rensselaer Polytechnic Institute, Troy, NY, Rensselaer Theses and Dissertations Online Collection
116. Szemes M, Greenhough A, Melegh Z, Malik S, Yuksel A, et al. 2018. Wnt Signalling Drives Context-Dependent Differentiation or Proliferation in Neuroblastoma. Neoplasia 20:335-50
117. Tabar V, Studer L. 2014. Pluripotent stem cells in regenerative medicine: challenges and recent progress. Nature Reviews Genetics 15:82-92
118. Tada S, Era T, Furusawa C, Sakurai H, Nishikawa S, et al. 2005. Characterization of mesendoderm: a diverging point of the definitive endoderm and mesoderm in embryonic stem cell differentiation culture. Development 132:4363-74
119. Taelman VF, Dobrowolski R, Plouhinec JL, Fuentealba LC, Vorwald PP, et al. 2010. Wnt Signaling Requires Sequestration of Glycogen Synthase Kinase 3 inside Multivesicular Endosomes. Cell 143:1136-48
120. Takada R, Satomi Y, Kurata T, Ueno N, Norioka S, et al. 2006. Monounsaturated fatty acid modification of Wnt protein: Its role in Wnt secretion. Developmental Cell 11:791-801
121. Takebe N, Ivy SP. 2010. Controversies in Cancer Stem Cells: Targeting Embryonic Signaling Pathways. Clinical Cancer Research 16:3106-12
122. Tan CW, Gardiner BS, Hirokawa Y, Layton MJ, Smith DW, Burgess AW. 2012. Wnt Signalling Pathway Parameters for Mammalian Cells. Plos One 7

123. Tanaka K, Kitagawa Y, Kadowaki T. 2002. Drosophila segment polarity gene product porcupine stimulates the posttranslational N-glycosylation of wingless in the endoplasmic reticulum. Journal of Biological Chemistry 277:12816-23
124. Taslimi A, Vrana JD, Chen D, Borinskaya S, Mayer BJ, et al. 2014. An optimized optogenetic clustering tool for probing protein interaction and function. Nature Communications 5
125. Tischer D, Weiner OD. 2014. Illuminating cell signalling with optogenetic tools. Nature Reviews Molecular Cell Biology 15:551-8
126. Tosi GM, Orlandini M, Galvagni F. 2018. The Controversial Role of TGF-beta in Neovascular Age-Related Macular Degeneration Pathogenesis. International Journal of Molecular Sciences 19
127. Vallier L, Touboul T, Brown S, Cho C, Bilican B, et al. 2009. Signaling Pathways Controlling Pluripotency and Early Cell Fate Decisions of Human Induced Pluripotent Stem Cells. Stem Cells 27:2655-66
128. Valvezan AJ, Zhang F, Diehl JA, Klein PS. 2012. Adenomatous Polyposis Coli (APC) Regulates Multiple Signaling Pathways by Enhancing Glycogen Synthase Kinase-3 (GSK-3) Activity. Journal of Biological Chemistry 287:3823-32
129. vandeWetering M, Cavallo R, Dooijes D, vanBeest M, vanEs J, et al. 1997. Armadillo coactivates transcription driven by the product of the Drosophila segment polarity gene dTCF. Cell 88:789-99
130. Vandewetering M, Oosterwegel M, Dooijes D, Clevers H. 1991. Identification And Cloning Of Tcf-1, A Lymphocyte-T-Specific Transcription Factor Containing A Sequence-Specific Hmg Box. Embo Journal 10:123-32
131. Varela-Nallar L, Rojas-Abalos M, Abbott AC, Moya EA, Iturriaga R, Inestrosa NC. 2014. Chronic hypoxia induces the activation of the Wnt/beta-catenin signaling pathway and stimulates hippocampal neurogenesis in wild-type and APPswe-PS1 Delta E9 transgenic mice in vivo. Frontiers in Cellular Neuroscience 8
132. Verras M, Papandreou I, Lim AL, Denko NC. 2008. Tumor Hypoxia Blocks Wnt Processing and Secretion through the Induction of Endoplasmic Reticulum Stress. Molecular and Cellular Biology 28:7212-24

133. Wang X, Chen X, Yang Y. 2012. Spatiotemporal control of gene expression by a light-switchable transgene system. Nature Methods 9:266-U64
134. Wehrli M, Dougan ST, Caldwell K, O'Keefe L, Schwartz S, et al. 2000. Arrow encodes an LDL-receptor-related protein essential for Wingless signalling. Nature 407:527-30
135. Willert K, Nusse R. 2012. Wnt Proteins. Cold Spring Harbor Perspectives in Biology 4
136. Wilson V, Manson L, Skarnes WC, Beddington RSP. 1995. The T-Gene Is Necessary For Normal Mesodermal Morphogenetic Cell Movements During Gastrulation. Development 121:877-86
137. Wodarz A, Nusse R. 1998. Mechanisms of Wnt signaling in development. Annual Review of Cell and Developmental Biology 14:59-88
138. Wu CY, Roybal KT, Puchner EM, Onuffer J, Lim WA. 2015. Remote control of therapeutic T cells through a small molecule-gated chimeric receptor. Science 350
139. Wu G, Xu GZ, Schulman BA, Jeffrey PD, Harper JW, Pavletich NP. 2003. Structure of a beta-TrCP1-Skp1-beta-catenin complex: Destruction motif binding and lysine specificity of the SCF beta-TrCP1 ubiquitin ligase. Molecular Cell 11:1445-56
140. Wu S-p, Cheng C-M, Lanz RB, Wang T, Respress JL, et al. 2013. Atrial Identity Is Determined by a COUP-TFII Regulatory Network. Developmental Cell 25:417-26
141. Xu Q, Wang YS, Dabdoub A, Smallwood PM, Williams J, et al. 2004. Vascular development in the retina and inner ear: Control by Norrin and Frizzled-4, a high-affinity ligand-receptor pair. Cell 116:883-95
142. Xu W, Zhou W, Cheng M, Wang J, Liu ZA, et al. 2017. Hypoxia activates Wnt/beta-catenin signaling by regulating the expression of BCL9 in human hepatocellular carcinoma. Scientific Reports 7
143. Yizhar O, Fenno LE, Davidson TJ, Mogri M, Deisseroth K. 2011. Optogenetics in Neural Systems. Neuron 71:9-34
144. Zakeri B, Fierer JO, Celik E, Chittock EC, Schwarz-Linek U, et al. 2012. Peptide tag forming a rapid covalent bond to a protein, through engineering a bacterial

adhesin. Proceedings of the National Academy of Sciences of the United States of America 109:E690-E7

145. Zeng X, Tamai K, Doble B, Li ST, Huang H, et al. 2005. A dual-kinase mechanism for Wnt co-receptor phosphorylation and activation. Nature 438:873-7
146. Zhang K, Cu B. 2015. Optogenetic control of intracellular signaling pathways. Trends in Biotechnology 33:92-100
147. Zhang X, Zhang MS, Li D, He WT, Peng JX, et al. 2016. Highly photostable, reversibly photoswitchable fluorescent protein with high contrast ratio for live-cell superresolution microscopy. Proceedings of the National Academy of Sciences of the United States of America 113:10364-9
148. Zuo Z, Liu H, Liu B, Liu X, Lin C. 2011. Blue Light-Dependent Interaction of CRY2 with SPA1 Regulates COP1 activity and Floral Initiation in Arabidopsis. Current Biology 21:841-7